The University of Nottingham

UNITED KINGDOM · CHINA · MALAYSIA

Faculty of Engineering
Department of Mechanical, Materials and Manufacturing Engineering

Development of Non-Destructive Small Specimen Creep Testing Techniques

Balhassn S. M. Ali, MSc.

Thesis submitted to the University of Nottingham

for the degree of Doctor of Philosophy

December 2013

ABSTRACT

Having knowledge of the current creep strength of service-aged components in high temperature installations such as nuclear power stations, oil refineries and chemical plants is essential for their safe and economic operation. Obtaining this knowledge may involve the use of small material samples. These small samples may be removed from weld regions or from component surfaces. Improving small specimens creep testing techniques, whereby a reliable uniaxial minimum strain rate and rupture data can be obtained, has been a major engineering concern for the last 20 years or so.

This thesis includes the development of the small ring creep testing specimen in order to allow the ring specimen to be manufactured and tested with various shapes and geometries. The shape and size of the available small material samples normally dictates the ring shape, e.g., circular or elliptical. However, changing the ring shape leads to a change in the conversion factors, which are used to convert the ring data to the corresponding uniaxial data. Therefore, the effects of the ring geometry with different thicknesses, on the conversion factors, are described in this work. The finite element analyses have been used to assess the effects of shear deformation on the ring behaviour and also to determine the optimum ring

geometry. Nickel base Superalloy 738 steel at 800°C and (Bar-257) P91 steel at 650°C have been used to validate the testing method.

Two new small sized creep test specimens are also described in this thesis, i.e., (i) a small (Two-bar) specimen, which is suitable for use in obtaining the uniaxial MSR and creep rupture data and (ii) a small notched specimen which is suitable for obtaining the multiaxial stress state parameter. The specimen testing techniques, modeling, loading and manufacturing are described for both specimen types in this work. Finite element analyses have been used to assess the effects of the two-bar specimen (TBS) dimensions on the conversion factors, the failure time, the minimum strain rate, and to determine optimum dimension ratio ranges for the specimen.

The two-bar specimen and the small notched specimen have been used to obtain a full set of material constants for two high temperature materials, i.e., (i) typical (as received) P91steel at 600°C and (ii) weak (Bar-257) P91 steel at 650°C. The results show remarkably good agreement between the data obtained from the two new small specimen testing techniques and the data obtained from corresponding uniaxial tests. The major advantages of the small ring specimen, the two-bar specimen and the small notched specimen testing techniques, over the existing small specimens testing techniques, are also included.

LIST OF PUBLICATIONS

Journal articles:

1. Hyde, T. H., Ali, B. S., and Sun, W., 2013, "Interpretation of Small Ring Creep Test Data," *The Journal of Strain Analysis for Engineering Design*, **48(4),** pp. 269-278.

2. Hyde, T.H., B.S.M. Ali, and W. Sun, 2013, "Analysis and Design of a Small, Two-Bar Creep Test Specimen". *ASME J. Engineering Materials and Technology*, **vol. 135(4)**, pp. 0410061-04100619.

3. Hyde, T. H., Ali, B. S. M., and Sun, W., 2013, "Small Two-Bar Specimen Creep Testing of (Bar-257) P91 Steel at 650ºC," *ASME J. Engineering Materials and Technology*, (under review).

4. Hyde, T. H., Ali, B. S. M., and Sun, W., 2013, "On the Determination of Material Creep Constants Using Miniature Creep Test Specimens," *ASME J. Engineering Materials and Technology*. (doi:10.1115/1.4026596).

Conferences:

5. Hyde, T. H., Ali, B. S. M., and Sun, W., 2012, "A Small Creep Test Specimen for Use in Determining Uniaxial Creep Rupture Data, *On Determination of mechanical properties of materials by small punch and other miniature testing techniques*," M. Karel, et al., eds., Ostrava, Czech Republic, pp. 42-53.

6. Ali, B. S. M., Hyde, T. H. and Sun, W., Determination of material creep constants for damage models using a novel small two-bar specimen and the small notched specimen. *ASME, Small Modular Reactors Symposium, 15-17 April 2014, Washington DC*. (accepted)

7. Sun, W., Hyde, T. H. and Ali, B. S. M. Small Tensile Bar Specimen Creep Tests for Use in determining Creep Deformation and Rupture Properties, *The 3th International Conference SSTT 2014, Determination of Mechanical Properties of Materials by Small Punch and Other Miniature Testing Techniques*, September 23 to 25, 2014, Ostrava, Czech Republic, (accepted)

Posters:

1. Ali, B. S. M., The effects of creep on engineering components, *the first Libyan engineers conference*, 20 September 2010, Nottingham University, UK

2. Ali, B. S. M., The importance of small specimens creep testing, *the first Libyan engineers conference*, 20 September 2010, Nottingham University, UK

3. Ali, B. S. M., Development of Small specimens Creep Testing for Power Plant Components, *East Midlands Universities PGR Student Conference, 6 September* 2013, Derby University, UK

ACKNOWLEDGEMENTS

NOMENCLATURE

a, b	Major and minor axes of the ellipse
A	Material constant in Norton's creep law, Kachanov and Liu-Murakami creep damage model
a	Crack length in CT specimen
B	Material constant in Kachanov creep damage model
b, d, L_o, k, D_i	Two-bar specimen dimensions Fig. 4-2
L, H, w, R, b, h	Small notched specimen dimensions Fig. 6-6
C	Material constant in Monkman-Grant relationship
C*	Fracture mechanics parameter to correlate the load-line displacement rates to the creep crack growth.
D	Reference Stress multiplayer
D_i , D_o	Inner and outer diameter of the tube
d_i	The average grain diameter in Hall–Petch relationship
D, d, b_0	Ring dimensions in Fig. 2-30
d'	Cylindrical indenter diameter
E	Modulus of elasticity
G	Modulus of elasticity (modulus of rigidity)
G_{MG}	Monkman–Grant constant
GL, d_{GL}	Gauge length and diameter of the gauge length, respectively
I	Second moment of area ($I = \int_A y^2 \, dA$)
I_n	Beam cross-section area property ($I_n = \int_A y^{1+(1/n)} \, dA$)
Int_2	Integral defined by equation (2.25)
k_e	Material constant related to the grain size in Hall–Petch relationship
K, β	Material constants in equation (2.4)
K_{sp}	Non-dimensional correlation factor for the small punch creep test
M	Material constant in both Kachanov, and Liu-Murakami creep damage models; $M = B(1+\phi)$
M, M_1, M_o	Bending moment, bending moment at $\theta = \pi/2$, bending moment at $\theta = 0$, respectively
n	Material constant in Norton's creep law, Kachanov and Liu-Murakami creep damage models

P	Applied load to the specimens
P_i	Internal pressure
PE , PS	Plane strain and plane stress, respectively
P_L	Limiting load
$\bar{\mathrm{p}}$	Pressure under the indenter in the impression creep test
q_2	Material constant in Liu-Murakami creep damage model
t_o, a_p	The small punch creep test specimen dimensions, Fig. 2-28
a_p, R_s, t_0	Dimensions of small punch creep test experimental set-up
t	Time
t_f	Failure time
T_m	Melting point
t_T	Transient time
r_o, R	Inner radios of the circular ring and the radios of the loading pin respectively
u_x, u_y, u_z	Displacement components in x, y and z direction, respectively
W, a	Compact tension specimen diminutions in Fig. 2-11
W, d_i, h, b	Impression creep test specimen dimensions in Fig. 2-17
X, Y, Z	Cartesian coordinates
α	Multiaxial parameter (material constant)
α'	Reference scaling factor
ε^c, $\dot{\varepsilon}^c$, $\dot{\varepsilon}^c(\sigma_{ref})$	Creep strain, minimum creep strain rate and minimum creep strain rate at reference stress, respectively
$\dot{\varepsilon}_{s.p.}$	Strain at skeletal point
$\dot{\varepsilon}_{ij}$	Creep strain rate tensor
ε_e	Elastic strain
$\dot{\varepsilon}_p$, ε_p	Primary creep strain and primary creep strain rate and, respectively
$\dot{\varepsilon}_{min}$	Minimum creep strain rate
ε_t	Transient (primary) creep strain
$\dot{\varepsilon}_f$	Strain rate at failure
ε_m	Membrane strain
S_{ij}	Deviatoric stress tensor
σ_{eq}	Equivalent, von Mises, stress
Δ^c	Creep displacement
Δ^{el}	Elastic displacement

$\dot{\Delta}_{ss}$	Steady state creep displacement rate
$\dot{\Delta}$	Creep displacement rate
Δ_{ep}	Elastic-plastic deformation
Δ_r	Stress redistribution deformation
$\dot{\Delta}_H, \dot{\Delta}_V$	Ring specimen horizontal and vertical displacement rates, Respectively
$\dot{\Delta}_{total}$	TBS total deformation rate measured at the loading pin
$\dot{\Delta}_{L_o}$	TBS Deformation rate which occurs in the parallel regions of the bars which are of length L_o
$\dot{\Delta}_{k\,(bending)}$	TBS deformation rate in the loading pin supporting material as result of the bending
$\dot{\Delta}_k^c$	Creep deformation rate in the loading pin supporting material
$\dot{\Delta}_k$	Total deformation rate in the loading pin supporting material
θ, θ'	The angular position from datum and the value of θ at M = 0, respectively
β' and η'	Impression creep test conversion factors
ν	Poisson's ratio
σ_1	Maximum principal stress
σ_m	Membrane stress
σ_{non}	Nominal stress
$\sigma_{m.d.h.s}$	Main diameter hoop stress
$\sigma_{s.p}$	Stress at skeletal point
σ_r	Rupture stress
$\sigma, \sigma_{ref}, \sigma_{nom}$	Stress, reference stress and nominal stress, respectively
σ_{ref}	Reference Stress
σ_y	Yield stress
σ_{y_o}	Yield stress of a very coarse-grained in Hall-Petch relationship
χ	Material constant in both Kachanov, and Liu-Murakami creep damage models
ω	Damage parameter, ranging from 0.0 (no damage) to 1.0 (full damage)
ϕ	Material constant in Kachanov creep damage model
β, η	Reference Stress parameters

Abbreviations

2D	Two dimensional
3D	Three dimensional
ASTM	American Society for Testing and Materials
CCG	Creep crack growth
CEGB	Central Electricity Generating Board
CEN	European Committee for Standardization
CT	Compact tension
EBW	Electron Beam Welding
EPRI	Electric Power Research Institute
ERA	Electric Research Association
EGL	Equivalent gauge length
EDM	Electric discharge machining
FE	Finite element
GTAW	Gas Tungsten Arc Welding
HAZ	Heat affected zone
MIT	Massachusetts Institute of Technology
MMA	Manual metal arc
Mo	Molybdenum
Mod.	Modified
MGR	Monkman–Grant relation
NDT	Non-destructive testing
MSR	Minimum strain rate
PM	Parent material
RSM	The Reference Stress Method
SSam	Surface Sampling System
TBS	Two-bar specimen
WM	Weld metal
JAERI	Japanese Atomic Energy Research Institute

TABLE OF CONTENTS

LIST OF FIGURES

LIST OF TABLES

CHAPTER 1.

INTRODUCTION

_____

1.1   SUMMARY

The overall aim of this work is to improve small specimen creep testing techniques and the associated testing specimens, which are used to assess creep strength for the high temperature components such as; chemical plants, power generation plants and oil refinery plants components. In addition, obtaining a full set of material creep constants, whereby a reliable residual life (or remaining life) can be predicted, using only small material samples taken from these components. These objectives were achieved firstly, by understanding the difficulties, limitations of the existing in use small specimen creep testing techniques and then developing one of the existing small creep testing specimens which is the small ring creep test specimen. In order to obtain a full set of material creep constants two novel small sized creep test specimens have been introduced (i) the small Two-bar specimen testing techniques which is suitable for use to obtain uniaxial data and (ii) the small notched specimen which is suitable for use to obtain the multiaxial stress state parameter for the material.

The developments of the small ring creep test specimen and introducing two novel small creep test specimens are the main innovations in the thesis. For validation purposes (i) Preliminary finite element (FE) analyses validations have been carried out and the results compared with the corresponding uniaxial experimental data (ii) experimental validation using different high temperature materials such as (Bar-257) P91 steel at 650°C, as received P91steel at 600°C and Inconel 738 (Nickel-based Superalloy) steel at 800°C. Remarkably good agreement was found between the results obtained from small specimen creep tests and those obtained from the corresponding conventional uniaxial creep tests.

1.2   BACKGROUND

In recent years, new, high temperature, materials have been developed and used to manufacture the power plant components. This has become necessary, in order to ensure the safe and efficient operation of conventional and other power generation plants, when operating under increasingly tough operating conditions, e.g., around 350 bars and 650°C, are used for ultra-supercritical power stations. Normally components in chemical plant, power plants, aero-engines, etc., operate at temperatures and stresses which are high enough for creep to occur [1, 2]. In the quest for improved efficiencies, lower emissions and fuel diversification, new materials are being

2

introduced and these are being subjected to increasingly severe loading conditions [3, 4]. In order to ensure the safe operation of components, improved understanding of the creep behaviour of the materials being used to manufacture them and improved inspection techniques are required [5]. One effect of the desire to improve understanding of material behaviour, and to obtain better inspection techniques, is the need, in some cases, to use small material samples [6]. This comes about because small scoop samples can be removed from some components, e.g. steam pipes and pipe bends, without adversely affecting their safe operation. Also, for some material zones, e.g. the heat-affected zones (HAZ) of welds, only small amounts of material are available for testing.

Conventional uniaxial creep test specimens are normally used to determine the creep strength of a material. However, the dimensions of a typical scoop samples are far too small to allow a conventional uniaxial creep test specimen to be extracted from it. Therefore, it has become necessary to develop small specimen test techniques. These include conventional, sub-size creep test specimens[7]. This test is the closest in behaviour to that of a conventional uniaxial creep test specimens. With this specimen a full creep curve can be obtained, i.e., including the primary, secondary and tertiary regions. In addition creep deformations can be converted to creep strain without the use of sophisticated conversion factors. However,

manufacturing and testing of this specimen type is rather complicated. Small punch creep test specimens also can be used [8], this testing technique has been around for many years, and it seems to be capable of obtaining the three typical creep regions. However, the interpretation of the small punch creep test data to obtain the corresponding uniaxial data remains a challenge in spite of the substantial amount of research that has been carried out to solve this problem. This is due to the complicated nature of the testing, i.e., large elastic/plastic deformation, contact and significant changes to the specimen shape during the test.

Alternatively the impression creep test specimen[9] and the small ring creep test specimens [10], can both be used to obtain the minimum creep deformation but they are unable to obtain creep rupture data. All these small creep testing methods including the specimens manufacturing, loading and testing procedure will be covered in this thesis. The conversion relationships which are used to convert the small creep test specimen's data to the corresponding uniaxial data are also discussed. Most of the conversion relationships presented in this thesis are based on the reference stress method in conjunction with the finite element (FE) method. Two novel, small creep test specimens, i.e., the two-bar specimen and the small notched specimen, are described and used to obtain minimum strain rate data, rupture data and a full set of material creep constants. Finite element

4

analyses have been used with Norton's creep law to obtain the conversion factors for the ring and for the two-bar specimen (TBS). Kachanov and Liu-Murakami damage models [3, 11] have been used to obtain the TBS and the small notch specimen failure times and locations. Various high temperature materials have been used to validate the ring, the TBS and the small notched specimen testing techniques. Very good correlation is found between the presented small specimens testing techniques results and results obtained from the corresponding uniaxial creep tests.

1.3   LAYOUT OF THIS THESIS

The literature review in Chapter 2 follows this introduction. This is mainly concerned with the creep in high temperature materials and creep mechanisms. It also includes the different types of creep testing techniques. The principles and the applications of the Reference stress method are also discussed in this chapter. The literature review also covers the most commonly used theoretical models for creep such as the Norton model, the Kachanov and the Liu-Murakami damage models. In addition it highlights the most commonly used high temperature materials for high temperature applications, e.g., power plants or chemical plant components, aero-engine components. The last part of Chapter 2 is a discussion and conclusions,

which highlight the areas which need to be strengthened in the small specimen creep testing techniques.

Chapter 3 presents the development of the small ring creep test specimen. This includes the use of finite element analyses to obtain the conversion factors η and β for various ring shapes and to assess the effects of shear deformation on the conversion factors. It also includes the differences between the η and β values obtained with two types of ellipses, i.e., "concentric-ellipse" and "offset-ellipse" geometries. The effects of the ring depth and thickness on the minimum strain rate and on the conversion factors are also investigated in Chapter 3. Experimental validation is included using a Nickel base Superalloy 738 at 800°C and a (Bar-257) P91 steel at 650°C. The minimum strain rates (MSRs) obtained from the small ring specimens are compared with those obtained from the corresponding uniaxial tests. The advantages of the ring specimen over the other small specimens creep testing techniques are also included in the last Section of Chapter 3.

The small two-bar specimen (TBS) creep testing technique, the testing method, the determination of Reference stress parameters, for the TBS, and the principle of the equivalent gauge length (EGL), are presented in Chapter 4. This chapter explains how the reference stress method is used in

conjunction with the finite element analysis (FE) method can be used to obtain the conversion factors, which are used to convert the TBS data to the corresponding uniaxial data. This chapter also includes the effects of the TBS dimensions on the reference stress parameters, MSR and the specimen failure time. The recommended specimen dimension ratio ranges are also included in this chapter. Preliminary validation for the testing technique using 3D- FE analyses and Norton's law, have been carried out to assess the accuracy of the conversion relationship and conversion factors. The final part of this chapter is a discussion and conclusions about the FE analyses and the effects of the specimen dimensions on the conversion factors.

Chapter 5 is mainly concerned with the small TBS creep testing and the validation of the testing method and also explains the specimens manufacturing and preparation, specimens loading and experimental setup. Two high temperature materials have been used to validate the TBS testing techniques, i.e., P91 steel at 600°C and (Bar-257) P91 steel at 650°C. The minimum creep strain rates and creep rupture data, obtained from the TBS are compared with those obtained from the corresponding uniaxial tests. The final part of this chapter is the discussion and conclusions; it highlights the advantages of the TBS testing method over the other small specimen creep testing methods. Recommendations and the advantages of the small TBS are also given in the last section of this chapter.

7

The full set of material constants for damage models are obtained in Chapter 6 using the TBS experimental results which are presented in Chapter 5, for (Bar-257) P91 steel at 650°C and P91 steel at 600°C. The experimental results for the ring and for the impression creep tests have been used in this chapter to obtain the material constants for Norton's creep law. The small notched specimen is also introduced in this chapter; this includes the specimen modeling, manufacturing and testing procedure. Chapter 6 also includes some FE analyses which are used to assess the effects of the notch radius on the specimen failure times and also to assess the failure location of the specimen. In addition the material constants which are obtained from the small creep test specimens, including the parameter α, are compared with those obtained from the full size creep test specimens. The final part of this chapter is the discussion and conclusions.

Finally, Chapter 7 presents a general discussion, the main conclusions and the suggestion for future work.

CHAPTER 2.

LITERATURE REVIEW

_____

2.1   INTRODUCTION

Many engineering components (see Fig. 2-1), operate in the creep range

therefore, they are subject to creep failure. Hence creep properties, creep

testing techniques and methods for estimating remaining lifetimes are

required by designers and are of interest for many researchers. This

literature review gives an overview of creep in general; it gives brief

descriptions of the creep behaviour and mechanisms for materials. This

chapter also describes the most common use of full size creep test specimens.

However, in some circumstances it is not possible to use full size creep test

specimens, because of the limitation of the material available for testing.

Therefore, this literature review will briefly cover the most common small

specimen creep testing techniques, which can be used when full size creep

testing specimens cannot be made from the material available. The

limitations, advantages and disadvantages of each small specimen creep

testing method are also included. Furthermore, the most commonly used

empirical, theoretical and numerical methods to interpret the small

specimens creep testing data to the corresponding, uniaxial data are also included.

The reference stress method is widely used to estimate the creep deformations and to interpret small specimen creep testing data. Therefore, a brief review of the reference stress method is included. The creep data obtained from small specimen types are compared with those obtained from the corresponding uniaxial creep tests. The most common material behaviour models, which are used to describe creep deformation, are also included in this chapter. Finally, the high temperature materials, i.e., P91, P92 and INCONEL 738, which have been used in the validation of the small specimen testing techniques, are briefly described.

Fig. 2-1: A tepecal power plant pipe creep failure, progression from cracking to rupture

2.2 CREEP

Creep is the time dependent, non-reversible, type of deformation which occurs in components operating at elevated temperature, normally 0.3 to 0.5 times the absolute material melting point (T_m). High temperatures are usually combined with stress below the material yield stress (σ_y). Time, Stress and temperature, are the three factors which control the creep strain (ε^c) [12] and therefore, the lifetime, of the engineering components which are undergoing creep, i.e.,

$$\varepsilon^c = f(t,\sigma,T) \tag{2.1}$$

where, t, σ and T are time, stress and temperature, respectively [13]. In order to avoid the failure of creeping engineering components, creep deformation has been studied, and component behaviour is monitored and assessed regularly, especially when the components are approaching the end of their design lifetime. The most common method used to test material creep strength (creep resistance) and to obtain the material creep properties, is by applying a constant tensile load on a cylindrical uniaxial specimen at elevated temperature. The test result is normally presented on a strain versus time curve, as shown in Fig. 2-2. Typical strain versus time creep curve exhibits three regions, i.e., primary, secondary and tertiary regions [14].
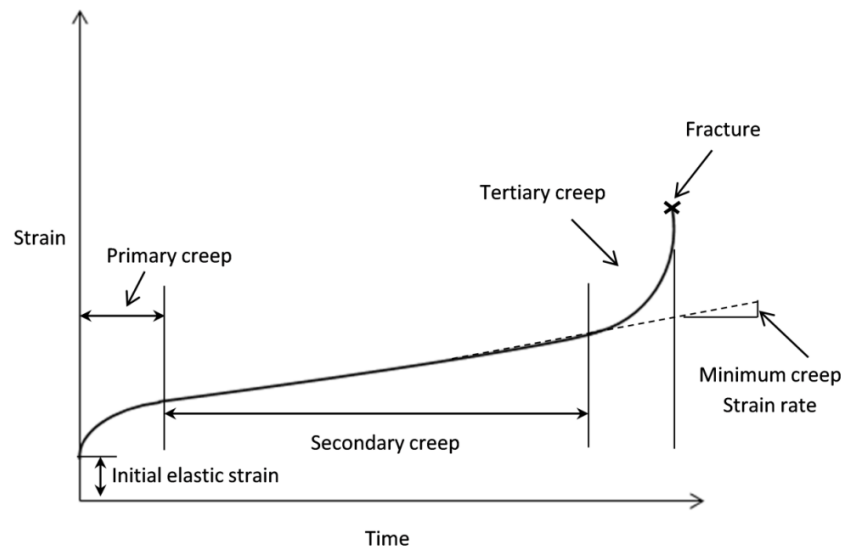
Fig. 2-2:   A typical creep strain time curve, at constant stress and temperature, for a uniaxial creep test specimen [15].

2.2.1 Primary and secondary creep

Primary creep occurs after a relatively small elastic deformation (instantaneous deformation), near the beginning of the primary region when the strain rate tends to be relatively high. However, because of the strain hardening which often occurs, the strain rate decreases during the primary region. In the secondary region the strain rate reaches a minimum value ($\dot{\varepsilon}_{min}$) being almost constant, as shown in Fig. 2-3. Most engineering components spend most of their creep life in the secondary creep region, which often makes the secondary region the most understood region. The constant strain rate in the secondary region, is due to the balance between two mechanisms, i.e., strain hardening and annealing (thermal softening) (Wu, Ramesh et al. 2003; Xue, Zhou et al. 2010). The equation most widely

used to describe the primary and steady creep strain rate is the power law relationship, i.e.

$$\dot{\varepsilon}^c = A\sigma^n t^m \qquad (2.2)$$

where A, n and m are material constants. Equation (2.2) can be used to describe the primary region when $m < 1$ and by taking $m = 0$, the equation (2.2) describes only the steady-state creep behaviour, i.e.

$$\dot{\varepsilon}^c = A\sigma^n \qquad (2.3)$$

Equation (2.3) is known as Norton's law [13].
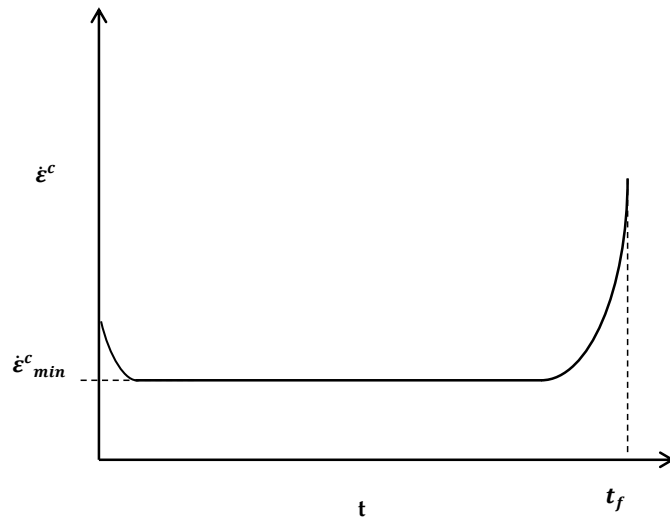
Fig. 2-3: A typical variation of creep strain rate with time, for a uniaxial creep test specimen under constant stress and temperature.

2.2.2 Tertiary creep and rupture

In conventional creep tests, with constant loading and temperature, the strain rate tends to increase throughout the tertiary region, until rupture

occurs, as seen in Fig. 2-3. Also, the specimen cross sectional area decreases in the tertiary region (necking), as a result of the growth of creep voids between the grains. For constant load creep testing, the reduction in the cross sectional area (necking region), cause an increase in the stress and in the number of voids in the necking area. Furthermore, during the tertiary stage of creep, creep voids initiate at an acceleration rate; this process is called creep cavitation. The increasing number of cavitations in a small area (necking region) finally leads to rupture [16, 17]. Equations (2.2) and (2.3) are unable to describe the creep strain rate in the tertiary region. Many equations have been proposed, in order to develop a mathematical model capable of describing the entire creep strain curve. Andrade (1915) introduced equation (2.4), to describe the secondary and tertiary creep strain [16], i.e.

$$\varepsilon = \varepsilon_e (1 + \beta t^{1/3}) \, e^{kt} \tag{2.4}$$

where ε, ε_e and t are creep strain, initial elastic strain and time respectively, β and k are material constants. Alternatively, Garofalo (1960) suggested that equation (2.4) can be used to include the primary creep component and hence gaining a better fit to experimentally obtained creep curves:

$$\varepsilon = \varepsilon_e + \varepsilon_t \left(1 - e^{-rt}\right) + \dot{\varepsilon}^c \, t \tag{2.5}$$

where ε_t is the transient (primary) creep strain, $\dot{\varepsilon}^c$ is the steady-state creep strain rate and r is the ratio of primary creep strain rate to the primary creep

strain at a given time, i.e., $r = \dfrac{\dot{\varepsilon}_p}{\varepsilon_p}$, where $\dot{\varepsilon}_p$ and ε_p are the primary creep

strain rate and the primary creep strain respectively [16]. Over the last

century many theoretical attempts have been made to model the entire creep

curve, including the Kachanov model. Kachanov in 1950, was the first to

model the entire creep strain time curve, including the tertiary creep, using a

single parameter, known as the damage parameter, ω, where (0 < ω < 1) [18].

More details about Kachanov model will be given in Section 2.6.

2.2.3   Creep mechanisms

The mechanisms of creep depend on both the stress and temperature levels

that a material is subjected to. When the material temperature is high enough

,i.e., ≈ 0.4T$_m$, the atoms become active enough to move from one position to

another, by processes known as dislocation or diffusion creep [14, 19].

Adding or creating obstacles to reduce the atoms movements through the

grains, is a well-known method used to increase the material creep

resentence. The boundaries between grains act as barriers to dislocation

movement and therefore, changing material grain sizes and orientations, as

well as strengthening the grain boundaries, usually results in changing the

creep properties [12, 20]. Normally a fine-grained material is harder and has

better creep resistance than a coarse-grained material, because smaller grains

mean shorter distances for atoms to travel within any one grain [21]. For

many materials the yield strength, σ_y, varies with grain size according to Hall-Petch equation, i.e.

$$\sigma_y = \sigma_{yo} + k_e \, d_i^{-(1/2)} \qquad\qquad (2.6)$$

where d_i is the average grain diameter, k_e is material constant related to the grain size and σ_{y_o} is the yield stress of a very coarse-grained material [22]. However, for both very large grained and extremely fine grained polycrystalline materials equation (2.6) is not valid. The size and number of the grains within a material is controlled by the rate of solidification from the liquid phase. Normally low solidification rates result in coarse-grained material, whereas on the other hand, high solidification rates result in fine-grained materials. Therefore, the solidification rate is considered to be a key factor in the material mechanical properties, including the creep properties [16, 17, 23, 24].

2.3   REFERENCE STRESS METHOD AND DATA INTERPRETATION

2.3.1   General

The Reference Stress idea was first proposed by Soderberg in the 1940s. Additions, clarifications and improvements to the method were made by MacKenzie and others [25]. The method is widely used for analysis and design of engineering components which are operating under creep conditions. The Reference Stress method (RSM) is a powerful, approximate

technique, used to describe a component deformation. The method predicts surprisingly accurate results considering the simplified nature of the method compared to other approaches [13]. The general concept of the method is to relate the plastic or creep deformation of a loaded component to a single uniaxial test deformation. This stress is called the "Reference Stress" for this particular component. The RSM is independent of the component material, it is only dependent on the geometry and loading method for the components [13]. Mackanzie in 1968 has introduced a general concept for the Reference Stress method; he proposed a simple solution for finding the displacement rate for a component, using a Reference Stress [25]. In some cases, it is possible to obtain an analytical solution for the steady state deformation rate using the reference stress method, for components with relatively simple geometries and loading, such as rectangular cross-section beams under pure bending, internally pressurized thick walled pipes and twist rate for a solid circular bar subjected to a torque[13, 26-28]. However, the vast majority of engineering components have complex geometries and/or loading. Therefore, analytical solutions for the steady state deformation rate cannot be obtained for these components. Numerical methods (e.g. FE), are widely used to obtain the $\dot{\Delta}_{ss}$ and $\sigma_{(ref)}$ for these components [29].

2.3.2   Approximate Reference Stress

2.3.2.1   Structure limit load solution

An approximate Reference Stress for a structure can be obtained based on the limit load and the yield stress of the structure [29]. The Reference Stress based on the lime load solution is given by:-

$$\sigma_{ref} = \frac{P}{P_L}\sigma_y \qquad (2.7)$$

where, P is the applied load acting on the component, P_L is the limiting load, in other words collapse load, and σ_y is the material yield stress [30]. The limit load method is useful when an analytical or numerical solution for the $\dot{\Delta}_{ss}$ is not available. The reference multiplayer D can also be obtained, as indicated in equation (2.8), based on the ratio of the elastic deformation in the structure to the elastic strain at the reference stress, i.e.,

$$D = \frac{\Delta^{el}}{\sigma_R / E} \qquad (2.8)$$

where E and Δ^{el} are Young's modulus and the elastic deformation respectively, for the structure. It should be noted that the reference multiplayer, D, is the same as the equivalent gauge length (EGL); more details about the EGL will be given in Chapter 4.

2.3.2.2 Skeletal point

For some components which have simple geometries and loading methods, e.g. beams in bending or thick cylinders subject to internal pressure, it is possible to identify a "Skeletal Point". As an example, the stress distribution for a rectangular cross-section beam made of a single material, subject to a pure bending moment, is a linear distribution in the elastic state. If the beam starts to creep under the same load, stress distributions no longer remain liner unless n=1. The stress distribution occurs in order for the beam to reach the compatibility during the creep deformation. Mackenzie has stated that for different stress exponents, n, the stress distribution curves intersect with the linear stress distribution line (elastic case, i.e., $n = 1$) at one point (see Fig. 2-4). This point is known as the Skeletal point and the stress at this point is equal to the reference stress for this component [25].
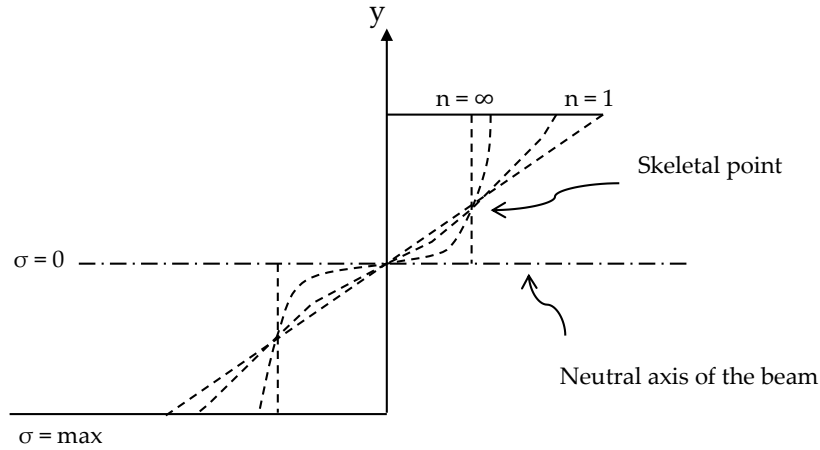
Fig. 2-4:   General stress distribution a cross a beam cross section under creep conditions, for various *n* values.

2.3.3 Applications of the Reference Stress method

The Reference Stress method is a powerful tool that can be used to predict the behaviour of a component undergoing creep or plastic deformation. Therefore, it has been widely used in the field of high temperature material design (Hyde, Yehia et al. 1993). The method has been used extensively to convert the deformation rates of small scale creep testing specimens, to equivalent uniaxial strain rates [9, 31, 32]. For convenience many researchers have used the references stress method to predict power plant components deformation, creep crack growth and remaining life [32]. Thick-wall tubes are widely used in power plants to transfer high temperature steam around the power plants. Therefore, it is a good example to demonstrate the usefulness of the Reference Stress method. If the reference stress for a tube is

obtained, then the deformation in the tube can be related to the deformation of a single conventional creep test, performed at a stress equal to the tube references stress. The deformation of the conventional creep test gives a close approximation to the actual tube deformation. Penny [13] obtained an expression for the tube Reference Stress, using the tube geometry and the internal pressure, i.e.

$$\sigma_{ref} = \frac{P_i}{Ln\left(\dfrac{D_o}{D_i}\right)} \tag{2.9}$$

where P_i is the applied internal pressure, D_0 and D_i are the outer and the inner diameters of the tube [13]. The strain rates and failure time of a thick-walled tube are close to those obtained from a uniaxial test preformed at a stress equal to the mean diameter hoop stress, σ_{mdh}, which is given by:-

$$\sigma_{mdh} = \frac{P_i}{2} \frac{\left(\dfrac{D_o}{D_i} + 1\right)}{\left(\dfrac{D_o}{D_i} - 1\right)} \tag{2.10}$$

The relationship between the Reference Stress and the mean diameter hoop stress at different ratios of D_o/D_i has been obtained [13]. Table 2-1 shows that for the same D_o/D_i ratio, the Reference Stress is almost the same as the mean diameter hoop stress. Therefore, many steel designers have used the reference stress for the pressure tubes and pipes to be the same as the mean diameter hoop stress for these components. It should be noted that the mean

diameter hoop stress, is the most important stress within the tubes or the pipes, and therefore it is used as the design stress for these components.

Table 2-1:   Correlation between the Reference Stress, σ_{ref}, and the mean diameter hoop stress, σ_{mdh} [13]

D_o/D_i	$\dfrac{\sigma_{ref}}{P} = \dfrac{1}{Ln\left(\dfrac{D_o}{D_i}\right)}$	$\dfrac{\sigma_{mdh}}{P} = \dfrac{1}{2}\dfrac{\left(\dfrac{D_o}{D_i}+1\right)}{\left(\dfrac{D_o}{D_i}-1\right)}$
1.1	10.49	10.5
1.5	2.47	2.5
2	1.44	1.5
4	0.72	0.83

2.4   CREEP TESTING TECHNIQUES AND TESTING SPECIMENS

2.4.1   Full size creep test specimens

Normally, to determine material creep properties, and to assess the material creep strength, a conventional creep test specimen (see Fig. 2-5 and Fig. 2-6) is used, with gauge diameter (5-10 mm) and relatively large gauge length (25–50 mm). A tensile load is applied to the specimen ends, in order to generate the required stress in the gauge diameter. The specimen can be used for constant or varying stresses and temperatures tests. However, most creep tests are carried out under constant load and temperature. The relatively large specimen dimensions, compared with the tested material grain size, allows accurate and easy strain measurement to be obtained [14, 27].
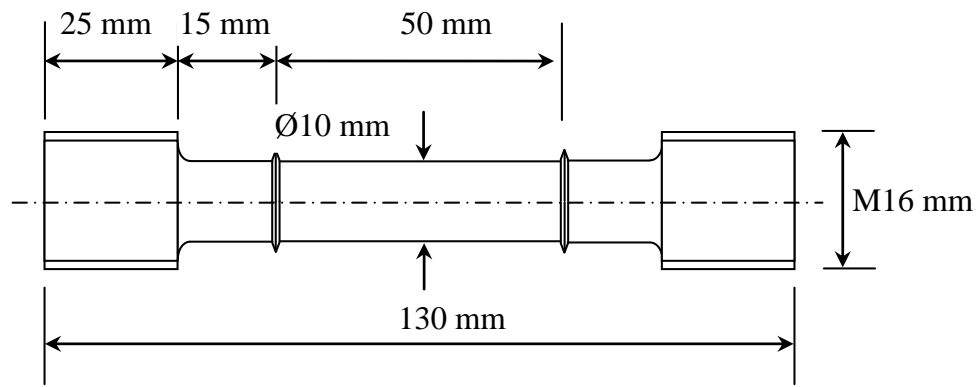
Fig. 2-5:   Conventional uniaxial creep test specimen (dimensions in mm) [33].

Fig. 2-6:   Photo of the conventional uniaxial creep test specimen

In many cases the high temperature engineering components which are operating undergoing creep condition are subjected to multiaxial stress and strain conditions, not only to uniaxial stress and strain. Therefore, a notched bar specimens with the dimensions shown in Fig. 2-7 have been developed, to obtain the multiaxial creep behaviour and determine the factor α which determines the rupture stress (σ_r) [33, 34]
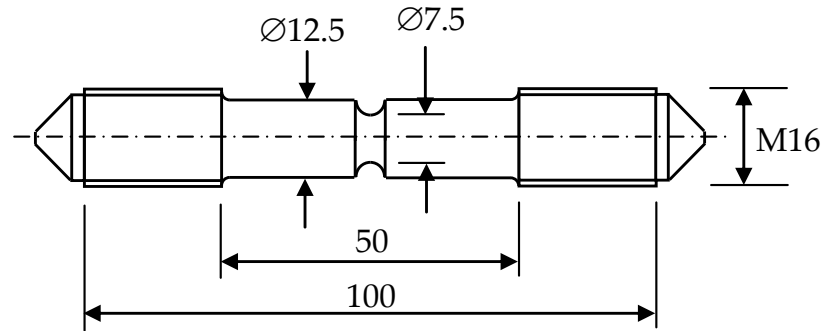
Fig. 2-7:   Notched bar creep test specimen (dimensions in mm) [33].

To obtain the creep properties for a single material, the notched bar specimen and the conventional uniaxial specimen (see Fig. 2-5), are enough to obtain the entire set of material constants for any creep model. However, in some cases the tested material consists of more than one metal, such as in weld regions. Generally, weld regions consist of three different materials, i.e., heat affected zone (HAZ), weld metal (WM) and parent material (PM). In order to obtain creep properties for the HAZ, other specimens types, such as cross-weld uniaxial specimens [35] can be used to obtain creep properties. Using this specimen type the weld metal (WM) and the HAZ are located in the central part of the specimen. Often, one of the HAZs is perpendicular to the loading direction, as shown in Fig. 2-8.
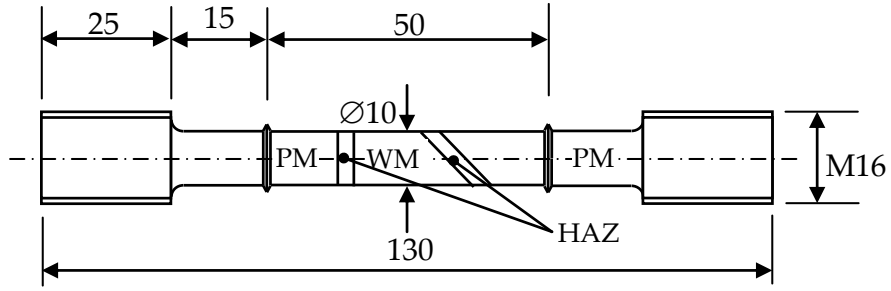
Fig. 2-8:   Cross-weld, uniaxial creep test specimen (dimensions in mm) [33].

The Cross-weld waisted specimen is another option to obtain creep rupture

data from the HAZ region, the specimen dimensions are shown in Fig. 2-9.

The cross-weld waisted specimens are normally positioned in such a way

that the HAZ is located in the centre of the uniform, waisted section as seen

in Fig. 2-10(a). In order to obtain the multiaxial creep behaviour, i.e., the

factor α for the HAZ material, cross-weld notched bar specimens are

normally used. The boundary between the HAZ and the PM is positioned in

the central of the notch section, as seen in Fig. 2-10(b). For the notched and

waisted specimens, the applied stress is taken to be the mean stress on the

minimum sections of the specimens [33, 35].
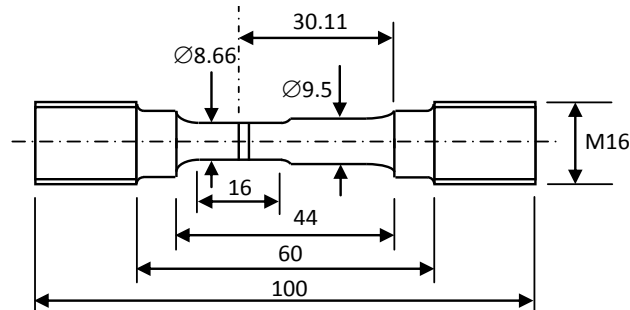
Fig. 2-9:   Cross-weld waisted creep test specimen (dimensions in mm) [33].

(a) Position of waisted specimen

(b) Position of the notched bar
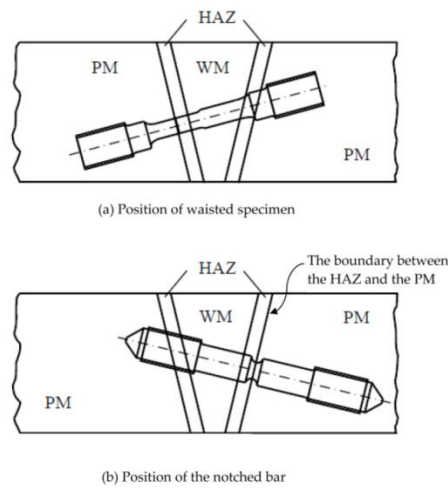
Fig. 2-10:   The material zone positions in cross-weld notched and waisted creep test specimens [33].

Another type of full size creep testing specimens is the compact tension specimen (CT specimen)[36, 37]. The specimen is widely used to assess the creep crack growth behaviour (CCG) in the PM, WM and HAZ materials; typical specimen dimensions are shown in Fig. 2-11. [38, 39]. The American Society for Testing and Materials (ASTM), which is an international standards organization, has set up standards to assess creep crack growth testing using CT specimens. Tensile load is applied to the specimen through loading pins, which forces the crack (a) to open. The measured creep load-line displacement rates and the crack growth rate are used to calculate the fracture mechanics parameter C* [40-42]. The C* factor is a function of the applied load, P, the load-line displacement rates and the crack growth rate. In the field of creep crack growth assessment, the C* parameter is a powerful

tool which can be used to relate the creep crack growth in the CT specimen, to the creep crack growth in the real component [40-42].
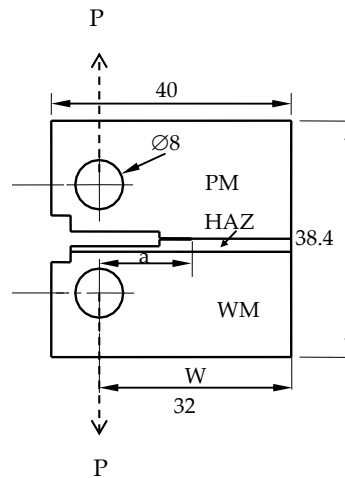
Fig. 2-11:   Cross-weld CT specimen consisting of PM, HAZ and WM (dimensions in mm) [43].

2.4.2 Small specimen creep testing (non-destructive testing techniques)

2.4.2.1 General

Normally a conventional uniaxial creep test specimen, with the dimensions shown in Fig. 2-5, is used to obtain the creep properties. However, for many practical creep testing situations, engineers must cope with cases where there is not enough material to construct the conventional uniaxial creep test specimen from it [32]. Therefore, it has become necessary to develop small specimen test techniques[44]. This comes about because small scoop samples

27

can be removed from some components, e.g. steam pipes and pipe bends, without adversely affecting their safe operation. Also, for some material zones, e.g., HAZ and WM of welds, only small amounts of material are available for testing. Rolls-Royce Company have developed a catting technique, known as the Surface Sampling System (SSam); the cutting machine is shown in Fig. 2-12. The cutting machine is attached to surface of the component as shown in Fig. 2-13. By using a thin, 50mm diameter hemispherical shell cutter, a sample is removed by spinning the cutter about its axis of symmetry at 9,000 rpm, while slowly advancing parallel to the rotation axis to feed the cutter into the base [32]. The SSam machine removes a small scoop sample of material typically about, (25-30 mm) in diameter and (3-4 mm) thick, as shown in Fig. 2-14. The dimensions and the size of the scoop sample will depend on the component geometry and the depth of cut setting. The cutting process can be categorized as a non-destructive testing (NDT) technique.

Fig. 2-12:   Image of a typical (SSam) sampler [45]
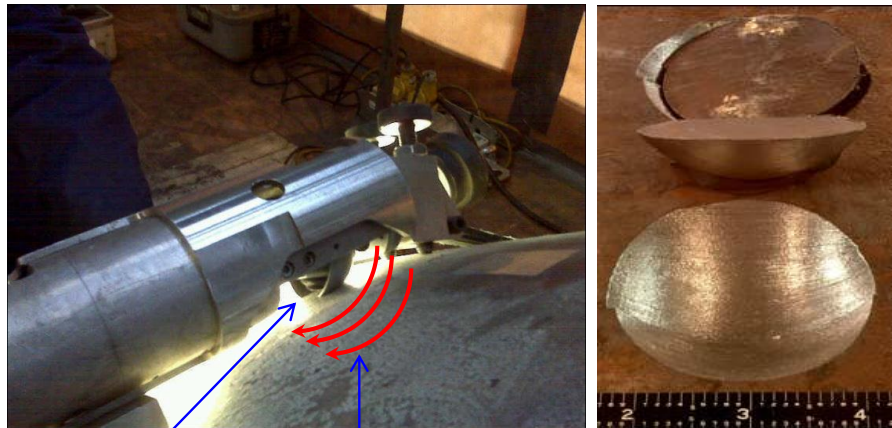
Hemispherical shell cutter

Cutting direction

(a)   (b)

Fig. 2-13:   Photographs of Scoop sampling in process on pipework (a), and A typical
scoop sample (b) [46].

(a) (b)
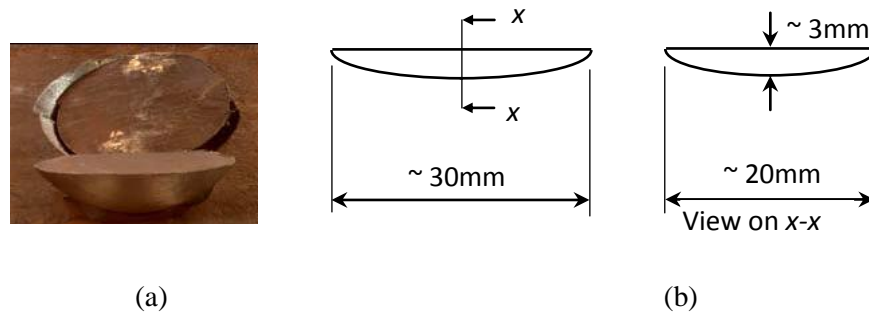
Fig. 2-14: Dimensions of a typical scoop sample [10],

However, the dimensions of a typical scoop sample, (see Fig. 2-14), are far too small to allow a conventional uniaxial creep test specimen (see Fig. 2-5) to be extracted from it. However, as many power plant components are now operating beyond their original design life, most of their components have to be creep assessed on a regular basis. Therefore, small scale sampling and testing techniques are becoming more attractive for remaining life evaluation (remaining life assessment of pressure components in the power plants). Furthermore, from an economic point of view these testing techniques are desirable, due to the ease and the low cost of assessing component creep strength using these testing methods

2.4.2.2 Conventional sub-size uniaxial creep test specimen

The conventional sub-size creep test specimen shown in Fig. 2-15 (c), is considered to be the closest version in its behaviour, to the conventional uniaxial creep test spacemen, among all developed small creep test specimens. The Small cylindrical specimen has relatively small gauge length

about (5–12 mm) and gauge diameter about (1-3 mm). These small

dimensions allow the specimen to be constructed from small scoop samples

(see Fig. 2-14). Loading the specimen is the critical part in this testing

technique, as the specimen has relatively small gauge length, a small

conventional end pieces have to be attached (welded) to the specimen ends

for loading purposes [7].
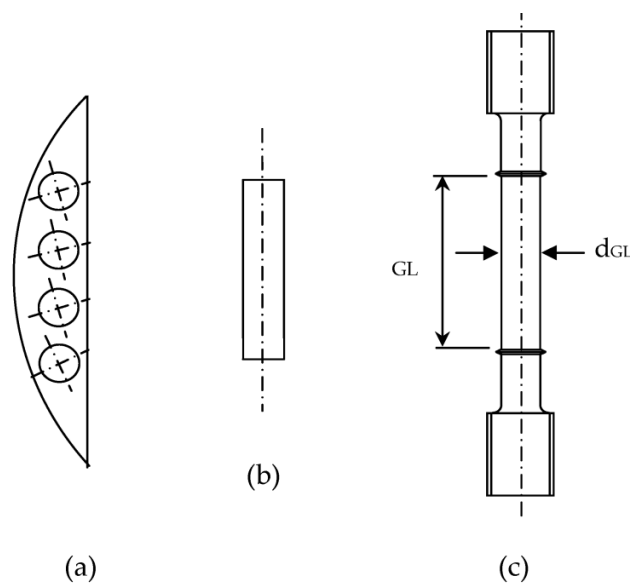
Fig. 2-15:   Positions of small cylindrical specimens in scoop samples (a), cylindrical
specimens (b) and conventional sub-size creep test specimen (c) [7].

As the gauge length is very small, the overall specimen deformation will be

limited; therefore, the deformation which occurs in the welded regions has to

be minimized and carefully taken into account, when measuring specimen

creep deformation. To weld the end pieces (grips), the electron beam

welding (EBW) technique is used, for the purpose of minimising the effects

of material recrystallization (softening) and type IV cracking (in the HAZ) on

the test results. The EBW generates relatively small weld regions, i.e. (HAZ and WM) compared with many other arc welding methods, such as Manual metal arc (MMA) welding, gas tungsten arc welding (GTAW) or gas metal arc welding (GMAW), as shown in Fig. 2-16. An example of the use of conventional sub-size uniaxial creep test specimens, is given by remaining life assessment projects, developed by Electric Power Research Institute (EPRI) and Central Electricity Generating Board (CEGB) [47].

(a) EBW joint

(b) GTAW joint
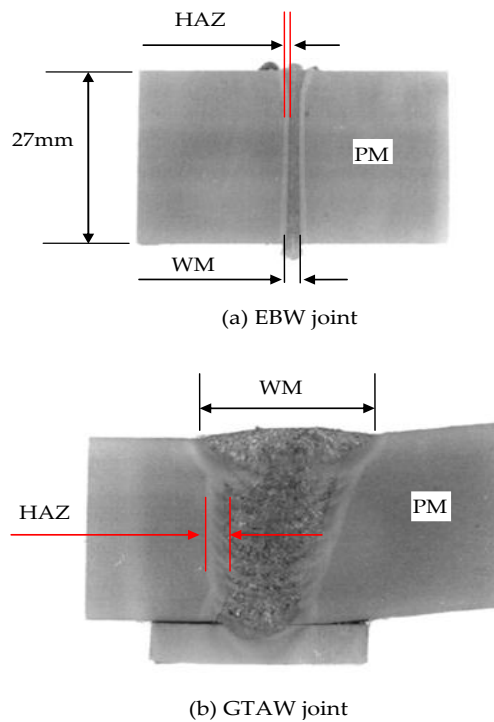
Fig. 2-16: Comparisons between a Gas Tungsten Arc Welding joint (GTAW) and an electron beam welding joint (EBW)[48].

However, for very small conventional sub-size creep test specimens with dimensions for d_{GL} of about 1 mm, the effect of oxidisation on the failure time, t_f, may be significant, especially for high temperature tests [7]. The effect of the oxidization on the specimen minimum strain rate (MSR) and

32

failure time can be minimised if the specimen is surrounded by "argon gas" during the test [49, 50]. The main advantage of conventional sub-size creep test specimens is that the specimen is capable of obtaining the full creep curves including the primary secondary and tertiary regions. The curves are identical to those obtained from the conventional uniaxial creep test specimens [49, 51]. The experimentally recorded elongation, Δ, at a given time, in the gauge length (GL), can be converted to creep strain without using any conversion relationship or correction factors, i.e.

$$\varepsilon = \frac{\Delta}{GL} \tag{2.11}$$

However, it should be noted that welding the extension pieces to the small cylindrical specimens in the correct position, where good aligning is achieved, between the specimen and the two extension ends, requires a rather sophisticated welding process [27]. Machining "smooth surface", uniform specimen cross-sections with small diameters (1-3) mm, is also a difficult task to perform. Furthermore, very small d_{GL} specimens, i.e. ≈ 1 mm requires complex creep testing machines with a constant argon gas flow rate and a very precise loading system.

2.4.2.3 Impression creep test

The impression creep testing technique (or indentation creep testing), was first reported in 1977; the technique was first used to test a material which

crept at room temperature [9]. The impression creep testing technique involves the application of a steady load (P) to a flat-ended indenter (rectangular or cylindrical), placed on the surface of a material (specimen), at elevated temperature, as seen in Fig. 2-17(a) [52, 53]. Creep allows the indenter to push its way into the surface of the specimen as shown in Fig. 2-17(c). The displacement time record from such a test is related to the creep properties of a relatively small volume of material in the vicinity of the material in contact with the indenter [5, 53]. The standard square impression creep test specimen shown in Fig. 2-17(b), has relatively small dimensions, i.e. (w = $b \approx 10$ mm, di ≈ 1 mm, h ≈ 2.5 mm, loading area is wd_i).

(a) Impression creep test with a rectangular indenter

(b) Square specimen

(c) A tested specimen
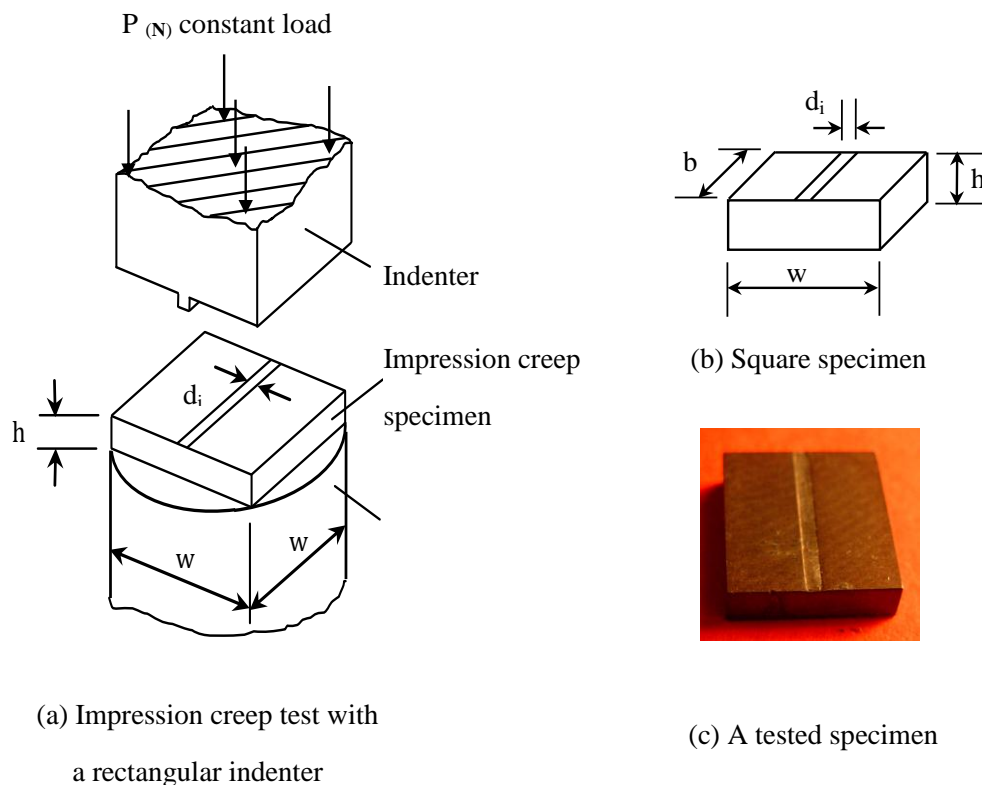
Fig. 2-17:   Impression creep testing and test specimen [54].

In some situations where the material available is insufficient for a standard impression creep test specimen to be constructed from it, the specimen dimensions can be reduced to w$\times$b$\times$h $\approx$ 8$\times$8$\times$2 mm with $d_i \approx$ 0.8mm [54]. Therefore, the method is suitable for testing local regions such as the HAZs and the WM of fusion welded joints as seen in Fig. 2-19. The specimen can be conveniently machined from small samples of material removed from the surface of the components, for example "scoop" samples removed on-site from power plants steam pipes (see Fig. 2-14), [54]. Therefore, the impression creep testing technique can be considered to be, effectively, a Non Destructive Testing techniques (NDT).

Impression creep test specimens can be easily loaded and tested using, for example, a creep testing machine shown in Fig. 2-18. Modern impression creep testing machines feature precise loading systems, temperature control and accurate measurement/recording deformation systems, etc. Most modern impression creep testing machines are designed to enable a constant flow rate of argon gas, which can be used during the test, if needed, to reduce the effects of oxidization on the test results. Generally the effect of the oxidisation depends on the characteristics of the specimen, i.e. material composition and geometry, test running time and testing temperature [49]. However, for high alloy steel (P91 and P92 high chromium steels), with testing temperature around 650°C oxidisation has an insignificant effect on

35

the impression creep testing results [55]. Typical impression creep test deformations versus time curves, subjected to steady loading are shown in Fig. 2-19 and Fig. 2-20.

Fig. 2-18:   Impression creep testing machine [52].
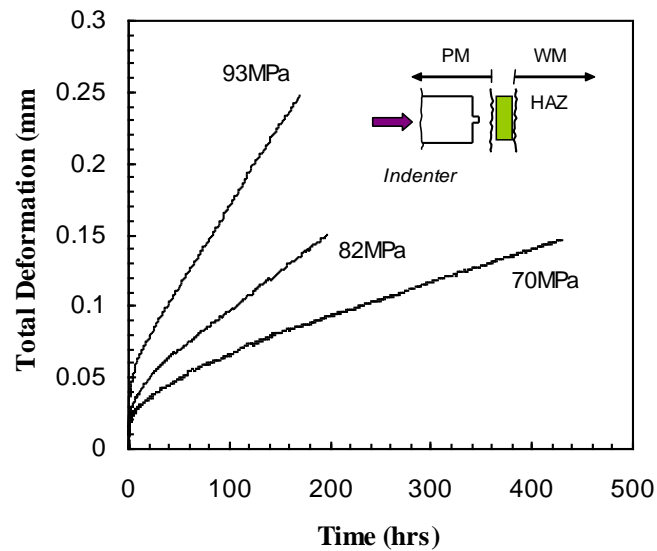
Fig. 2-19:   Impression creep test deformations of the HAZ material in a P91 weld at 650°C, subjected to steady loading from the parent material side [5].
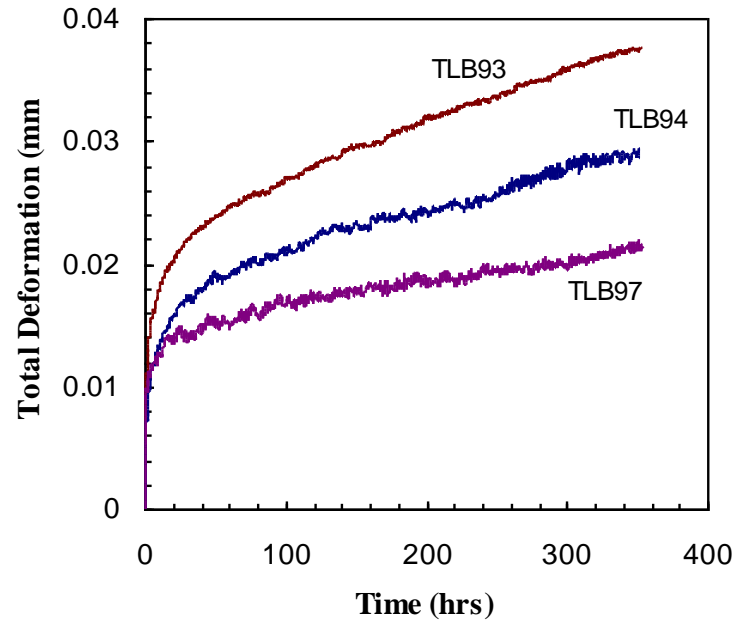
Fig. 2-20: Total impression creep test deformations with time at 90 MPa and 600°C obtained from three different ex-service ½CrMoV steam pipe samples [54].

The impression creep test is limited to primary and secondary creep regions and there is no indication of the tertiary region, as can be seen from Fig. 2-19 and Fig. 2-20. In order to obtain the minimum creep strain rate, using the impression creep test, equation (2.11) cannot be used directly to convert the load-line indenter displacement or displacement rate to creep strain or strain rate. Many researchers have effectively used a trial-and error approach to correlate the impression creep test data with conventional uniaxial minimum creep data using a cylindrical indenter [31]. Conversion factors are needed to convert the pressure under indenter, $\overline{p}$, to the equivalent uniaxial stress, σ, i.e.

$$\sigma = \eta' \overline{p} \qquad (2.12)$$

and also to convert the steady state indenter displacement rates, $\dot{\Delta}^C$, to the corresponding uniaxial minimum creep strain rate, $\dot{\varepsilon}^C$, i.e.

$$\dot{\varepsilon}^C = \frac{\dot{\Delta}^C}{\beta' d'} \qquad (2.13)$$

where β' and η' are experimentally determined factors and d' is the cylindrical indenter diameters. Several researchers have obtained β' and η', using different materials at various temperatures, and the values of the conversion factors are reported in Table 2-2. From this table, general agreement can be observed, leading to values of β' and η' of approximately 1.0 and 0.3 respectively. Most of the researchers described the conversion factors as geometric correlation factors [31].

Table 2-2: Summary of β' and η' factors obtained for experiment impression creep tests for various materials [31].

Material	Test temperature (C°)	Stress exponent (n)	η'	β'
Succinonitrite (single crystal)	37	4	0.303	1
B Tin	60-203	4-5	0.256-0.357	1
LiF (single crystal)	-	-	0.1493	2.6
Al 99.999%	300-400	6.1	0.415-0.416	1
1018 steel*	-	-	0.345	0.67
Al	-	-	0.287	1
Cu	-	-	0.347	1
Ni	-	-	0.345	0.625
Al 90.74% alloy*	-	-	0.303-0.333	1

Hyde and co-authors derived a mechanics-based approach to the impression creep problem, by using the Reference Stress method to obtain the Reference

Stress parameters (conversion factors), β and η are used to convert the mean pressure under the indenter, $\bar{p}$, to the corresponding uniaxial stress, σ, i.e.

$$\sigma = \eta \bar{p} \tag{2.14}$$

and to convert the steady state indenter displacement rates, $\dot{\Delta}^c$, to the corresponding uniaxial minimum creep strain rate, $\dot{\varepsilon}^c$, i.e.

$$\dot{\varepsilon}^c = \frac{\dot{\Delta}^c}{\beta d_i} \tag{2.15}$$

where $\dot{\varepsilon}^c$ is the corresponding uniaxial minimum creep strain rate, η and β are the reference stress parameters (conversion factors) and d_i is the relative indenter dimension see Fig. 2-17(a) [56]. As an example, the conversion relationship, i.e. equation (2.15), has been used to convert the indenter minimum displacement rate, to the equivalent uniaxial minimum creep strain rate, using a 316 stainless steel at 600°C and a 2-1/4Cr1Mo weld metal at 640°C [57]. The minimum creep strain rates obtained from the impression creep tests, and plotted together with the minimum creep strain rates obtained from the corresponding conventional uniaxial creep tests against stress in Fig. 2-21. A very good agreement is found between the two sets of data.
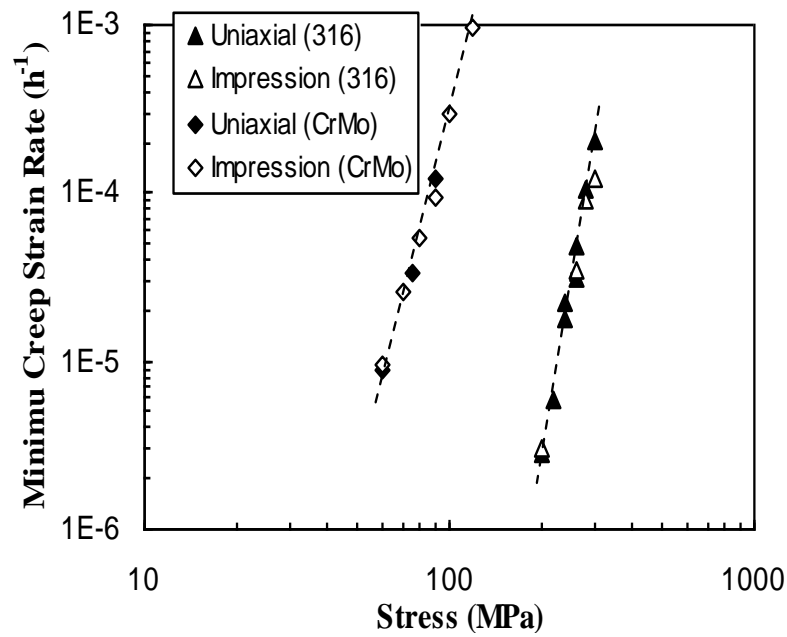
Fig. 2-21:   Minimum creep strain rate data for 316 stainless steel at 600°C and 2-1/4Cr1Moweld metal at 640°C, obtained from uniaxial and impression creep tests [57].

Generally the conversion factors are independent of the tested material properties [31]. However recent FE analyses have been carried out by Hyde and co-authors, which shows that the conversion factors are sensitive to the specimen height to the indenter width ratio, i.e. (h/d), for a given specimen width to indenter width ratio, i.e. (w/d), and specimen width to length ratio, i.e. (w/b), [5]. However, care must be taken during the experiment setup and specimen preparation to ensure that there is full contact between the indenter and the specimen surface when applying the load.

One of the main challenges facing users of the impression creep testing technique is that the testing of high creep resistance materials, which are

similar in creep strength to the indenter, is not possible. The indenter material has to have much higher creep resistance than the tested material, in order to ensure that the indenter does not deform significantly during the test, [5]. Hyde and *et al.* at the University of Nottingham have developed the impression creep test by extending the traditional single-step impression creep testing method to stepped temperature and stepped-load testing. In a stepped-temperature test, the indentation loading is held constant, but the temperature is increased (or reduced). In the stepped-load test, the indentation loading is increased (or reduced) when a sufficient section of the deformation curve has been obtained from the previous step, the temperature remaining constant. For either the stepped temperature or stepped-load tests, a sufficient time must be given between the steps in order to ensure that steady state creep is achieved for the new load or temperature step [54, 56].

Service aged 1/2Cr1/2Mo1/4V steel, at 565°C, has been used as an example to validate the stepped-load test; the deformation curves obtained from the test is shown in Fig. 2-22. The minimum strain rates obtained from the impression creep test deformation curves, with or without a previous loading history are plotted together with the corresponding uniaxial minimum creep strain rates against the applied stress in Fig. 2-23. Good agreement is found between the minimum creep strain rates obtained from

the stepped-load tests, and the corresponding uniaxial tests, which is a good

indication of the stepped-load testing accuracy [56].
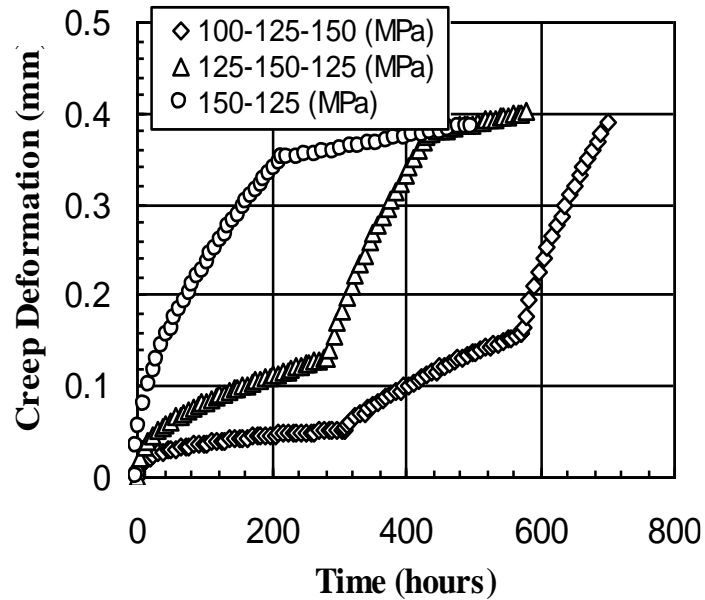
Fig. 2-22:   Deformation curves for a 1/2Cr1/2Mo1/4V steel at 565°C, obtained from
stepped-load impression creep tests [56].
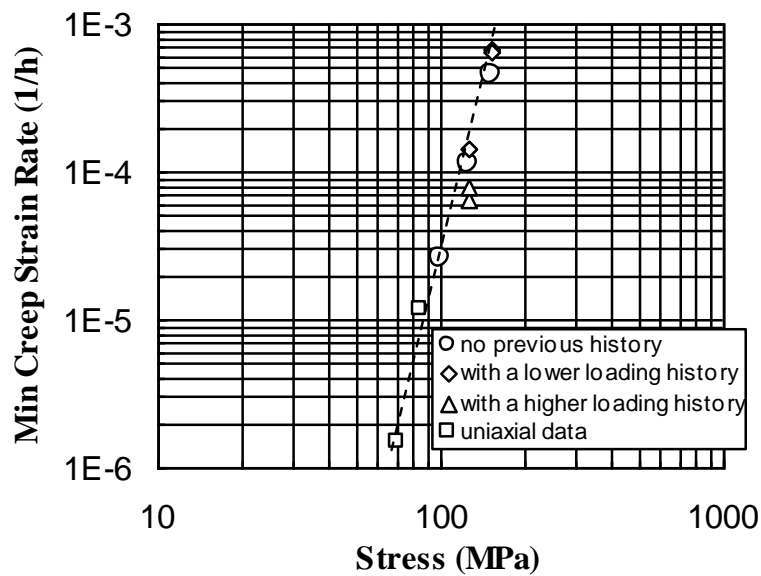
Fig. 2-23:   Minimum creep strain rate data for the 1/2Cr1/Mo1/4V steel at 565°C, obtained
from steped-load impression tests and uniaxial creep tests [56].

An ex-service, ½CrMoV, steam pipe material, at 40 MPa, has been used as an example of stepped-temperature testing. The testing temperature was increased six times (630, 640, 650, 660, 670 and 680) °C, the deformation-time curves obtained from the stepped-temperature tests are shown in Fig. 2-24. For these stress and temperature levels, the corresponding uniaxial data are not available [54]. However, the validity and the accuracy of the stepped-temperature testing technique can be assessed in the future, by comparing the step-temperature tests minimum creep strain rate with conventional creep test specimen data.
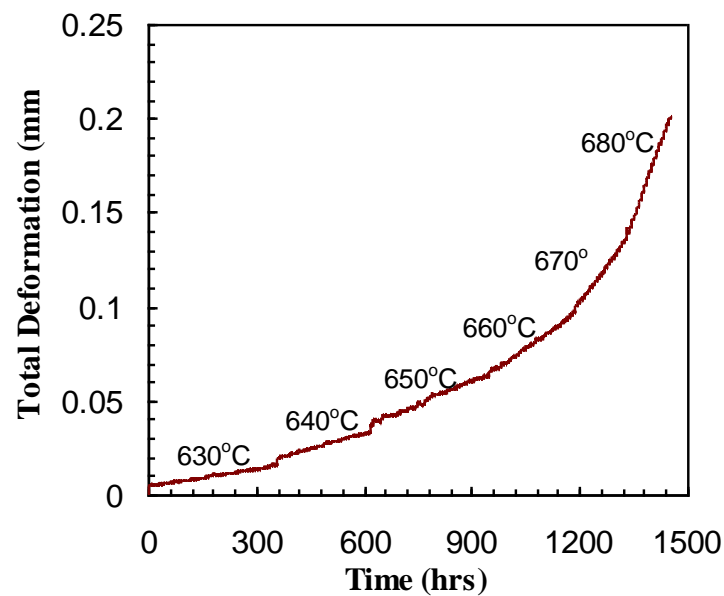
Fig. 2-24:   Variation of total impression deformation with time for an ex-service ½CrMoV steam pipe material (MSC9/MT572), subjected to stepped-temperatures, at 40 MPa [54].

Although the impression creep testing technique is limited to primary and secondary creep, it is possible to obtain a reasonable estimation to the rupture life using this testing technique. The Monkman–Grant relationship

43

(MGR) between secondary creep strain rate and rupture life can be used to predict the time to failure, i.e.

$$\dot{\varepsilon}^c \times t_f \quad \text{Constant} = C_{MG} \tag{2.16}$$

where C_{MG} is the Monkman–Grant constant, $\dot{\varepsilon}^c$ is the minimum creep strain rate and t_f is the time to failure. The Monkman–Grant relationship is found to be valid for most materials, including high alloy steel [58]. The Monkman–Grant constant (C_{MG}), can be found conveniently using the minimum creep strain rate and t_f obtained using a conventional creep test specimen. Since the minimum creep strain rates obtained from the impression tests correspond reasonably well to those obtained from the conventional uniaxial creep tests (see Fig. 2-21), the impression creep test results can be easily used with the Monkman–Grant relationship to estimate the t_f for the material [57].

One of the main advantages of impression creep testing is the ease of manufacturing the specimens. Several tests can be performed on the same specimen (by changing the indenter position on the specimen surface after each test). Specimen dimensions do not change significantly during the test and therefore, the conversion factors are approximately constant during the test duration. The impression creep testing technique can be used for stepped-load and stepped-temperature testing. The very good correlation

44

between the minimum creep strain rates obtained from impression creep tests and the corresponding conventional creep tests (see Fig. 2-23), is an indication of the accuracy of this testing technique [52, 57].

2.4.2.4 Small punch creep test

The small punch test (SPT) was developed in the late 1970s in the USA, at the Massachusetts Institute of Technology (MIT)[59]. The technique was introduced mainly to identify the ductility loss in steels due to temperature effects [60]. The small punch creep testing technique has been widely used for material creep testing in Japan, at the Japanese Atomic Energy Research Institute (JAERI) and, later, further developments were made at Tohoku University in the 1980s. More improvements to the testing method were later made in the USA and in Europe in the 1990s. Swansea University and the UK Electric Research Association (ERA) have shown great interest in this testing method and they have made substantial contributions to the development of small punch creep testing.[61]. The small punch creep test (SPCT) seems to be a promising technique for use in obtaining primary, secondary and tertiary creep properties, using small amount of material. The method is considered to be a non-destructive technique (NDT), because specimens can be made from very small amounts of material. Specimens can be machined from HAZ or WM regions of weldments. [32, 46].

A small punch creep test involves the application of a constant load, through a spherical punch or a ball, to a thin disc, at high temperatures. The typical small punch creep test specimen is approximately 0.5 mm thick and around 8 to 10 mm in diameter. The specimen can be conveniently machined from small scoop samples removed from the component surface (see Fig. 2-14). The small disc specimen is rigidly clamped into a test rig which comprises upper and lower ring shaped dies, which clamp the edges of the specimen. A constant load is then applied to the disk specimen as shown in Fig. 2-25 [62].
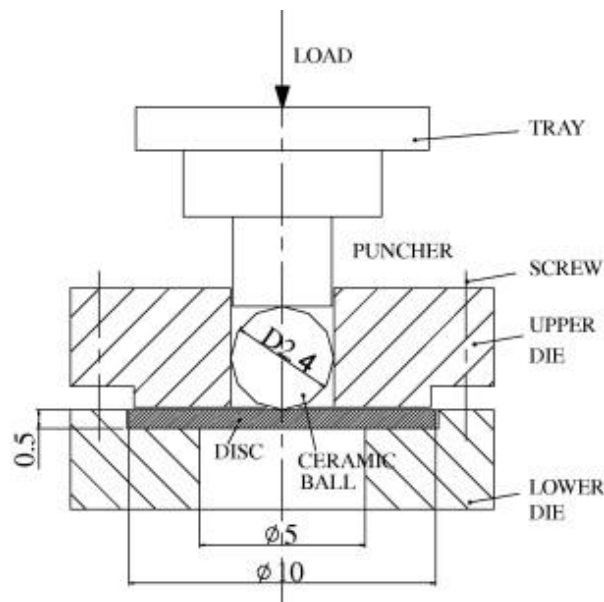
Fig. 2-25:   Small punch experiment set-up [62].

During the test a ceramic ball is used to force the specimen into a hemispherical shape and this finally leads to failure of the specimen, as shown in Fig. 2-26 [63].
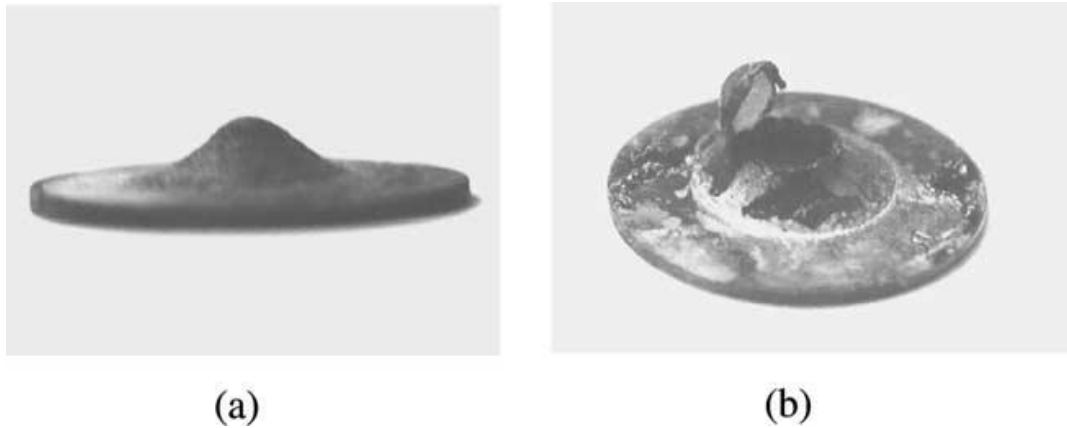
Fig. 2-26:   Typical appearance of tested small punch creep test specimen before failure
with F = 217.6N (a) and after failure, with F= 1226N (b) for 12Cr1MoV steel ,
at 540 $^{\circ}$C [64].

The test involves large deformations relative to the specimen dimensions as can be seen from the typical, failed specimen, shown in Fig. 2-26(b). The deformation of the specimen (plastic and creep deformation) is recorded by measuring the displacement of a tray, using a mechanical measuring device [65, 66]. The outcome from a SPCT is normally plotted as a deformation versus time curve (see Fig. 2-27).
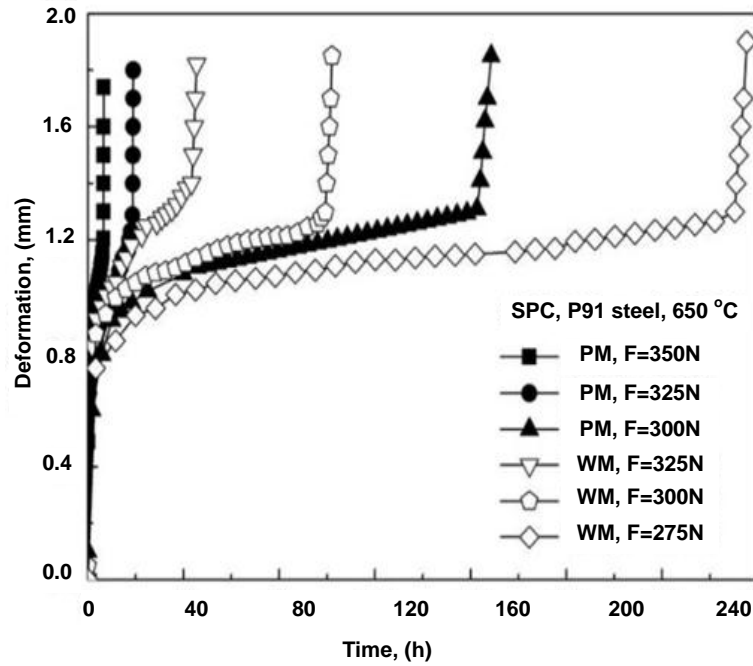
Fig. 2-27: Small punch creep test data for PM and WM zones of P92 steel welded joint material at 650°C under various loadings [65].

By comparing small punch deformation versus time curves, i.e. (Fig. 2-27) with uniaxial specimen creep strain versus time curves,(see Fig. 2-2), it can be seen that small punch creep curves exhibit the typical three creep regions, i.e., Primary, secondary, and tertiary regions It is also noticeable that the instantaneous deformation in the small punch curves is much higher than that in uniaxial specimen strain versus time curves. However, converting the SPCT deformation to the equivalent uniaxial strain is not an easy task. The high instantaneous elastic deformation response and the existence of high plastic deformation during the test, make it difficult to distinguish creep deformation from the elastic and plastic deformations [8]. The increasing contact area between the loading ball and the specimen surface makes it

difficult to determine the appropriate load magnitude which will generate the exact constant equivalent uniaxial stress during the test duration. Furthermore, the significant change of the overall specimen geometry, adds further difficulties in determining universally approved conversion factors, to convert the specimen deformation to equivalent uniaxial strain [32, 67].

A European draft code of practice (CEN CWA15627 2006) provides a formula which can be used to estimate the equivalent uniaxial stress σ_{eq}, for the SPCT, using a correlation factor, and geometric parameters of a SPT set-up, i.e. a_p, R_s, and, t_0, where a_p is the inner radius of the lower die, R_s is the radius of the ball and t_0 is the specimen thickness at the beginning of the test, i.e.

$$\frac{P}{\sigma_{eq}} = 3.33 K_{sp} \ a_P^{-0.2} \ R_s^{1.2} \ t_0 \tag{2.17}$$

where K_{sp} is a non-dimensional correlation factor, which can be obtained by comparing the failure life obtained from conventional uniaxial creep tests and the SPCTs. However, the correlation factor (K_{sp}) is found to be in a range of 1.0 to 1.3. Yang and Wang (2003), proposed a relationship, for SPT set-up with a_p = 2.5mm, R_s =1.2 mm and t_0 = 0.5 mm, in order to convert the central SPCT deformation Δ, to the equivalent uniaxial strain, ε_{eq}. [64]

$$\varepsilon_{eq} = 0.2111 \Delta^2 + 0.3299 \Delta \tag{2.18}$$

For a similar SPT set-up with a_p = 2 mm, R_s =1.25 mm and t_0 = 0.5 mm, similar empirical relationships have been obtained, e.g. equation (2.20), to determine the equivalent uniaxial strain. The relationship is between the equivalent strain at the edge of contact, ε_{eq}, and the total deformation, Δ.[8, 46, 68] i.e.,

$$\varepsilon_{eq} = 0.0044\Delta^3 + 0.09357\Delta^2 + 0.17959\Delta \qquad (2.19)$$

For the same dimensions, a similar empirical relationship between the applied load, P, and the "membrane stress", σ_m, has been obtained, i.e.,

$$P / \sigma_m = 1.72476\Delta - 0.05638\Delta^2 - 0.17688\Delta^3 \qquad (2.20)$$

Many other promising empirical attempts have been obtained to convert the SPCT data to the corresponding uniaxial data, including those reported in Hyde, Stoyanov et al. 2010. Hyde and *et al* at the University of Nottingham have devolved an approximate theoretical model (see Fig. 2-28) to describe the overall behaviour of an SPCT specimen.
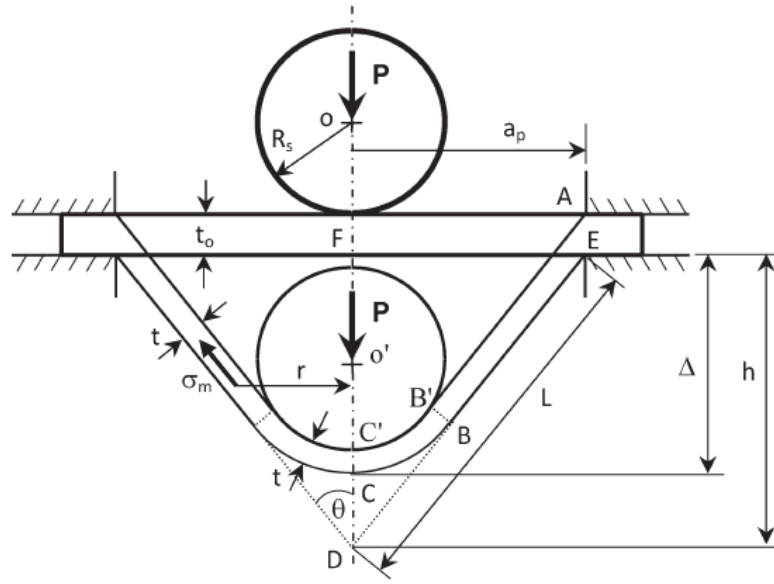
Fig. 2-28: Initial and deformed (assumed uniform thickness) shape of the SPT specimen [67]

This model assumes that the specimen's thickness (t_o) is very small compared to the other dimensions in the experimental set-up. Also, it is assumed that the thickness of the specimen remains constant as the punch test progresses. The general strain level, or the membrane strain, ε_m, in the SPT specimen is given by equation (2.21), while equation (2.22) is an approximate relationship to calculate the change of the angle θ in Fig. 2-28, at each change of the displacement [67].

$$\varepsilon_m = \ln\left[\frac{1}{\sin\theta} - \frac{R_s}{a_P \times \tan\theta} + \frac{R_s}{a_P}\left(\frac{\pi}{2} - \theta\right)\right] \tag{2.21}$$

$$\Delta \approx \frac{a_P\sqrt{1-\sin^2\theta}}{\sin\theta} - \frac{R_s}{\sin\theta} + R_s \tag{2.22}$$

Using a membrane assumption, the membrane stress σ_m can be also estimated using the model shown in Fig. 2-28, [67].

$$\sigma_m = \frac{P}{2\pi r t_0} \frac{\sqrt{1+(1/\tan^2\theta)}}{\cos\theta} \qquad (2.23)$$

Both the "membrane stress" and the correlation factor "K_s" approaches could be used to estimate the equivalent uniaxial stress and strain using the applied load and specimen dimensions. For the purpose of validation, the P91 material has been used to manufacture SPC test specimens with the recommended dimensions and uniaxial creep test specimens. All specimens were creep tested at 650°C, using various stress levels. the SPC tests results and the corresponding uniaxial tests results are plotted in Fig. 2-29. However, it is important to highlight the fact that, up to this point, there is no general agreed method for the interpretation of SPCT data; i.e., there is no universally accepted way of converting the SPC test data to the corresponding uniaxial data [32, 67, 69]
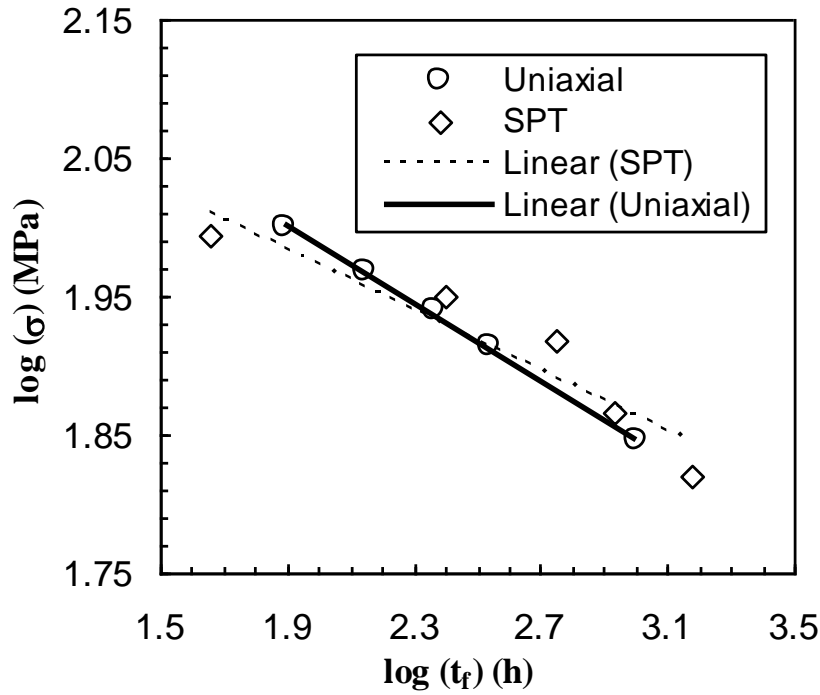
Fig. 2-29:   Converted creep rupture data obtained from a SPT on (Bar-257) P91 steel at 650° C, compared with corresponding uniaxial data [28]

2.4.2.5 Small ring creep test

The small ring test method was proposed by Hyde and Sun, 2009, at the University of Nottingham. This novel creep testing method has been patented by the "United States Patent" on the 12th November 2013 under Patent Number US 8,578,784 B2. The small ring creep test method is used to obtain uniaxial secondary creep data from small samples of material. The small specimen size (see Fig. 2-30), allows it to be constructed, for example, from small scoop samples (see Fig. 2-13), removed from critical parts of power plants [27]. In this section, an analysis of the creep behaviour of small, ring type specimens, and the associated test procedures, are briefly

described. This includes the determination of the conversion factors, which are used in the conversion relationships. The method has been described in detail in [27, 47]. Therefore, only a brief description will be given in this section.
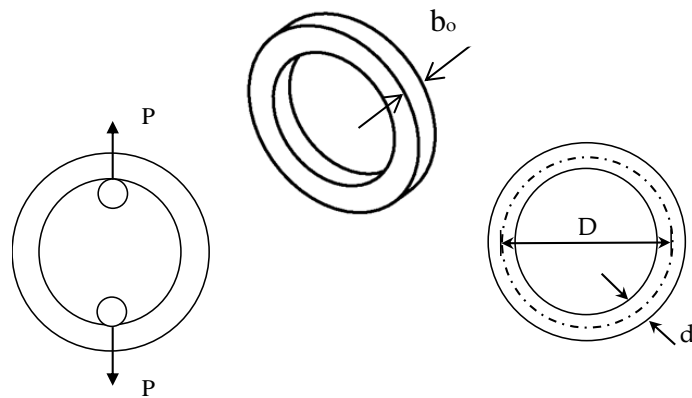
Fig. 2-30: Circular ring creep test specimen loading arrangement and dimensions (D≈5-20 mm; d≈1-2 mm and ring depth (b_o)≈1-2 mm)

Fig. 2-31: Ring specimen test loading application

Small ring specimens (circular or elliptical) are easily loaded through pin connections, as in Fig. 2-31 and the load-line displacement between the two loading pins, are recorded throughout the test duration. The conversion relationship for the small ring testing technique is based on the Reference Stress method; which enables the minimum load-line displacement rates ($\dot{\Delta}_{ss}$) obtained from testing the rings, to be converted to equivalent uniaxial minimum creep strain rates ($\dot{\varepsilon}_{eq}$). Reference Stress parameters (conversion factors), are used to relate (i) the specimen load and dimensions to the corresponding uniaxial stress and (ii) the spacemen load-line displacement rate and dimensions to the corresponding uniaxial strain [47]. Hyde and Sun, 2009 have presented a thin ring (plane stress) analytical solution based on beam theory. Analytical solution for the stationary state "load-line" deformation rate ($\dot{\Delta}_{ss}$) of an elliptical ring, see Fig. 2-32, has been obtained [27]. An analytical conversion relationships also obtained based on the Reference Stress approach, to convert the load-line deformation rate and the applied load (*P*) to the corresponding uniaxial strain rate and Reference Stress, respectively [27, 47]. For an elliptical ring made from a material, obeying the Norton creep law, $\dot{\varepsilon}_{min} = A\sigma^n$, the solution for the load-line displacement rate is given by:-
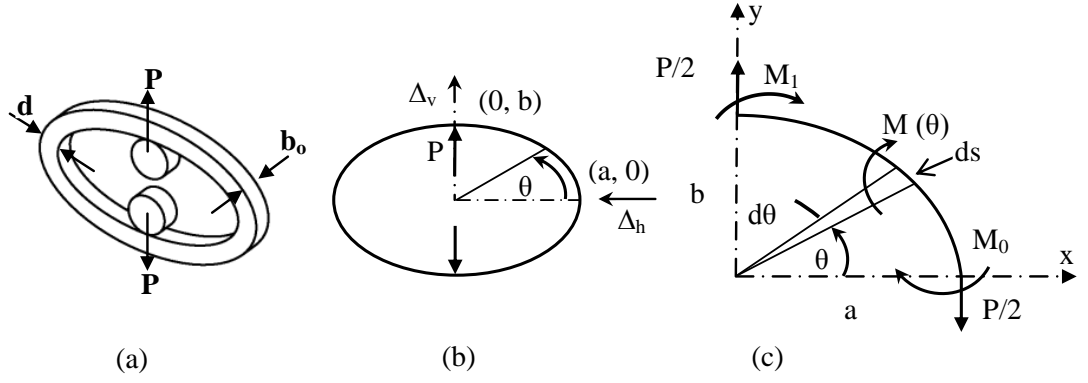
Fig. 2-32: Analytical model of the elliptical ring specimen: (a and b) elliptical ring shape and geometry definition; and (c) free body diagram [27]

$$\dot{\Delta}_{ss} = \frac{2Aab}{(I_n)^n}\left(\frac{Pa}{2}\right)^n Int_2\left(n,\frac{a}{b}\right) \tag{2.24}$$

where $I_n = \int_A y^{1+\frac{1}{n}} dA$ (A is the area and y is the vertical direction (see Fig. 2-32) to the bending axis)

$$Int_2 = -\int_0^{\theta'}\left(\cos\theta - \cos\theta'\right)^n \left(1-\cos\theta\right)\sqrt{\left(\frac{a}{b}\right)^2 \sin^2\theta + \cos^2\theta}\, d\theta + \int_{\theta'}^{\frac{\pi}{2}}\left(\cos\theta' - \cos\theta\right)^n$$

$$\left(1-\cos\theta\right)\sqrt{\left(\frac{a}{b}\right)^2 \sin^2\theta + \cos^2\theta}\, d\theta \tag{2.25}$$

and

$\theta' = \cos^{-1}(1 - \frac{2M_0}{Pa})$, for more details about θ' and M_0 see [27]. M_o is the internal bending moment at $\theta = 0$, as in Fig. 2-32 (c). Therefore, for a rectangular cross-sectioned beam, equation (2.24) can be rewritten as:-

$$\dot{\Delta}_{ss} = \left(\frac{2n+1}{n}\right)^n Int_2\left(n,\frac{a}{b}\right)\frac{4ab}{d}A\left(\frac{Pa}{b_0 d^2}\right)^n \tag{2.26}$$

56

where, n and A are material constants, a and b are the major and minor axes of the ellipse, d and b_0 are the thicknesses in the radial and axial directions, respectively, and P is the applied load [27]. Using Mackenzie's method [25] to determine the Reference Stress, it can be shown that $\sigma_{ref} = \alpha\, \sigma_{nom}$, so that equation (2.26) can be rewritten, giving:-

$$\dot{\Delta}_{ss} = \left(\frac{2n+1}{n}\right)^n \frac{Int_2\left(n, \frac{a}{b}\right)}{\alpha^n} \frac{4ab}{d} A\left(\alpha\, \sigma_{nom}\right)^n \tag{2.27}$$

where, for the ring specimen, $\sigma_{nom} = \frac{Pa}{b_0 d^2}$. The value of α $(= \eta)$ which makes $\left(\frac{2n+1}{n}\right)^n \frac{Int_2\left(n, \frac{a}{b}\right)}{\alpha^n}$ practically independent of the value of n, is the Reference Stress conversion factor (β). This leads to the following expression for the minimum displacement rate:-

$$\dot{\Delta}_{ss} = \beta\, \frac{4ab}{d} A\left(\alpha\, \sigma_{nom}\right)^n \tag{2.28}$$

where β is a constant, which is purely a function of ring dimensions, see [27] for a more detailed derivation of β. The value of the Reference Stress (σ_{ref}) is given by:

$$\sigma_{ref} = \eta\left(\frac{Pa}{b_0 d^2}\right) \tag{2.29}$$

From equation (2.28), the equivalent uniaxial creep strain rate at a Reference Stress (σ_{ref}) can be obtained as follows:

$$\dot{\varepsilon}^c(\sigma_{ref}) = \frac{d}{4\beta ab} \dot{\Delta}_{ss} \tag{2.30}$$

For a circular ring, i.e. (a/b) = 1, the Reference Stress and the equivalent uniaxial creep strain rate, at the Reference Stress, are given by:-

$$\sigma_{ref} = \eta \left(\frac{P R}{b_0 \, d^2} \right)$$ (2.31)

and

$$\dot{\varepsilon}^c (\sigma_{ref}) = \frac{d}{4 \beta R^2} \dot{\Delta}_{ss}$$ (2.32)

where R is the mean ring radius. The theoretically obtained η and β values for a range of major to minor axes, i.e. a/b ratios, is presented in Fig. 2-33. It can be seen that the value of β varies approximately linearly with a/b while the value of η is practically independent of the a/b ratio, [47].
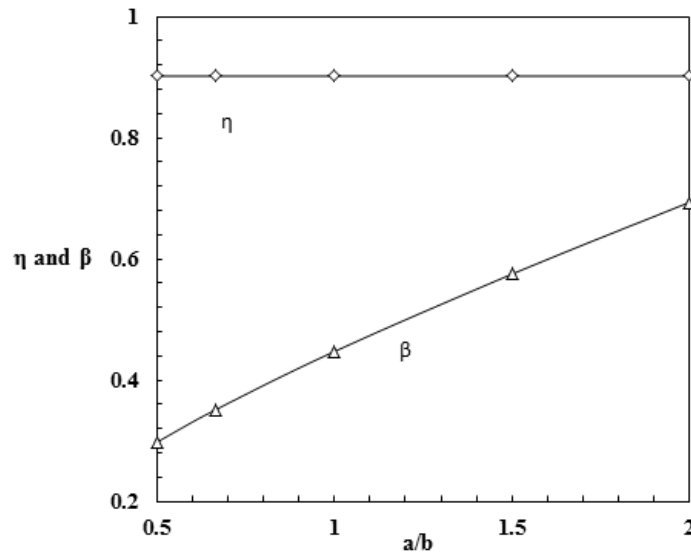
Fig. 2-33:   The variations of the η and β parameters with the a/b ratio [27]

Equations (2.30) and (2.32) give the equivalent gauge length (EGL), for the elliptical and the circular specimens respectively, whereas equations (2.29)

and (2.31) give the equivalent uniaxial stress for the elliptical and the circular specimens, respectively. Also an approximate reference stress and equivalent gauge length for a structure can be obtained from the limit load and the material elastic properties [13], i.e.

$$\sigma_{ref} \approx \frac{P}{P_L} \sigma_y \tag{2.33}$$

where P_L is the limit load (collapse load) for the structure and the σ_y is the yield stress for the structure, and P is the applied load, and

$$EGL \approx \frac{\Delta^e}{(\sigma_{ref} / E)} \tag{2.34}$$

An approximate limit load for a circular ring has been published by Hyde and Sun, 2009, i.e.

$$P_L \approx \frac{b_o\, d^2}{R} \sigma_y \tag{2.35}$$

See [27] for more details about P_L for the ring specimen. From equations (2.35) and (2.33) a definition of the reference stress for the circular ring specimen can be obtained, i.e.

$$\sigma_{ref} \approx \frac{PR}{b_o\, d^2} \tag{2.36}$$

Using the theoretical expression for the circular ring minimum strain rate, i.e., equation (2.28) and the β value for the circular ring specimen, see Fig. 2-33, which is ≈ 0.448, an expression for the circular ring EGL can be obtained

$$EGL = 1.792 \frac{R^2}{d} \qquad\qquad (2.37)$$

Similarly, the EGL for an elliptical specimen with (a/b=2), for example, can be obtained, i.e.

$$EGL = 2.8 \frac{a^2}{d} \qquad\qquad (2.38)$$

For an elliptical ring with $a/b = 2$ and with $a = 10$ mm, $b = 5$mm, $b_o = 2$ mm and $d =$2mm, say, the EGL value is about 140 mm. It is clear that this EGL value is significantly larger than the equivalent gauge length value applicable to the commonly used small specimen types.

The ring specimen testing method has been validated, both numerically and experimentally. FE analyses, using the ABAQUS software [70], were performed (under plane stress conditions). The analysis was carried out using circular ring specimen, with R=10 mm and b_0=1mm, for a number of R/d values. The FE steady state load-line deformation rate, together with the predictions of the deformation rates obtained from the corresponding analytical solutions, are plotted against R/d, in Fig. 2-34. It can be seen that the deformation rates obtained from both methods are practically the same, especially for high R/d ratios, when the effects of the shear deformation on the ring specimen is negligible [27].
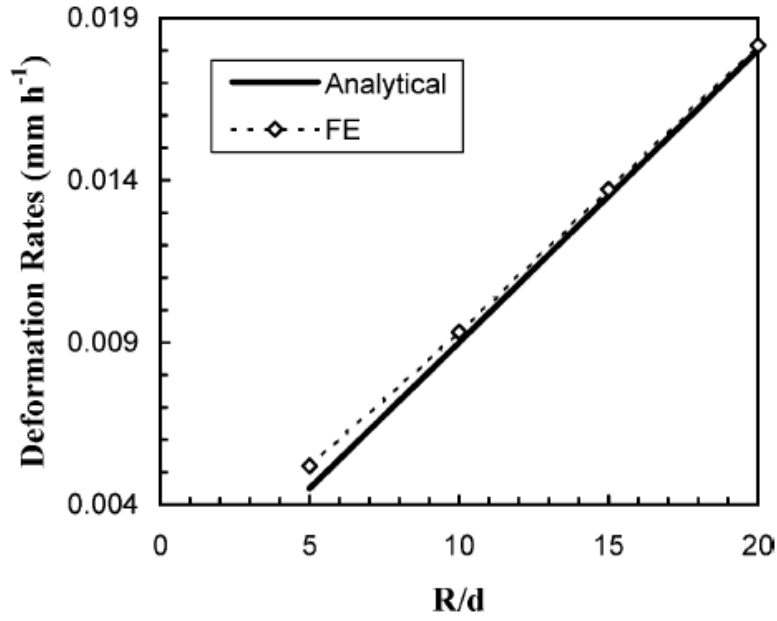
Fig. 2-34: Variation of a circular ring load-line deformation rates under steady-state creep with R/d, for $\sigma_{nom}(=PR/b_0d^2)=100$MPa, obtained from analytical solutions and FE (plane stress with $n=6$ and $A=1\times 10^{-16}$ [27].

Experimental validations were achieved by comparing the minimum creep strain rates obtained from the ring specimens with those obtained from conventional uniaxial creep tests. Conventional uniaxial creep test specimens (see Fig. 2-5), and circular ring specimens were manufactured using a P91 material and creep tested at 650°C. Equation (2.31) has been used to calculate the load for the circular ring specimens based on the ring dimensions and the corresponding uniaxial stress. Equation (2.32) has been used to convert the rings minimum deformation rates to equivalent uniaxial minimum strain rates. The minimum creep strain rates obtained from the uniaxial and ring creep test specimens are plotted together in Fig. 2-35. A remarkably good agreement, between the two sets of data, is found.
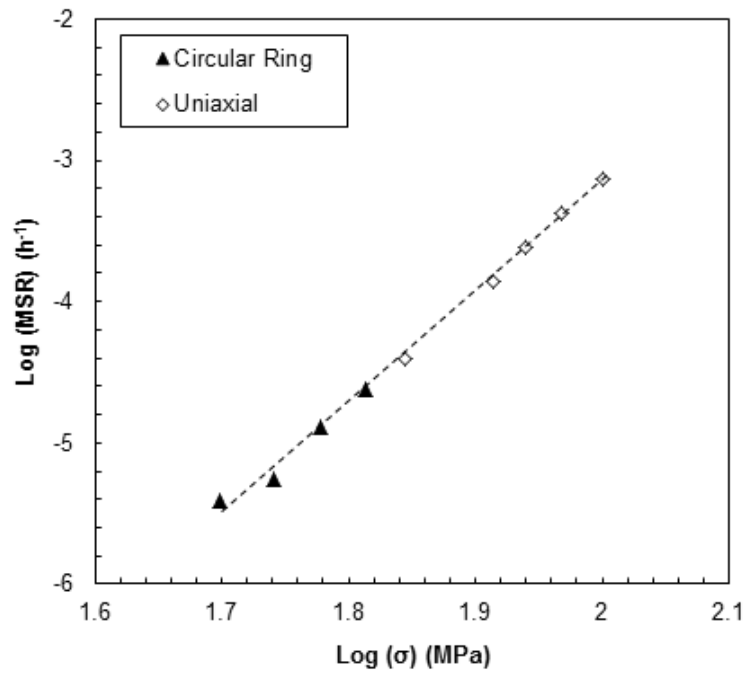
Fig. 2-35:   Minimum creep strain rate (MSR) data for (Bar-257) P91 steel obtained from uniaxial and circular ring creep tests at 650°C [27]

Ring specimens are easily machined and loaded, compared with conventional specimens. For the ring specimen, creep deformation is relatively large compared to the specimen dimensions, which makes the effect of the small thermal deformation on the test result is insignificant [47]. Unlike impression creep testing, the ring testing method can be used for a wide range of materials, including those with high creep strength, i.e. with similar creep strength to the loading pins. The experimental set-up, and the aligning procedures used are simple to perform. The specimen's surface finishing is not critical because the ring specimens are designed to obtain only steady state creep strain rate data, not creep rupture data. Furthermore, the equivalent gauge length for ring specimens is significantly higher than

all other commonly used small specimen creep testing techniques, see equations (2.38) and (2.37); which allows easily measurable strains to be obtained [27].

2.5   HIGH TEMPERATURE MATERIALS

In recent decades, power plant operating temperatures and/or stresses have increased significantly, in order to meet energy needs. Therefore, engineering components within the power plants have had to be more creep and corrosion resistant, in order to withstand these more severe working conditions [71]. In addition, the very high maintenance and replacement costs of these components make it necessary for them to be constructed from high creep and corrosion resistance materials. Unscheduled interruptions to power plants working plan, normally result in high costs for the operating companies .Therefore, the power plants are normally designed to have a relatively long lifespan. For all these reasons the useable material creep and corrosion resistance is a key point of the chosen material criteria [71, 72]. Furthermore, most aero engine parts, chemical plant components and oil refinery components, are very safety critical engineering components and are designed to be reliable with high operating safety factors. All these requirements have to be carefully considered by designers in order to avoid catastrophic failures in these components. Therefore, modifications to the

alloying compositions of the existing, in use, high temperature materials

become necessary [73]. A commonly used material in aero engine

applications is the Nickel-Base Superalloy "INCONEL". There are various

versions of this material with slight differences in alloy compositions, i.e.

600, 617, 625, 718 and X-750. One of the most commonly used versions is the

Inconel 718 which has been widely used in aerospace industry; the Inconel

718 chemical composition is given in Table 2-3.[74, 75]

Table 2-3:   Chemical compositions of Inconels 718 (weight %) [75]

N_i+C_o	Cr	Fe	$Nb+T_a$	M_o	S_i	Al	c	M_n	T_i	S	P	B
50	17	Bal.	5.5	1.0	0.35	0.7	0.02	0.35	1.15	0.015	0.015	0.002

In general, the Inconel Superalloy is used to manufacture some aeroplane

engine parts, petrochemical and nuclear reactor parts. The material has very

good creep resistance and high corrosion and oxidation resistance with a

wide range of temperatures [74, 76]. However, in many other high

temperature applications, less creep resistant materials can be used, such as

P91 and P92 [77, 78]. These materials are widely used in power plants pipe-

work, oil refinery pipe-work and in nuclear reactors cooling systems.

Generally, in the design of such components, the weight of the components

is not a major factor in the component design (as would be the case when

designing an aeroplane engine). The P91 material is a modified version of

(9Cr 1M$_o$ steel) material; it has high allowable stress, which enables engineers to design pipes and tubes with thinner wall thickness. Thinner pipes and tubes store less thermal energy and, hence, are subjected to lower thermal stresses [79]; the P91 material chemical composition presented in Table 2-4. The P92 material [3, 79] and [80]. was made by substituting Molybdenum (*Mo*), in P91 material, by tungsten (*W*). The P92 material has good steam corrosion resistance and excellent creep properties and low thermal expansion. However, P92 is a relatively new material for use in manufacturing boiler components of supercritical and ultra-supercritical power stations; the chemical composition for P92 material is given in Table 2-5, [3, 79] and [80].

Table 2-4:   Limits of the chemical composition of P91 (weight %) [79]

	C	*Mn*	*P*	*S*	*Si*	*Cr*	*W*	*Mo*	*V*	*Nb*	*N*	*B*	*Al*	*Ni*
Min%	0.08	0.3	-	-	0.2	8	-	0.85	0.18	0.06	0.03	-	-	-
Max%	0.12	0.6	0.02	0.01	0.5	9.5	-	1.05	0.25	.1	0.07	-	0.04	0.4

Table 2-5: Limits of the chemical composition of P92 (weight %)[79] and [80].

	C	*Mn*	*P*	*S*	*Si*	*Cr*	*W*	*Mo*	*V*	*Nb*	*N*	*B*	*Al*	*Ni*
Min%	0.07	0.3	-	-	-	8.5	1.5	0.3	0.15	0.04	0.03	0.001	-	-
Max%	0.13	0.6	0.02	0.01	0.5	9.5	2	0.6	0.25	0.09	0.07	0.006	0.04	0.4

2.6   MATERIAL BEHAVIOUR MODELS

Many material behaviour models have been developed over time to describe material deformation under creep condition. Penny and Marriott have presented some of the material behaviour models in their Book [13], some of the models describe the creep deformation as functions of stress such as:-

Norton $$f_1(\sigma) = A\sigma^n \tag{2.39}$$

Soderberg $$f_1(\sigma) = A_2 \left\{ \exp\left(\frac{\sigma}{\sigma_0}\right) - 1 \right\} \tag{2.40}$$

Mc Vetty $$f_1(\sigma) = A_3 \sinh\left(\frac{\sigma}{\sigma_0}\right) \tag{2.41}$$

while others describe the creep deformation as functions of temperature, i.e.

Andrade $$f_2(t) = \left(1 + n_1 t^{\frac{1}{3}}\right) \exp(n_2 t) - 1 \tag{2.42}$$

Bailey $$f_2(t) = H_1 t^{n_1} \tag{2.43}$$

Mc Vetty $$f_2(t) = H_1\left(1 - e^{-n_1 t}\right) + H_2 t \tag{2.44}$$

The stress function models are commonly used to study creep deformation and failure. The most widely used constitutive equation is the Norton power law relationship, between the creep strain rates of primary and steady-state creep and the applied stresses, i.e. equation (2.39) where A and n are material constants [13].

2.6.1 Kachanov model

The constitutive damage equations proposed by Kachanov, i.e., equation (2.45) and (2.46) are commonly used to describe creep deformation and failure in the components. In these two equations Kachanov introduced a damage parameter, ω, to represent the creep damage in the material.

$$\frac{d\varepsilon_{ij}^c}{dt} = \frac{3}{2} A \left(\frac{\sigma_{eq}}{1-\omega} \right)^n \frac{S_{ij}}{\sigma_{eq}} t^m \tag{2.45}$$

$$\frac{d\omega}{dt} = B \frac{(\sigma_r)^{\chi}}{(1-\omega)^{\phi}} t^m \tag{2.46}$$

where

$$\sigma_r = \alpha\sigma_1 + (1-\alpha)\sigma_{eq} \tag{2.47}$$

in which t is the time, ε_{ij}^c is multiaxial creep strain components, S_{ij} is the deviatoric stress component, ω is the damage parameter, where $0 < \omega < 1$. Also, σ_{eq}, σ_1 and σ_r are the equivalent (von-Mises), maximum principal and rupture stresses, respectively. A, n, B, χ, ϕ, m are material constants and α is the multiaxial stress state parameter. The constant α is normally obtained by comparing the failure times of the FE analyses for a notched bar specimen using a variety of α values with the experiment failure time for the notched specimen. The rupture stress, i.e., equation (2.47) is a function of the equivalent stress σ_{eq}, the maximum principal stress σ_1 and the multiaxial rupture parameter α [81].

The material constants can be obtained by curve fitting to the uniaxial creep curves; the determination of the material constants will be explained in Section (2-7) [43]. For the uniaxial conditions $\frac{S_{ij}}{\sigma_{eq}} = 1$ in equation (2.45) and $\sigma_r = \sigma_{eq}$ in equation (2.46) . Integration of equation (2.46) between the limits $\omega = 0$ (no damage) and $\omega = 1$ (failure), under uniaxial conditions stress, leads to an expression for the uniaxial failure time as follows:-

$$t_f = \left[\frac{m+1}{B(1+\phi)\sigma^{\chi}} \right]^{\frac{1}{m+1}} \tag{2.48}$$

Similarly, the uniaxial creep strain versus time relationship can be obtained, i.e.

$$\varepsilon^c = \frac{A\sigma^{(n-\chi)}}{B(n-\phi-1)} \left(\left[1 - \frac{B(1+\phi)\sigma^{\chi} t^{m+1}}{m+1} \right]^{\frac{\phi+1-n}{\phi+1}} - 1 \right) \tag{2.49}$$

However, for FE rupture analyses using Kachanov model, the analyses may be difficult to converge. As can be seen from the constitutive equations (2.45) and (2.46) there is an inverse dependency on (1-ω) for creep strain and damage rates. Therefore, as ω approaches unity, the strain/damage rates approach infinity [40]. As a result, the computing time increases significantly, and the analyses terminate without converging. In order to avoid the very high damage and strain rates, which occur with the Kachanov model, other material behaviour models are needed [82].

2.6.2   Liu-Murakami model

Unlike the Kachanov model, the Liu-Murakami damage model addresses the issue of the very high damage/strain rates which occur as the damage parameter ω approaches unity [11, 41]. The Liu-Murakami model can be used to represent primary, secondary and tertiary multiaxial creep deformations. This model also consists of a pair of coupled creep/damage equations, i.e.

$$\frac{d\varepsilon_{ij}^{c}}{dt} = \frac{3}{2} A\sigma_{eq}^{n-1} S_{ij} Exp\left[\frac{2(n+1)}{\pi\sqrt{1+3/n}}\left(\frac{\sigma_{1}}{\sigma_{eq}}\right)^{2} \omega^{3/2}\right] \tag{2.50}$$

$$\frac{d\omega}{dt} = \frac{M[1-Exp(-q_{2})]}{q_{2}}(\sigma_{r})^{\chi} Exp(q_{2}\omega) \tag{2.51}$$

As with the Kachanov model, the rupture stress σ_{r}, can be represented by equation (2.47). Integration of equation (2.51), under uniaxial conditions, leads to:-

$$\omega = -\frac{1}{q_{2}} Ln\left[1-\left(1-e^{-q_{2}}\right)\frac{t}{t_{f}}\right] \tag{2.52}$$

Also, creep strain increments, for the uniaxial case, can be calculated using the following relationship:-

$$\Delta\varepsilon^{c} = A\sigma^{n} Exp\left[\frac{2(n+1)}{\pi\sqrt{1+3/n}}\omega^{3/2}\right]\Delta t \tag{2.53}$$

where

$$t_{f} = \frac{1}{M\sigma^{\chi}} \tag{2.54}$$

69

As in the Kachanov model, the material constants A, n, M, χ and q_2 it can be obtained by curve fitting to the uniaxial creep curves [83].

2.7   DETERMINATION OF MATERIAL PROPERTIES

In order to predict the deformation of components which are undergoing creep, the material creep constants for the components must be known and precisely determined [84]. Material constants of high temperature materials change over time, especially when they are exposed to extremely high temperatures and/or stresses. Therefore, the creep properties of these materials used in the power plants, for example, have been a major concern to material scientists and engineers, for many years. Accurate determination of material creep properties, together with appropriate material behaviour models, can give a very close estimation to the components creep deformation and failure [85].

Most material constants mentioned in Section 2.6, can be obtained experimentally. The constants A and n in Norton's law are temperature dependent; together they control the secondary creep strain rate. They can be obtained by plotting the uniaxial minimum creep strain rates against the applied stresses (log-log scale). The constants B, χ and ϕ, control failure through controlling the acceleration of the tertiary creep strain rate, and they

can be obtained from curve fitting to the experimental strain-time curves [40]. The multiaxial stress state parameter α lies between 0 and 1; it determines the value of the rupture stress, by quantifying the contribution of the maximum principal stress and equivalent von Mises stress. The multiaxial stress state parameter α can be obtained by comparing the results of notched bar specimens test results and FE notched bar analyses results. By modifying the α value in the FE analyses until the FE analyses failure time correspond to the experiment failure time, this α value can be taken as the correct α value for the material [40, 86]. Tanner *et al* [74] have obtained the Inconal 718, P91 and P92 material constants for damage constitutive equations [40, 74]; the constants are reported in Table 2-6, Table 2-7 and Table 2-8

Table 2-6: The (Bar-257) P91 steel constants for damage models at 650°C (σ in MPa and time in hour) [40].

Material	A	n	m	B	ϕ	χ	α	q_2
PM	1.092×10^{-20}	8.462	-4.754×10^{-4}	3.537×10^{-17}	7.346	6.789	0.3125	3.2
WM	1.370×10^{-20}	7.65	-0.0361	1.600×10^{-20}	11.463	7.950	0.59	5.0
HAZ	2.300×10^{-20}	8.462	0	1.522×10^{-14}	7.346	5.502	0.75	2.8

Table 2-7: The P92 Material constants for damage constitutive equations at 675°C (σ in MPa and time in hour) [3].

Material	A	n	m	B	ϕ	χ	α	q_2
PM	4.335×10^{-20}	7.659	0.0	3.377×10^{-17}	8.3	6.459	0.383	3.0
WM	1.065×10^{-17}	6.485	0.0	1.499×10^{-15}	7.5	5.671	0.187	3.0

Table 2-8: The Inconal 718 material creep damage constants for Kachanov model, at 620°C, (σ in MPa and time in hour) [72, 74].

Material	A	n	m	B	ϕ	χ	α
PM	2.037×10^{-61}	19.300	0.0	4.322×10^{-47}	12.0	14.728	0.1
WM	5.260×10^{-56}	17.984	0.0	2.623×10^{-50}	4.0	16.367	0.2

2.8 CREEP IN WELDS

For many years; the welded regions in components operating in the creep range have been a major concern for designers [87]. The welded regions are often considered to be the weakest regions in components. The weld region consists of three different materials, i.e. parent material (PM), weld metal (WM) and heat-affected zone (HAZ). The three materials in the weld regions have different microstructures, (see Fig. 2-36), different grains sizes, and different creep strengths and therefore the three materials creep at different rates [88]. The HAZ can also be divided into three sub-zones, i.e. fine grained (FG) HAZ, coarse grained (CG) HAZ and intercritical HAZ as shown in Fig. 2-36. The recrystallization of the material in the HAZ is dependent on the welding temperature, weld speed, the cooling and the solidification rates and the properties of the welded material [89]. The recrystallization in the HAZ is usually accompanied by an increase in the ductility, reduction in the hardness and of the creep strength of the material [89, 90].

The size of the HAZ and the WM manly depend on the welding method used to weld the joint. Generally arc welding have relatively large HAZ and WM zones, whereas laser or electron beam welding results in relatively narrow HAZ and WM regions, compared to the overall specimen dimensions [91, 92]. Normally the application of the welded joints determines the type of weld which should be used. Different types of creep test specimens have been developed to obtain creep properties from the weld. One of the main uses of the recently developed small specimen creep testing techniques is to examine the creep strength and to determine the creep properties in weld regions [32].
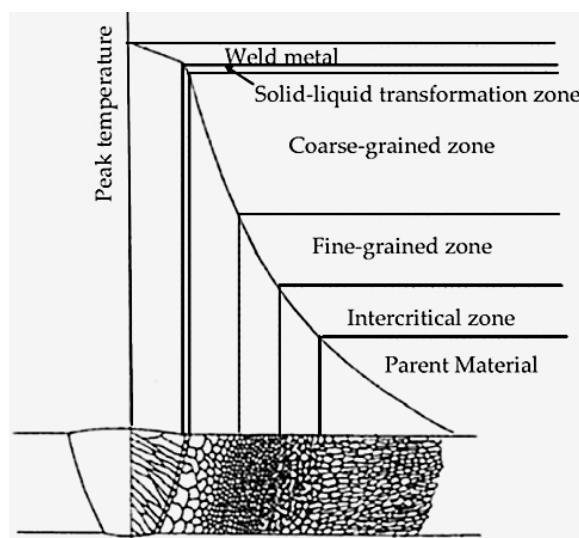
Fig. 2-36: Diagram of the cross section of a weld, showing typical microstructural zones [88].

2.9   SUMMARY AND CONCLUSION

The majority of creep testing techniques and their associated specimens (full size and the small size) specimens have been briefly covered in the literature review. It has been found that, the full size creep test specimens are capable of providing the full set of material creep constants for any material behaviour models. However, as mentioned in Section 2.4.2, in some circumstances, full size specimens are unpractical to be used, because of insufficient volume of material available for testing. In such situations, the small specimens testing play a vital role in determining the creep properties and for assessing the creep strength of the material.

It is also noticeable from this literature review that the secondary creep region (steady state region) has been described reasonably well by the existing small testing techniques (Impression and small ring) creep tests. However, the tertiary creep properties and the time to failure have not been successfully represented by existing small specimen creep testing techniques, despite the extensive efforts and the continued attempts using the SPCT to solve the problem. Therefore, a major part of the work presented in this thesis is related to research in order to obtain creep properties using small specimens. This thesis contains further development of the existing small ring creep test method, in order for the ring specimen to be able to

accommodate various shapes of the small samples. This thesis also contains a

new small specimen testing technique which is capable of obtaining the full

creep curve up to rupture.

CHAPTER 3.

DEVELOPMENT OF SMALL RING CREEP TESTS SPECIMEN
_____

3.1   INTRODUCTION

This chapter describes new aspects and further development of the work done by Hyde and Sun (2009) for the small ring creep testing method [27, 47]. The small ring creep test can be used to generate approximately uniaxial secondary creep strain rate data from small samples of material. The technique which is used is based on the reference stress method; it enables the load-line displacement rates, obtained from ring tests, to be converted to equivalent uniaxial creep strain rates. The method has been detailed in [27, 47] and therefore only a brief description will be given in this chapter. In effect, the analytical solution presented by Hyde and Sun, neglects the contribution that shear deformations make to the ring deformation. Also, it neglects the effect of the axial length, b_o, of the ring on the ring deformation and thus the reference stress parameters β and η.

 In this chapter the effects of shear deformation and the axial length, b_o, on the reference stress parameters β and η, have been studied using FE analyses. In previously published work, a/b is either 1 (circular) or 2 (elliptical) with a/d

= 5 and b_o/d = 1[27]. In some circumstances, it may be convenient to use rings with a/b and b_o/d which are not closely related to the published thin ring geometries. Also, the testing of specimens with higher and lower ellipse ratios (a/b) may be advantageous. Therefore, the finite element (FE) method has been used to obtain the variations of the conversion factors, η and β, with b_o/d and a/d, for a range of a/b ratios. The applicability of the η and β values obtained from the thin ring plane stress, plane strain and 3D analyses are also assessed. Accurate conversion relationships and reference stress parameters are required, in order to ensure that accurate creep properties are obtained. A comparison of experimental results, obtained from small ring creep tests, with corresponding uniaxial creep test data also have been made, using Inconel 738 (Nickel-based Superalloy) parent material at 800°C and P91 parent material at 650°C. Conclusions about the practical implacability of the work are provided in the last section of this chapter.

3.2   FINITE ELEMENT ANALYSES

3.2.1   Scope of investigation

The analytical solution for the ring specimen presented in Chapter 2 does not include the contribution that shear deformation makes to the overall deformation [27] and hence it does not include the effect that shear deformation has on the conversion factors, η and β. In order to assess the

effect, a series of elastic-creep finite element analyses, using Norton's creep law, have been performed using a range of a/d, b_0/d and a/b values. Under steady-state conditions, the stresses and deformation rates are independent of time. From the results of the finite element analyses, the variations of the conversion factors with the geometric parameters (a/d, b_0/d, and a/b) have been obtained. A limited study was also carried out, to assess the effects of the small geometry changes on the ring deformation behaviour. The ABAQUS finite element software package [70] was used for the FE investigations.

3.2.2 Geometries, meshes and boundary conditions

The two extremes of behaviour, i.e. plane stress and plane strain, were investigated using meshes consisting of 8-noded, plane stress, PS, and 8-noded, plane strain, PE, elements, respectively. The intermediate behaviour was investigated using 3D meshes which consist of 20-noded brick elements. Limited mesh sensitivity study was carried out in order to determine the mesh size used for the study. Because of the symmetry, it was only necessary to model one quarter of the ring and one half of the ring thickness for the 3D case; typical FE meshes are shown in Fig. 3-1. The boundary conditions, $u_x = 0$ on plane A, $u_y = 0$ on plane B, and $u_z = 0$ on plane C, are also indicated in Fig. 3-1.

It was reasonable to use rigid elements to model the loading pin, because (i) the loading fixture is normally made from a materials which has a much higher creep resistance than the tested material and (ii) the loading pin stiffness is much higher than the ring, because normally the diameter of the loading pin is much larger than the ring thickness, d, i.e. $D/d \geq 2.5$, where D is the loading pin diameter. Therefore, the small deformation in the loading pin during the creep deformation has been neglected. Reduced integration elements were employed in the analyses, because the finite element (FE) method calculates the element stiffness matrix and then inverts it to find the displacements in the nodes and then calculates the strains and stresses in the element. For complicated finite element problems, when using high order elements (quadratic), it becomes necessary to use numerical integration within the elements to calculate the stiffness matrix.

Reduced integration uses a lesser number of points within the elements when computing the integrals (solving the integral). Clearly, the more integrations points used for each element, the more accurate the solution will be, but this has to be weighed up against the cost of the computation time. Displacement-based FE formulations always over-estimate the stiffness matrix and the use of fewer integration points should produce a less stiff

element. Therefore, in some cases, particularly in non-linear problems such as creep, it is actually advisable to use reduced integration instead of full integration. The slight loss of accuracy is counteracted by the improvement in the approximation of real-life behaviour.
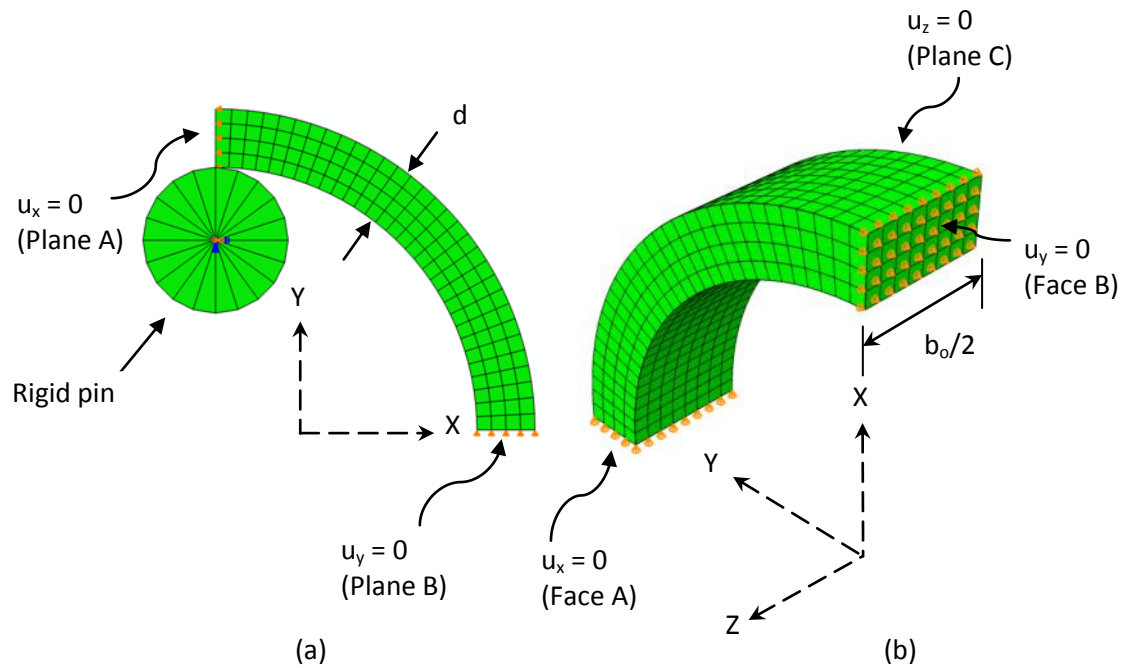
Fig. 3-1:   Typical finite element meshes used for (a) PS and PE cases and (b) 3-D cases

3.2.3   Elliptical ring geometries

Two methods have been used to create the elliptical ring geometry in the FE analyses (see Fig. 3-2 (*a*) and (*b*)). The simplest method is to create two concentric-ellipses (see Fig. 3-3 (a)); this results in a variable thickness, *d*, in the elliptical ring. The thicknesses are the same (i.e. the required *d*-value) at the positions of the major and minor axes. An alternative method, which

produces a uniform thickness, *d,* is the "offset-ellipses" method which is created using an ellipse as the mid-thickness geometry. The inside and the outside surfaces are then traced out by the position of the centre of a pin of diameter, *d*, which is imagined to be rolled around the mid-thickness ellipses, as illustrated in Fig. 3-3 (b, c).

(a)　　　　　　　　　　　　　　　　(b)
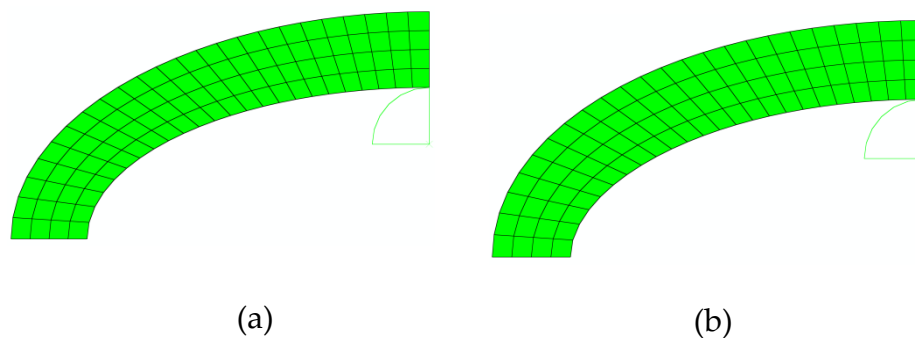
Fig. 3-2:　Example of FE meshes for Elliptical rings , Concentric-ellipses with a variable thickness, *d,* (a), Offset-ellipses with a constant thickness, *d,* (b).
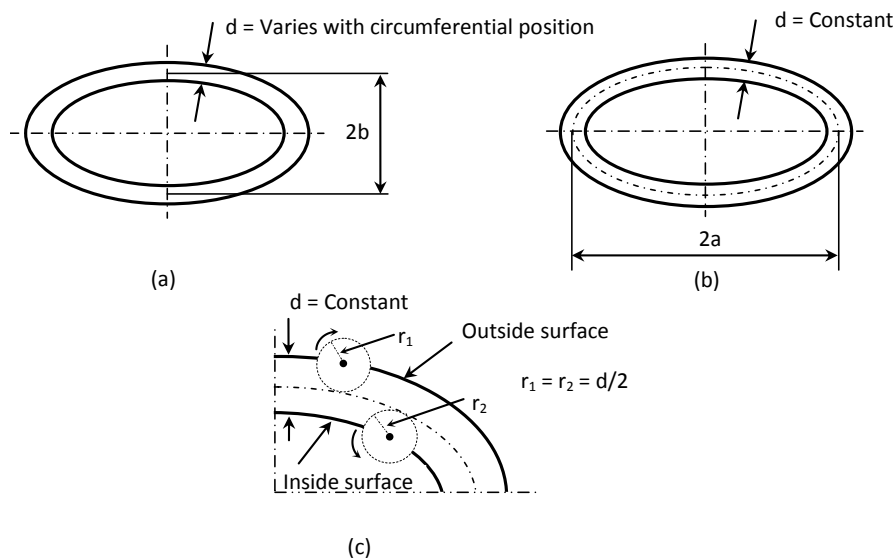
Fig. 3-3:　Elliptical ring geometries, Concentric-ellipses (a), Offset-ellipses(b) and The method used to define the offset-ellipse geometry(c)

3.3   MATERIAL BEHAVIOUR MODEL AND RING GEOMETRIES USED FOR THE ANALYSES

For the FE analyses Norton material behaviour model, i.e.

$$\dot{\varepsilon}^c = B\sigma^n t^{\mathrm{m}} \tag{3.1}$$

was used in all of the calculations performed, where $\dot{\varepsilon}^c$ and σ are minimum creep strain rate and the applied stress respectively, B, n and m are temperature dependent material constants, which can be obtained by curve fitting from experimental results[13]. Equation (3.1) can model just the primary and the secondary creep reigns and shows that the relationship between stress and strain is a power-law. In the primary creep stage, the strain rate decreases monotonically with time (hardening process); the n parameter in equation (3.1) is usually greater than 1, while m<1. When m is equal to zero the model used to describe the secondary creep region. The model is widely used for the description of steady state creep of metals and alloys, because of its simplicity and accuracy compared with other creep models. However, Norton's model is limited to the primary and secondary creep therefore, it is unable to model the entire creep curve till rupture.

In all calculations, the a-value was kept constant with a nominal value of 10mm; note that when the results are normalised, the a-value chosen is

unimportant. Analyses were performed with a/b = 0.5, 0.66, 1, 1.5 and 2, for d-values of 0.5, 1.0, 1.5, and 2.0 mm. As with the dimensions used in the analyses, the actual value of B used is not important because the results have been normalised. FE results were obtained for n-values, in the range 1 to 10. The stress / strain contours and the deformed shape of the circular ring specimen, i.e. a/b=1, under the steady state creep is show in Fig. 3-4. It is necessary to use a range of n-values in order to determine the specific value of α', which makes the log(β') value, i.e., $log\left[\dfrac{\Delta_V}{\frac{4ab}{d}B\left(\alpha'\frac{Pa}{b_0\,d^2}\right)^n}\right]$ practically independent of the n-values used. This specific α'-value, which produces a horizontal line in Fig. 3-5 (the $\log\beta' - n$ plot) is equal to the required η-value. The procedure is described in detail in [5]. The value of $\log\ (\beta')$ can be obtained from the intercept between fitted line and the $\log\ (\beta')$ axis.
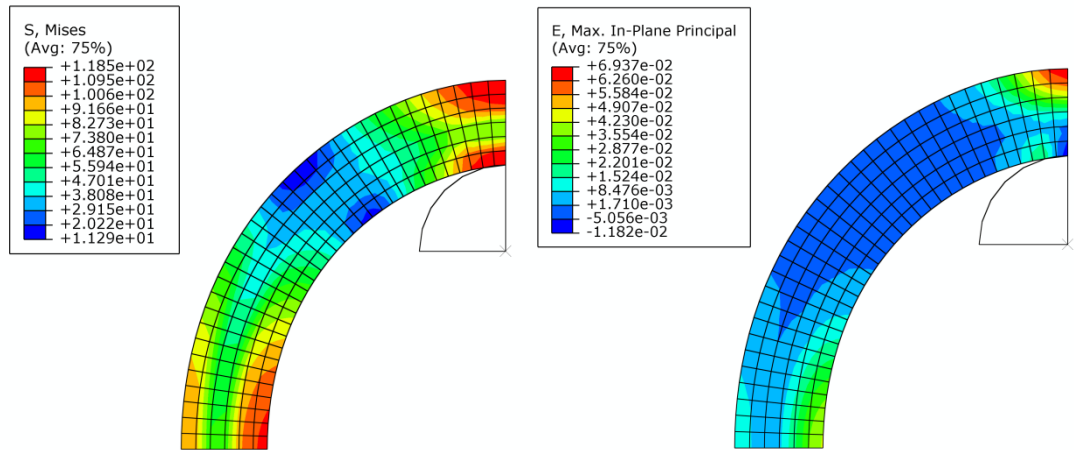
Fig. 3-4:   Stress and strain contours for the circular ring specimen, with R=10mm and d=2mm, under the steady state creep.
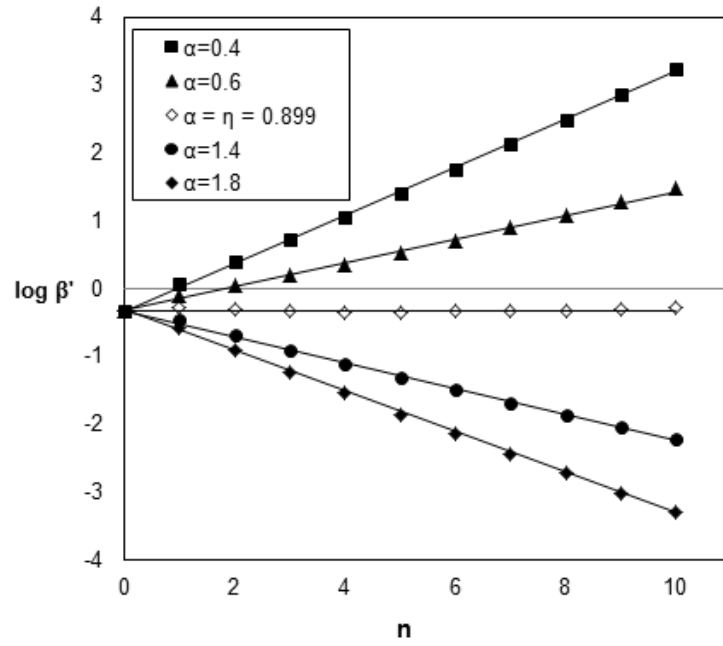
Fig. 3-5:   Determination of β and η values, for a ring specimen with $d=1$, $a/b=1$ and $a/d=10$

3.4   RESULTS OF THEORETICAL AND FE INVESTIGATIONS

3.4.1   Differences between the η and β values obtained with "concentric-ellipses" and "offset-ellipses" geometries

Depending on whether the ellipse geometry is created using "concentric" or "offset" ellipses, the relative thicknesses will be different at different angular positions, θ (see Fig. 2-32). Hence the η and β values will be different. The variations of the η and β values with d/a, under plane stress conditions, for the two ellipse geometry types, with a range of ellipticity ratios, a/b, are shown in Fig. 3-6. The β values obtained for the concentric-ellipses see Fig. 3-3 (a), are found to be slightly higher than the values obtained from the

offset-ellipses, see Fig. 3-3 (b), for all a/b ratios examined, except for the circular ring, where $a/b = 1$. These differences can be related to the fact that concentric-ellipses have non-uniform thicknesses, especially when $a/b \leq 0.66$ and $a/b \geq 1.5$. As a consequence of the slightly lower cross-section area, i.e. $d \times b_0$, the displacement rates are greater, when compared with those obtained with offset-ellipses, for the same a/b and d/a values. Therefore, the β values for the "concentric-ellipses" are greater than the corresponding values for the "offset-ellipses", as can be seen in Fig. 3-6. However, the η values are practically independent of the modelling procedure, and result in η value of about 0.9 for all of the a/b and d/a ratios used in this study, for both of the geometry modelling types.
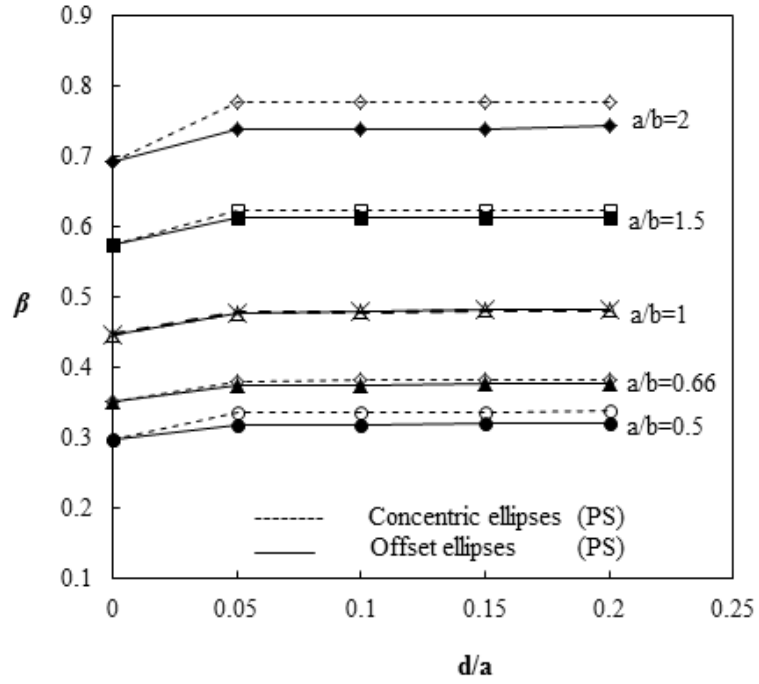
Fig. 3-6: Comparison of the β values obtained for offset-ellipses with those obtained for concentric-ellipses

3.5 EFFECTS OF DIMENSION RATIOS ON THE CONVERSION FACTORS VALUES FOR CIRCULAR SPECIMENS

3.5.1 Effect of b_o/d ratio on the η and β values

The FE analyses were carried out using plane stress, plane strain and 3D models, with offset-ellipse geometries, to assess the effect of the b_o/d ratio on the β and η values. Various ring depth (b_o) were used, while all other ring dimensions were kept constant for the analyses. The 3D specimen model dimensions are shown in Fig. 3-1, where the values for b_o, in the 3D analyses, were taken to be 0.25 to 40 mm. The results, Fig. 3-7 and Fig. 3-8, show that under plane stress conditions, where b_o is very small, i.e., close to zero, β and

η have the highest values, which are 0.482 and 0.91, respectively. Under

plane strain conditions, where b_o is large i.e. the b_o/d ratio is effectively

infinite, β and η have the lowest values, which are 0.415 and 0.79,

respectively. The β and η values obtained from the 3D analyses varied

between those obtained from the plane stress and the plane strain conditions,

i.e. as b_o decreases, (see Fig. 3-9 (a)) the values of β and η become very close to

those obtained for plane stress conditions, whilst as b_o increases, (see Fig. 3-9

(b))the β and η values become practically constant, being nearly equal to the

values obtained for plane strain conditions.
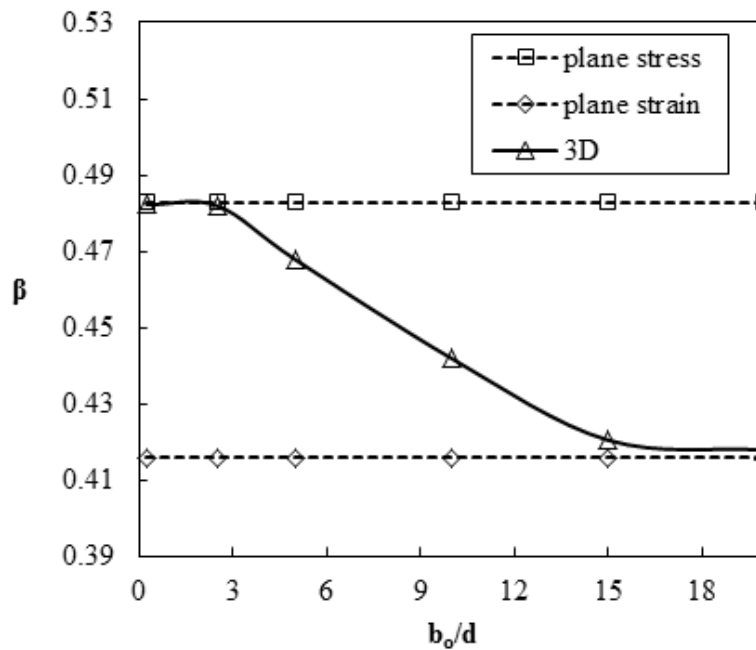
Fig. 3-7:   The values of β for plane stress, plane strain and 3D analyses, for circular
specimens with d=2 mm, and various b_o/d ratios
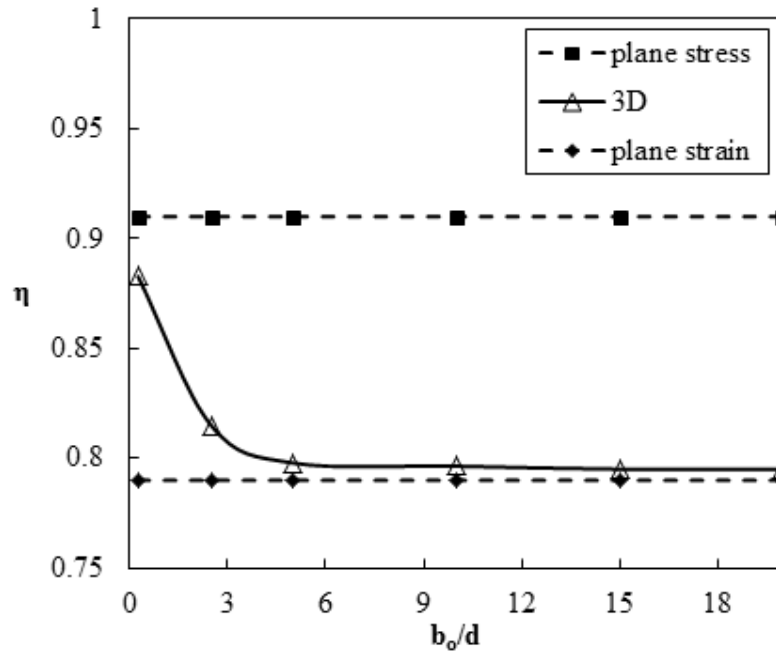
Fig. 3-8:   The values of η for plane stress plane strain and 3D analyses, for circular specimens with d=2 mm, and various b_o/d ratios

(a)   (b)
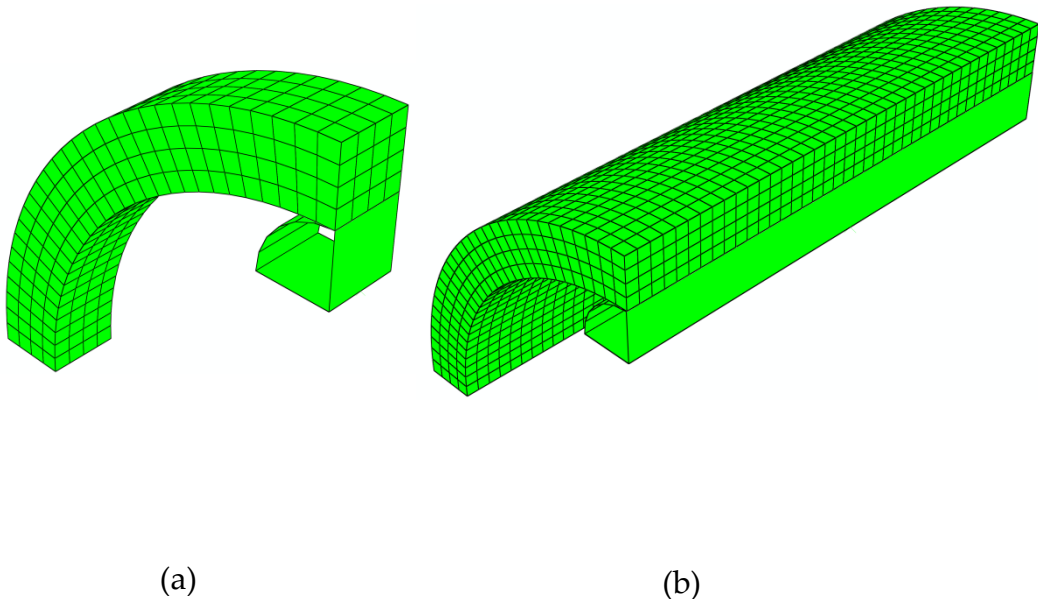
Fig. 3-9: Typical 3-D finite element meshes for the circular ring specimen with R=10mm, d=2mm and b_o=2mm (a) and with R=10mm, d=2 and b_o=20mm (b)

3.5.2 Effect of d/a on the conversion factors η and β

Plane stress analyses were carried out in order to study the effects of the d/a ratio, for offset-ellipse geometries, on the β and η values, with various a/b ratios. The analyses show that for all of the a/b ratios used, the β values increase slightly as the d/a ratio increases, as shown in Fig. 3-10. Moreover, it can be seen that, the β values vary approximately linearly with d/a for all a/b ratios. This indicates that when the ring thickness, d, is close to zero (represented by the theoretical solution) the effects of shear deformation are negligible, and the β value is low for all a/b ratios used; β gradually increases as the d/a ratios increases. In contrast, the η values were found to be practically constant, being around 0.9 for all ring geometries analysed. The results show that the effects of shear deformation on the β and η values, for all d/a ratios in the range d/a = 0.05 to 0.20, and for all a/b ratios in the range a/b = 0.5 to a/b = 2.0, are very small. Therefore, for practical purposes the effects of shear deformation can be neglected, as shown in Fig. 3-10.
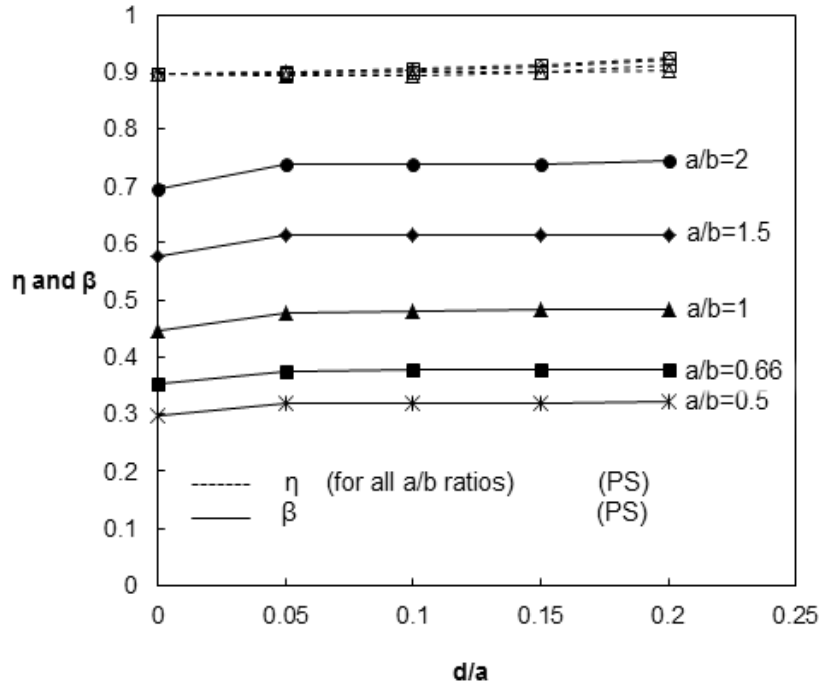
Fig. 3-10:   The effects of *d/a* on *β* and *η* values, for various *a/b* ratios

3.6   TRANSVERSE DEFORMATIONS

Deformations occur during a ring specimen test, in particular the measured load-line displacement, $\dot{\Delta}_V$, is accompanied by the transverse displacement, $\dot{\Delta}_H$. As a result, slight changes in the aspect ratio, a/b, occur because the a-value decreases and the b-value increases, for the case of "tensile loading" as indicated in Fig. 3-11. From this perspective, it is desirable to use a ring geometry (i.e. a/b) for which the small changes in a/b which occur during a test have an insignificant effect on η and β values. Analytical, expressions for the displacement rates in the vertical (increasing b) and horizontal (decreasing a) directions have been obtained, for ring specimens under plane stress creep condition using Equations (11) and (12), i.e.

$$\dot{\Delta}_H = \frac{2Bb^2}{(I_n)^n} \left(\frac{Pa}{2}\right)^n Int_3\left(n, \frac{a}{b}\right) \tag{3.2}$$

$$\dot{\Delta}_V = \frac{2Bab}{(I_n)^n} \left(\frac{Pa}{2}\right)^n Int_2\left(n, \frac{a}{b}\right) \tag{3.3}$$

Details of the derivation of these equations and the definitions Int_2 and Int_3 have been published [47]. The displacement rates in the vertical and horizontal directions have also been obtained using FE analyses with various a/b ratios; offset ellipses were used for this purpose and plane stress condition were used. The ratios of $\frac{\dot{\Delta}_H}{\dot{\Delta}_V}$ are obtained from the FE analyses and the analytical results, and are plotted against the a/b ratio in Fig. 3-12. It can be seen that there is a good agreement between the analytical and FE results [93].
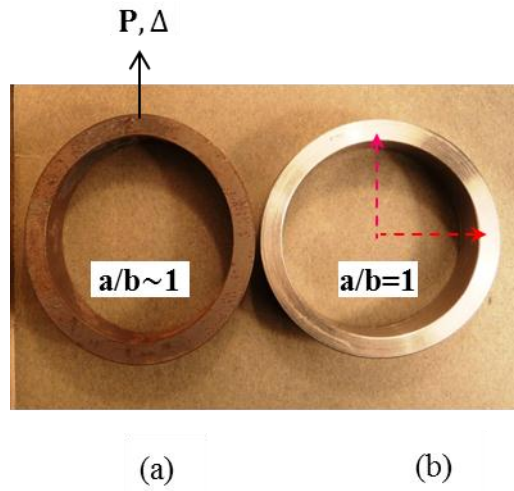
Fig. 3-11:　The appearance of (a) the tested and (b) untested circular ring specimens i.e. R= a = b.
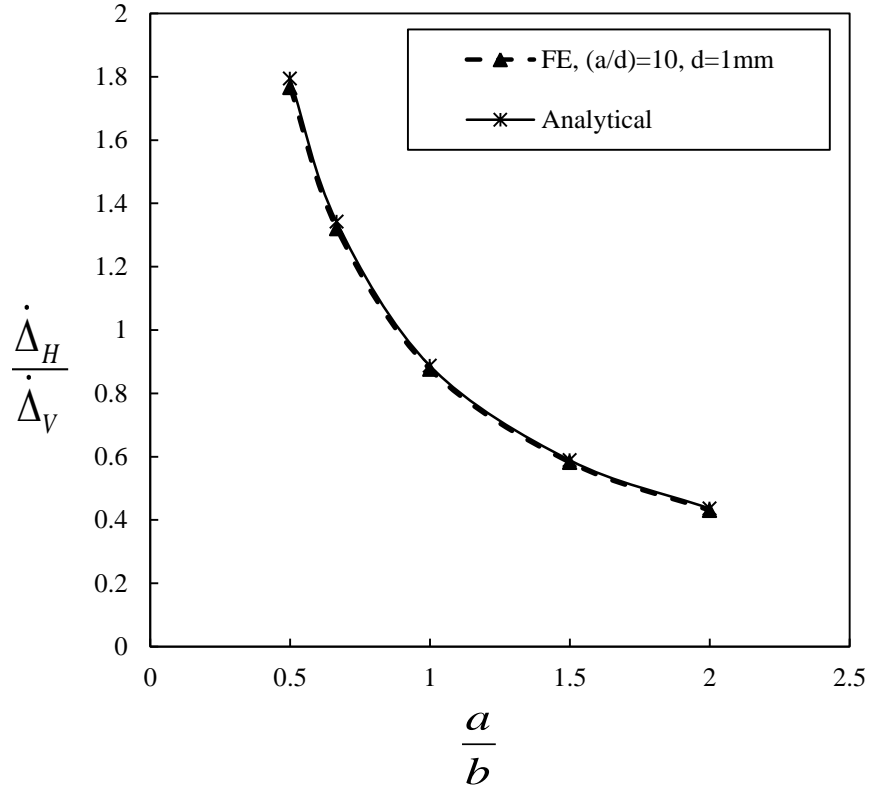
Fig. 3-12: Variations of $\frac{\dot{\Delta}_H}{\dot{\Delta}_V}$ with a/b analytical and FE analyses results.

Based on the results of the analytical and FE analyses for a circular ring, the ratios of the $\frac{\dot{\Delta}_H}{\dot{\Delta}_V}$ were found to be approximately unity [93].; the small increase in the b-value and decrease in the a-value, which occurs as a result of the creep deformation, were found to be almost the same. Therefore, the change in the ring geometry which occurs during a test for relatively small deformation may be neglected for the case of circular rings.

3.7   EXPERIMENTAL WORK

3.7.1   Specimens preparation

The specimens have been manufactured within the faculty of engineering at the University of Nottingham using electrical discharge machining AQ 750L (EDM) see Fig. 3-14. It was convenient to use this cutting machine to manufacture the specimens, because of the small dimensions of the ring specimen. The ring cutting operation is described in Fig. 3-13, and the cutting operation specification is included in Table 3-1. The cutting was performed in the presence of circled cooling liquid [94, 95]. The cooling liquid plays a significant role in the ring specimen surface finishing and in the cutting operation in general. However, the major benefits of the cooling liquid can be summarised by the flowing points:-

i.   Reducing the spark between the cutting wire and the specimen, resulting in in good surface finish

ii.   Constant cooling liquid flow is a key factor to control the temperature in the cutting region

iii.   Maintaining the cutting wire in good condition, resulting in less interruptions to the cutting operation and it extends the lifespan of the wire

iv.   The method allows smaller wire cutting diameter to be used, which is useful in the case of the manufacturing of small size specimen.

Table 3-1:   Standard cutting operation properties and specifications for the EDM machine

Cutting speed (straight line cutting)	6.0 mm/min
Wire diameter	0.25 mm
Wire rotating speed (r.p.m.)	Wire feed = 8.0 m/min
Cooling liquid temperature(cutting temperature)	Approximately 8000 to 12000 ^{o}C at the actual cutting gap.
Voltage/ DC magnitude	Machining voltage = 40.0 volts
Cooling liquid type	De-ionised water
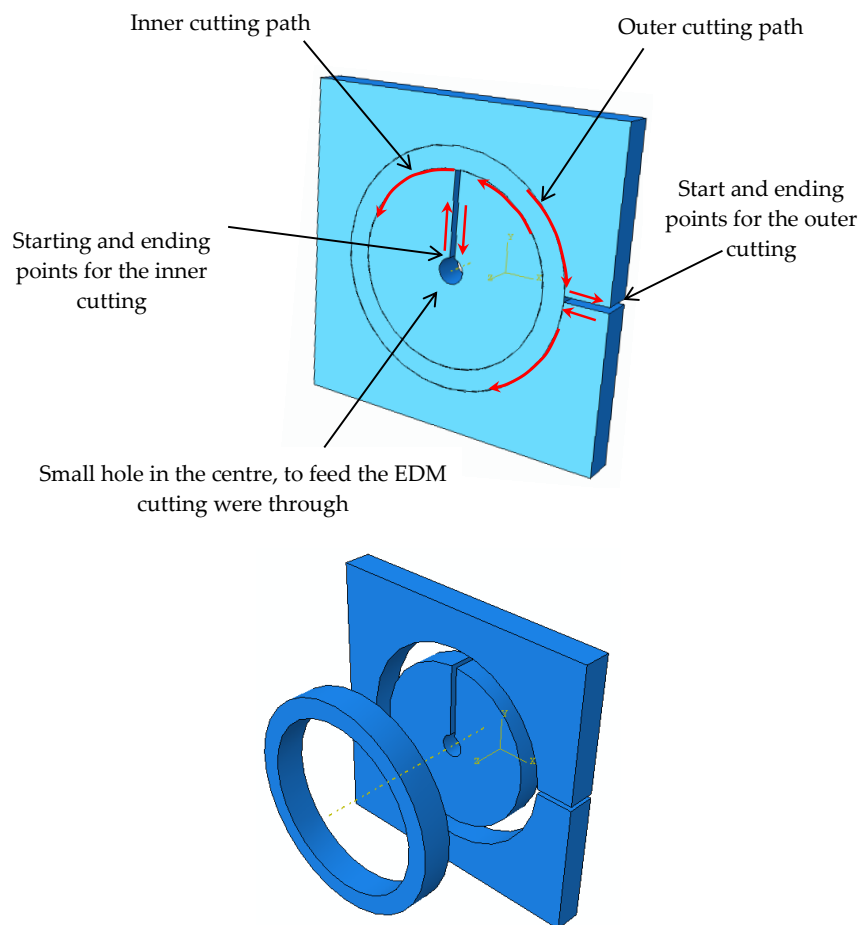
Fig. 3-13:   Drawing to demonstrate the ring specimen cutting procedure using an EDM machine.

3.7.2 Comparison of Nickel base Superalloy 738 Material uniaxial creep data with predictions based on small ring creep tests

Experimental validations were performed in order to compare the minimum creep strain rates obtained from the ring specimens with those obtained from the corresponding conventional uniaxial creep test specimens, using Nickel base Superalloy 738 Material at 800°C. The specimens were manufactured from an ex-service Inconel 738 Material of third stage blade from a heavy-duty gas turbine using an electric discharge cutting machining (EDM). The root of the blade was selected for creep testing because this area is not exposed to high stresses and temperature; therefore, it can be used to represent the material in its virgin condition [46]. It is common practice to use the root of gas turbine blades as a reference of the as-cast and heat-treated material which can be used for metallurgical evaluation.

Fig. 3-14:   Electrical discharge machining (EDM) AQ 750L
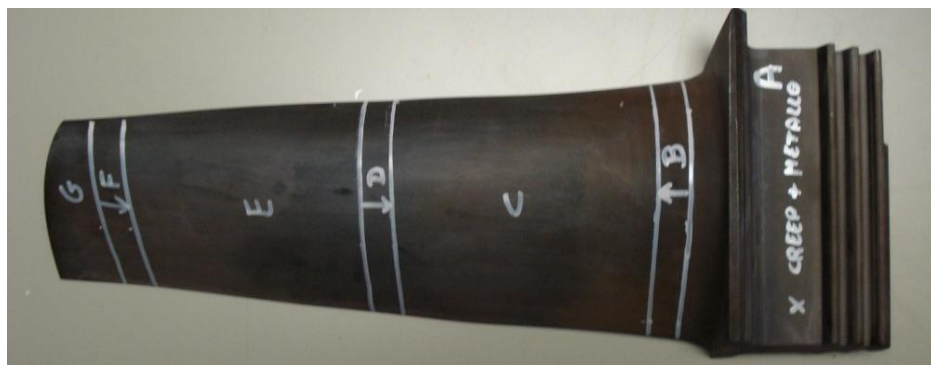
Fig. 3-15:   Third stage gas turbine blade from a heavy-duty gas turbine [46].

A small section of the root was removed along the main direction of the blade (see Fig. 3-16). This small section has been used to extract six small circular ring specimens, as shown in Fig. 3-17.

Fig. 3-16: Piece of root extracted along the main direction of the blade.
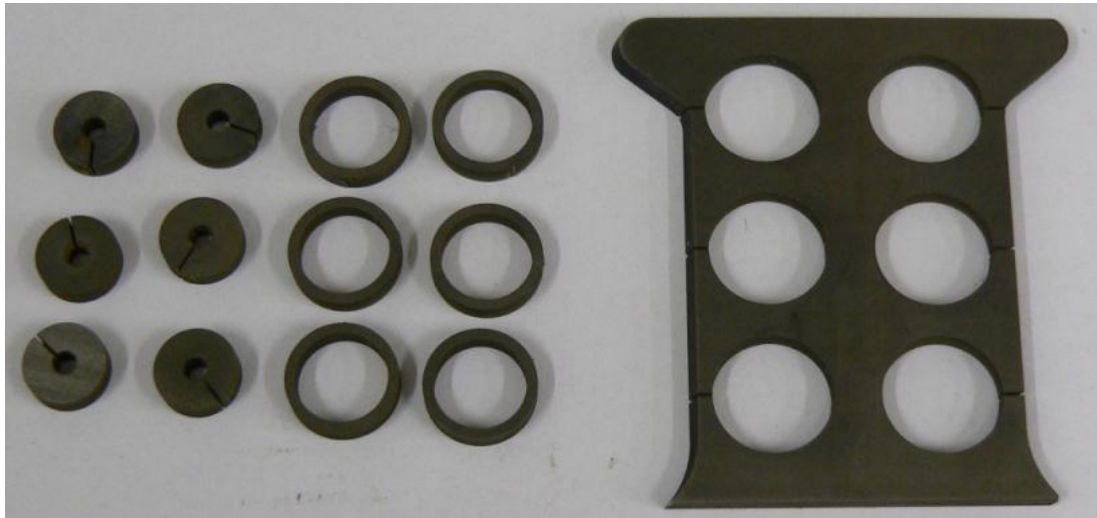
Fig. 3-17: Ring specimens and remains from EDM operations condition [46].

The ring specimens (see Fig. 3-17), were creep tested at 800°C using stress levels of 250, 300, 350 and 400 MPa. The circular ring dimensions b_0, R and d were 2, 10 and 2 mm, respectively. Equation (3.4) has been used to calculate the required load magnitude (P) for the circular rings, i.e.

$$\sigma_{ref} = \eta \left(\frac{PR}{b_0 d^2} \right) \qquad (3.4)$$

Conventional uniaxial creep test specimens (see Fig. 2-5), were also made of nickel base superalloy 738 material and creep tested at 800°C using various stress levels including those used for the circular ring, i.e. 250, 300, 350 and 400 MPa. [28]. The specimens were tested using a "Tinius Olsen H25KS" creep testing machine, see Fig. 3-18. This is a sensitive creep testing machine which can be conveniently used for small load applications, i.e. low stress levels and/or testing of small size ring specimens. The machine has a precise loading system and the applied load can be as small as 0.01N. Equation (3.5) has been used to convert the minimum displacement rates to the equivalent uniaxial minimum creep strain rates, i.e.

$$\dot{\varepsilon}^c(\sigma_{ref}) = \frac{d}{4\beta R^2} \dot{\Delta}_{ss} \qquad (3.5)$$
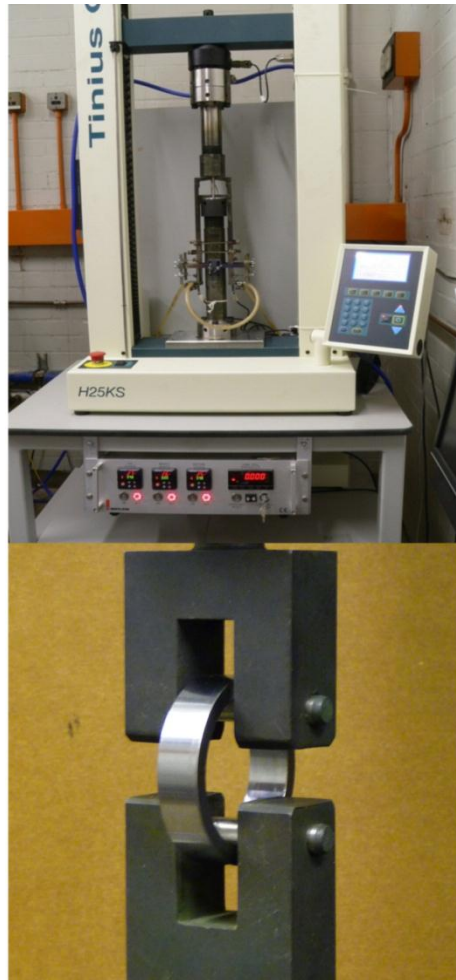
Fig. 3-18 Creep testing machine "Tinius Olsen H25KS" used for ring specimen creep testing (a) and ring specimen loading application (b).

The circular ring creep deformation is plotted against time in Fig. 3-19, from which it can be seen that the results exhibit primary and secondary creep strain regions. The minimum deformation rates obtained from the circular ring specimens, were converted to minimum creep strain rates using equation (3.5). The converted minimum creep stain rates obtained from the ring specimens together with the corresponding uniaxial minimum creep strain rates are plotted in Fig. 3-20, using log-log scale. Good correlation was found between the two sets of results.
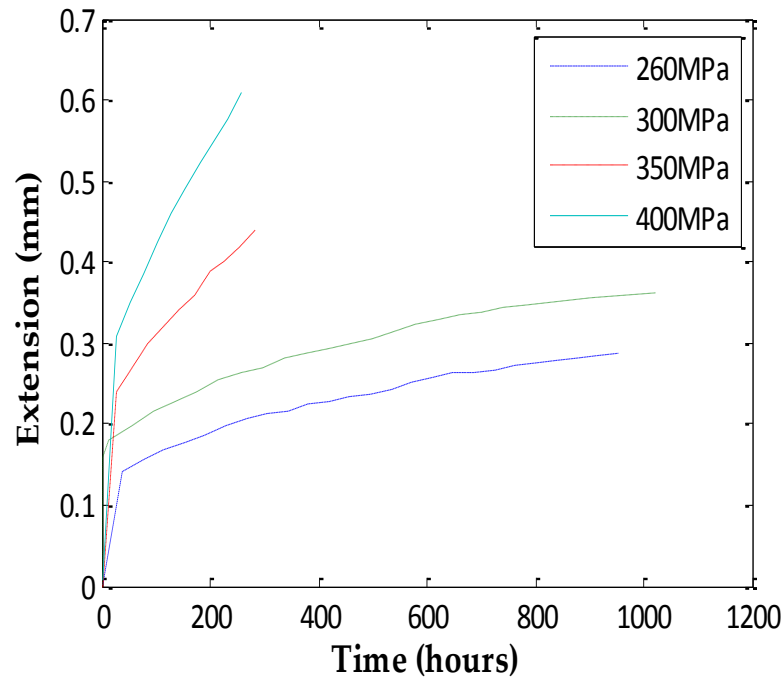
Fig. 3-19:   Small ring creep test deformation curves, for Inconel 738 (Nickel-based Superalloy) at 800°C [46].
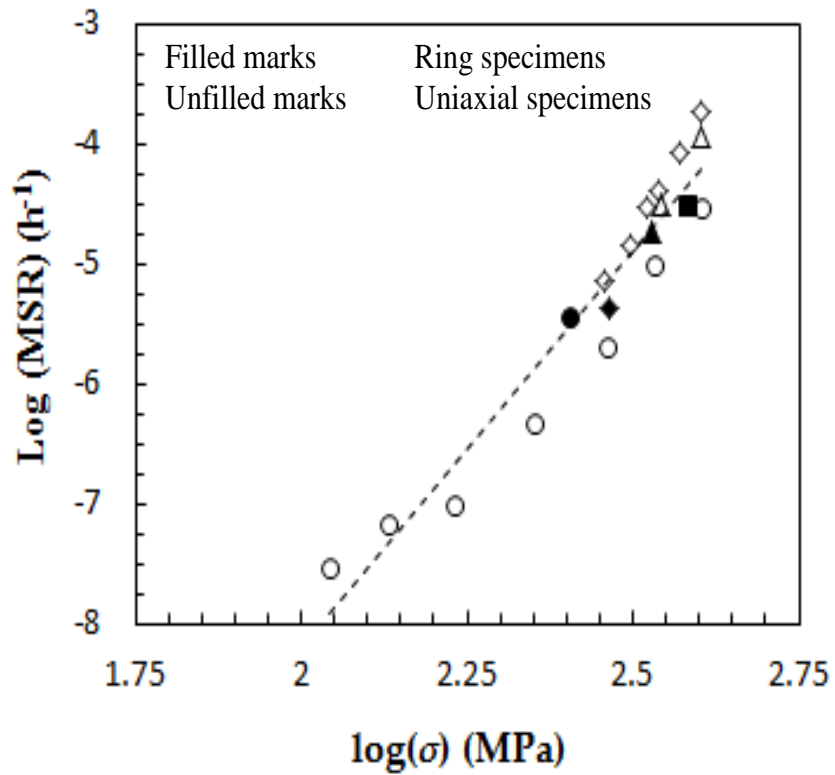
Fig. 3-20:   Minimum creep strain rate data for Inconel 738 (Nickel-based Superalloy) at 800°C obtained from uniaxial and ring tests at various stress [96].

3.7.3 Comparison of (Bar-257) P91 steel uniaxial creep data with predictions based on small ring creep tests

(Bar-257) P91 steel was also used to validate the ring testing technique. Elliptical ring specimens, circular ring specimens and conventional uniaxial creep test specimens were manufactured from the same batch of P91 steel and creep tested at 650°C. The uniaxial specimens creep curves obtained for stresses of 70, 82, 87, 93 and 100 MPa are shown in Fig. 3-21, from which it can be seen that the creep behaviour is typical of that for many materials; it exhibits primary, secondary and tertiary regions. The elliptical and the circular ring specimen geometries and dimensions are shown in Fig. 3-22. The specimens were tested with loads corresponding to uniaxial stresses of 50, 55, 60 and 65 MPa. However, the displacement time curves obtained from the circular and elliptical rings show no indication of the tertiary regions, as shown in Fig. 3-23 and Fig. 3-24. Equations (3.4) and (3.6) have been used to determine the loads for the circular and the elliptical rings, respectively, i.e.,

$$\sigma_{ref} = \eta \left(\frac{Pa}{b_0 d^2} \right) \qquad (3.6)$$

whereas equations (3.5) and (3.7) have been used to convert the minimum displacement rates to the equivalent uniaxial minimum creep strain rates, for the circular and the elliptical rings, respectively, i.e.,

$$\dot{\varepsilon}^c(\sigma_{ref}) = \frac{d}{4\beta ab} \dot{\Delta}_{ss} \qquad (3.7)$$

The β values for the tested circular and the elliptical ring geometries were 0.48 and 0.78 respectively, whereas the η values were constant at 0.9 for both geometries. These values have been obtained numerically using the FE analyses in order to include the small effects of shear deformation on the specimen deformation. The minimum creep strain rate (MSR) obtained from the ring specimens and the uniaxial specimens are plotted together, versus the stress (using log-log scales) in Fig. 3-25. The correlation between the uniaxial and the small ring data is remarkably good.
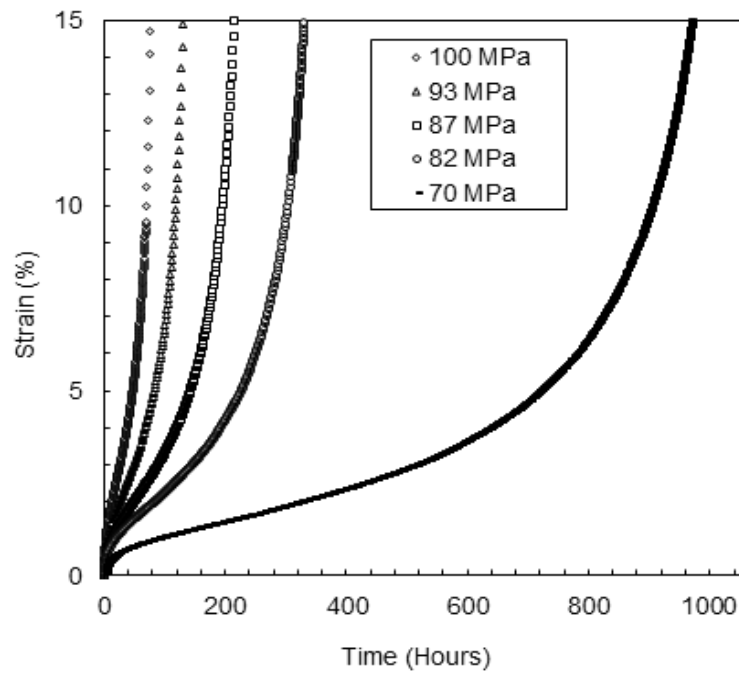
Fig. 3-21:   Creep strain versus time curves obtained from uniaxial tests for (Bar-257) P91 steel at 650°C [10]
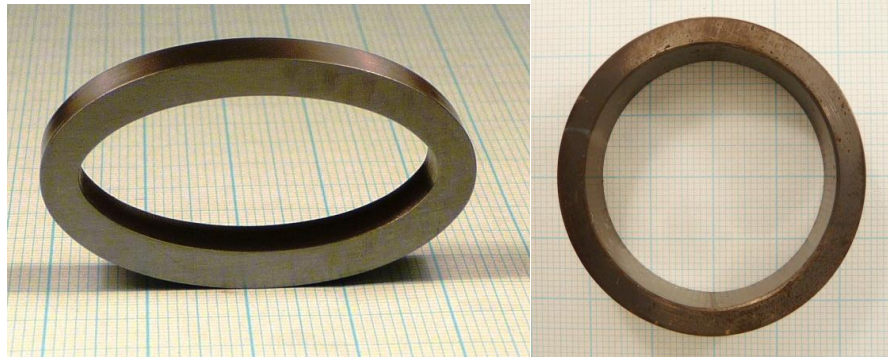
(a)   (b)

Fig. 3-22:   The tested ring specimens dimensions, (a=20mm, b=10mm, b_o =2mm and d=2mm) for the elliptical rings (a) and (R=10 mm, d=2mm and b_o=2mm) for the circular rings (b)
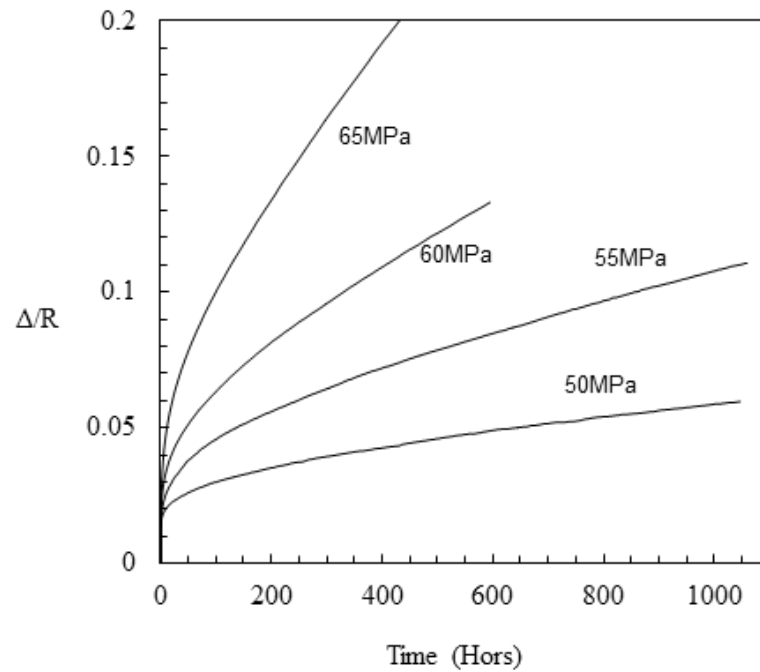
Fig. 3-23:   Variation of Δ/R with time obtained from creep tests for diametrically loaded circular rings, made of (Bar-257) P91 steel at 650°C [10]
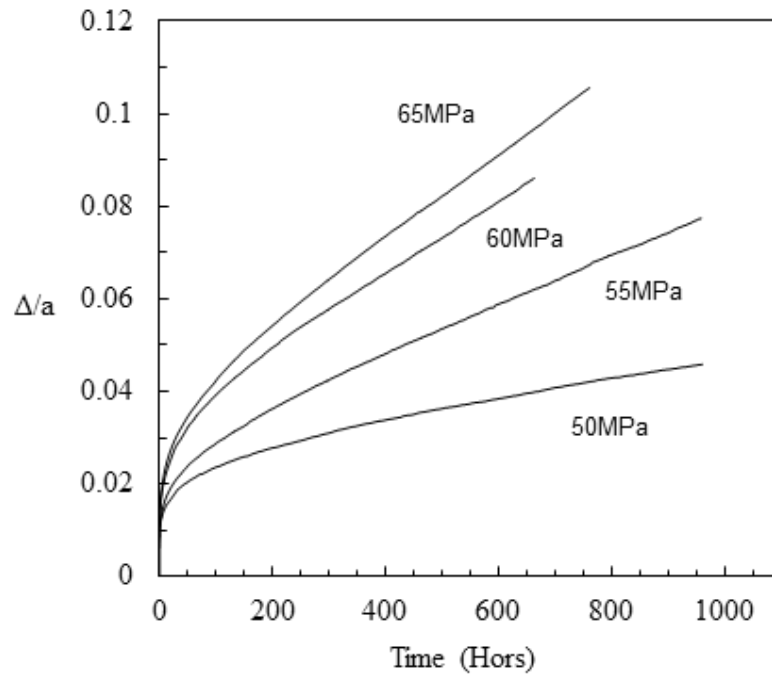
Fig. 3-24: Variation of Δ/a with time for diametrically loaded elliptical rings made of the (Bar-257) P91steel at 650°C.
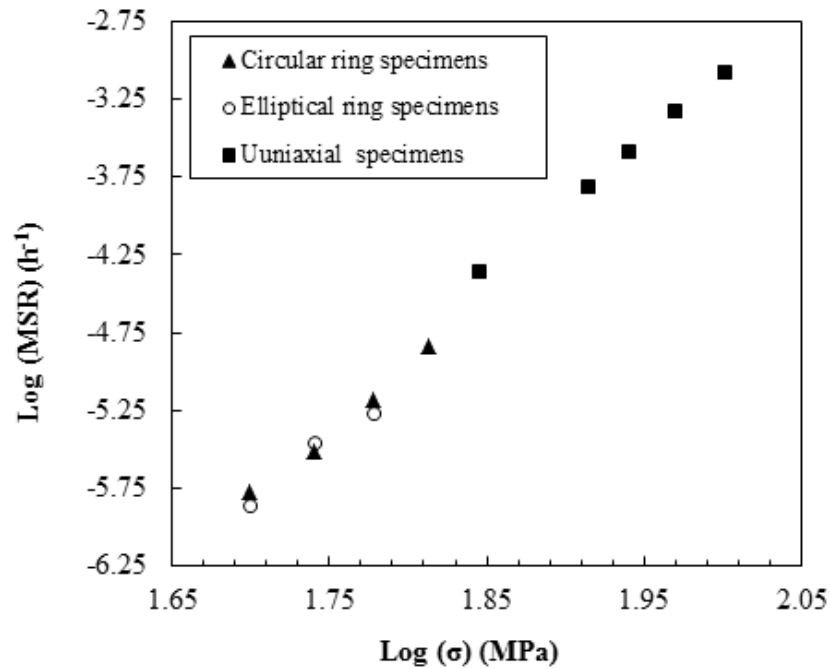
Fig. 3-25 : Minimum creep strain rate (MSR) data obtained from the uniaxial creep tests and the ring specimens (circular and elliptical) for the (Bar-257) P91steel at 650°C.

In order to further verify the ring specimen testing technique, FE analyses (under plane stress conditions) were carried out using an elliptical ring, with a =10mm, d=1mm and a/b = 0.66, for a number of a/d values. The material properties (A and n) for the elliptical ring material were 1×10^{-16} (based on unite of stress in MPa and the time in hour) and 6, respectively. The applied load magnitude corresponded to a stress of 100MPa. Equations (3.6) and (3.8) were used to calculate the load magnitude in the FE analyses and the theoretical minimum displacement rates, i.e.

$$\dot{\Delta}_{ss} = \frac{4\,\beta\,a\,b\,A(\eta\sigma)^{n}}{d} \tag{3.8}$$

The appropriate conversion factors η and β were chosen based on the elliptical a/b ratio. The variations of FE steady state load-line deformation rates and the analytical estimation for the minimum deformation rate are plotted together, against the a/d rations, in Fig. 3-26. It can be seen that the deformation rates obtained from both methods are practically the same.
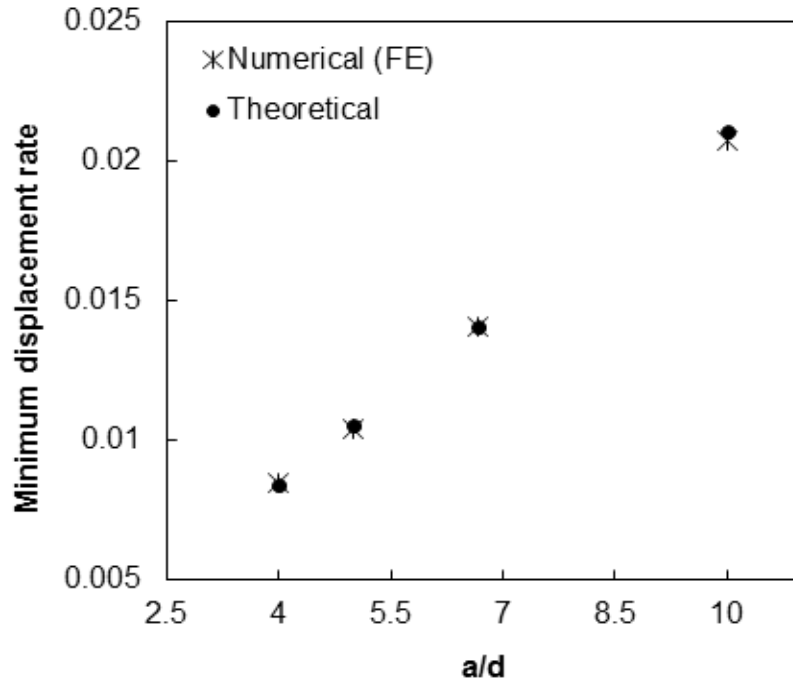
Fig. 3-26:   Variation of the minimum deformation rates (analytical and FE) with *a/d* ratios
for an elliptical ring with *a/b*=0.66.

Additional verification using FE analyses has been carried out, to compare

the minimum displacement rates obtained theoretically for circular ring

specimen, i.e.

$$\dot{\Delta}_{ss} = \frac{4\,\beta\,R^2 A(\eta\,\sigma)^n}{d}$$ (3.9)

with the displacement rates obtained numerically using FE analyses, (under

plane stress conditions) for a number of stress exponent *n* values. The

circular ring dimensions were *R*=10mm, *d*=1mm and b_o=1mm, the material

constant *A* was chosen to be 1×10^{-16} and *n* = 6.00. Equation (3.4) was used

to calculate the load in the FE analyses; the load magnitude corresponds to a

constant stress of 100MPa for all cases. The analytical and numerical results

are presented in Fig. 3-27; Again, remarkably good agreement was found between the two sets of results.
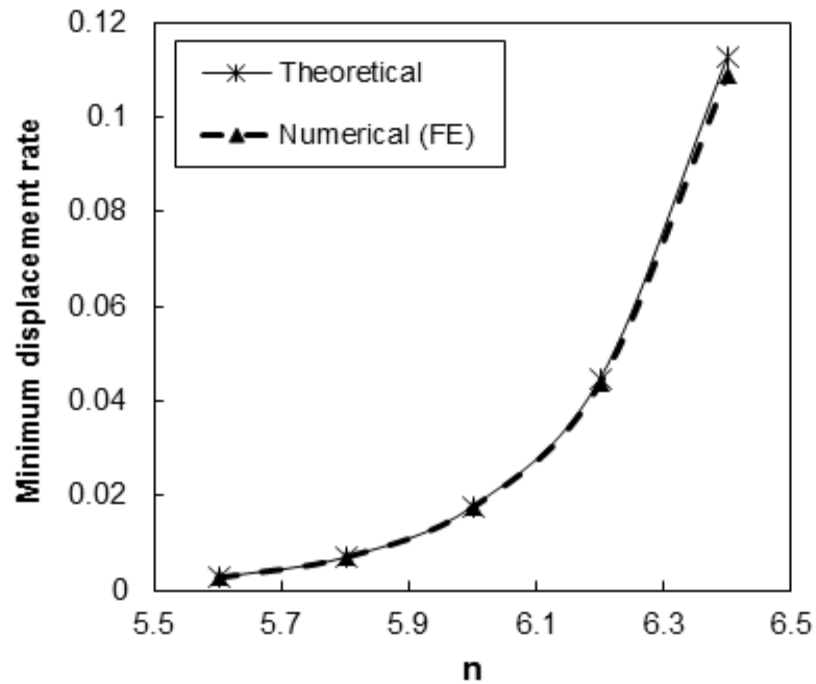
Fig. 3-27:   variations of circular ring specimen minimum displacement rates (theoretically and numerically), with *n* values.

3.8   DISCUSSION

Small ring creep testing is useful in a number of practical engineering situations; it can be used, for example, to obtain the current creep strength of a service-aged material. The specimens can be easily made from small material samples. They can be constructed, for example, from small scoop samples removed from a component surface; or from the HAZ region of a weld [27], i.e., a circular ring specimen with the dimensions of R~5 mm, b_o~2 mm and d~2 mm, and can be easily made from a HAZ region of the GTAW joint, which is about 1~3 mm in width see Fig. 3-28 [97]. The ring specimen

also can be used to determine the relative creep properties of materials produced as part of an alloy development programme e.g. [4, 98]. The minimum creep strain rate, obtained from a service-aged material, can be used, with the Monkman-Grant relationship, to estimate component life. The usefulness of a particular small ring specimen test method depends on the ease with which specimens can be manufactured and tested and the ease with which the measured deformations can be converted to corresponding uniaxial creep data.
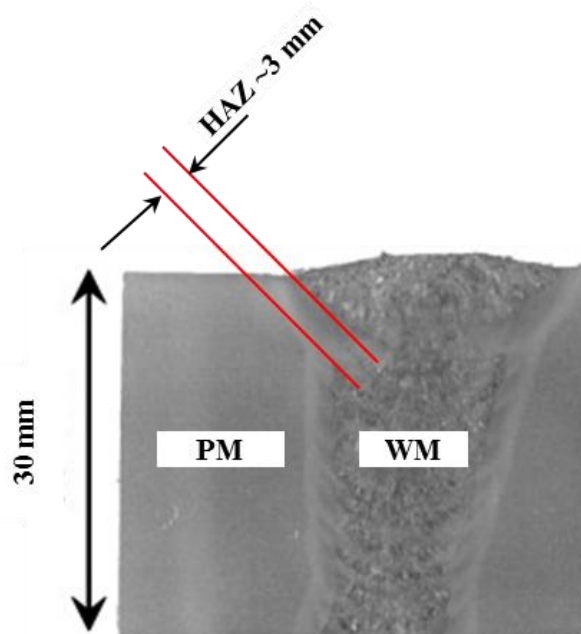
Fig. 3-28:   Cross-sectional view of the GTAW joint with single bevel groove[92].

Small ring specimens, particularly circular rings, can be manufactured and tested as easily as any other commonly used small specimen type (i.e. small punch, impression creep and sub-size uniaxial test specimens). Creep testing of circular, small ring specimens, is made easy by the self-centering property

of the specimen. Also, the measured deformation is not related to localised creep strains which occur at the region of contact between the test specimen and loading device (e.g. the impression creep test method); it depends on the bending which occurs at every circumferential position of the ring. Hence, it is not necessary to have a loading device with significantly higher creep strength than the tested material. The sensitivity of the measured deformations is very important if the predicted creep strains, corresponding to uniaxial data, are to be produced with reasonably high accuracy. A simple measure of the relative sensitivities of particularly small specimen test types is given by the equivalent gauge length (EGL). Typical ring test dimensions, i.e. , $R = 5$ and $d = 1$ mm, result in a β-value of about 0.5, leading to an EGL of about the same magnitude as a conventional uniaxial creep test specimen (see Fig. 2-5) with a 50 mm gauge length.

The b_o value chosen for a test may have a significant effect on both the η-value and the β-values. Small b_o/d values (i.e. $b_o/d < 2$) correspond to plane stress conditions see Fig. 3-7 and Fig. 3-8. Large b_o/d values (i.e. $b_o/d > 15$) correspond to plane strain conditions (see Fig. 3-7 and Fig. 3-8). It should be noted that the expressions for the σ_{ref} value, e.g. equation (3.6), and the $\dot{\varepsilon}^c(\sigma_{ref})$ value, e.g. equation (3.7), do not contain any material properties, i.e., the conversion process (from small ring specimen data to corresponding

uniaxial data) is material independent. In some situations, the dimensions and shape of the small samples of material available may make it more beneficial to test elliptical, rather than circular, specimens. In this case, two types of geometry have been investigated, i.e., "concentric-ellipses" and "offset-ellipses". Essentially, the difference is that the offset-ellipse geometry produces a constant thickness, d, as is the situation assumed when deriving the analytical solution (Chapter 2). The offset-ellipse approach is recommended, because the concentric-ellipse geometry has a variable thickness, d, (see Fig. 3-3) which causes an increase in the ring deformation rate with consequential increases in the β value (see Fig. 3-6). The variations of η and β with a/b (the ellipticity ratio) is shown in Fig. 3-6.

In general, the small changes in shape which a specimen undergoes as a test progresses, has a relatively insignificant effect on the σ_{ref} and $\dot{\varepsilon}$ (σ_{ref}), which exist during a test. The experimental results (see Fig. 3-20 and Fig. 3-25) indicate that the small ring test data can be converted into corresponding uniaxial data, with remarkably good accuracy. It is concluded that the small ring test method is capable of producing data which corresponds to uniaxial creep data. Also, it is recommended that circular ring with $b_o/d \approx 1$ and R/d ≈ 5 should be used where practical; these circular ring ratios allow easy interpretation of the test data. Equation Section (Next)

110

CHAPTER 4.

ANALYSIS AND DESIGN OF A SMALL, TWO-BAR CREEP

TEST SPECIMEN

_____

4.1   INTRODUCTION

There is a strong desire to develop miniature specimen types and the associated testing techniques from which reliable creep deformation and creep rupture data can be conveniently and economically derived, from small amounts of material. In this chapter, a new small-sized (two-bar) specimen type is described; it is suitable for use in obtaining both uniaxial creep strain and creep rupture life data. The (two-bar) specimen can be machined from small samples removed from the surface of a component, without adversely affecting the safe operation of the component. The specimen has a simple geometric shape and can be conveniently manufactured and loaded (through pin-connections) for testing.

Conversion relationships between the applied load and the corresponding uniaxial stress, and between the measured load-line deformations and the corresponding uniaxial minimum creep strain rate, have been obtained,

based on the reference stress method, in conjunction with finite element analyses. Using finite element analyses the effects of the specimen dimensions and loading pin diameter on the reference stress parameters have been investigated. On this basis useful ranges of relative specimen dimension ratios are recommended. Using the Liu-Murakami damage model, the effects of specimen depth on the specimen minimum displacement rate and failure time have also been investigated. FE analyses are used to provide preliminary validation of the technique and to assess the accuracy of the conversion relationship. The advantages of the TBS over other small specimen testing methods are described and the recommendations are summarized in Section 4.8.

4.2 REFERENCE STRESS METHOD AND EQUIVALENT GAUGE LENGTH

4.2.1 Creep Deformation and Reference Stress Method (RSM).

For some components and loading modes, it is possible to obtain analytical expressions for steady-state creep deformation rates, $\dot{\Delta}_{ss}^{c}$, [99]. For a material obeying a Norton's power law, i.e. $\dot{\varepsilon}^{c} = A\sigma^{n}$, these show that the general form is:-

$$\dot{\Delta}_{ss}^{c} = f_1\left(n\right) f_2\left(dimensions\right) A(\sigma_{nom})^{n} \tag{4.1}$$

where $f_1(n)$ is a function of the stress index, n, and f_2 *(dimensions)* is a function of the component dimensions and σ_{nom} is a conveniently chosen nominal stress for the component and loading [25, 31]. By introducing a scaling factor, α, for the nominal stress, equation (4.1) can be rewritten as:

$$\dot{\Delta}_{ss}^c = \frac{f_1(n)}{\alpha^n} f_2(dimensions) A(\alpha\sigma_{nom})^n \tag{4.2}$$

An α value ($\alpha = \eta$) can be chosen so that the function $\frac{f_1(n)}{\eta^n}$ in equation (4.2), becomes independent (or approximately independent) of n, where n is the stress index in Norton's law. Equation (4.2) can be further simplified, i.e.

$$\dot{\Delta}_{ss}^c \approx D \, \dot{\varepsilon}^c(\sigma_{ref}) \tag{4.3}$$

where D is the so-called reference multiplier, i.e.

$$D = \frac{f_1(n)}{\eta^n} f_2(dimensions)$$

and $\dot{\varepsilon}^c(\sigma_{ref})$ is the minimum creep strain rate obtained from a uniaxial creep test at the so-called reference stress, i.e.

$$\sigma_{ref} = \eta \, \sigma_{nom} \tag{4.4}$$

The reference multiplier, D, has the units of length, and can usually be defined by $D = \beta d$, where d is a conveniently chosen, "characteristic", component dimension. Therefore, for the known loading mode and component dimensions, σ_{nom} can be conveniently defined, and if the values of η and β are known, the corresponding equivalent uniaxial stress can be

obtained by σ_{ref} (= $\eta\sigma_{nom}$), and the corresponding uniaxial minimum creep strain rate can be obtained using equation (4.3) if $\dot{\Delta}_{ss}^c$ is known.

4.2.2 Determination of Reference Parameters

If an analytical solution for the component steady-state creep deformation rates can be obtained, substituting two values of n in the expression $\frac{f_1(n)}{\eta^n}$ and equating the two resulting expressions allow the value of η to be determined. Hence, σ_{ref} (= $\eta\,\sigma_{nom}$), and D can be obtained. This approach was proposed by MacKenzie [25, 31, 100]. However, analytical solutions for the component steady-state creep deformation rates only exist for a small number of relatively simple components and loadings [100].

 If computed (e.g. finite element) solutions to a creep problem are obtained using several stress index n values, but keeping all other material properties, loading and component dimensions the same, then σ_{ref} can be obtained. This is done by taking several values of α, normalising the steady-state value of deformation rate, $\dot{\Delta}_{ss}^c$, with respect to $A(\alpha\sigma_{nom})^n$ and hence finding the value of α which renders $[\dot{\Delta}_{ss}^c/(A(\alpha\sigma_{nom})^n]$ independent of n. This process is most easily visualised by plotting log $[\dot{\Delta}_{ss}^c/(A(\alpha\sigma_{nom})^n]$ for various values of α against n, as illustrated in Fig. 4-1. It can be seen that approximately straight line fits are produced, using all of the α values, and their fits have

approximately the same intercept on the log $[\dot{\Delta}_{ss}^{c}/(A(\alpha\sigma_{nom})^{n}]$ axis. This intercept is equal to the logarithm of the reference multiplier, D.
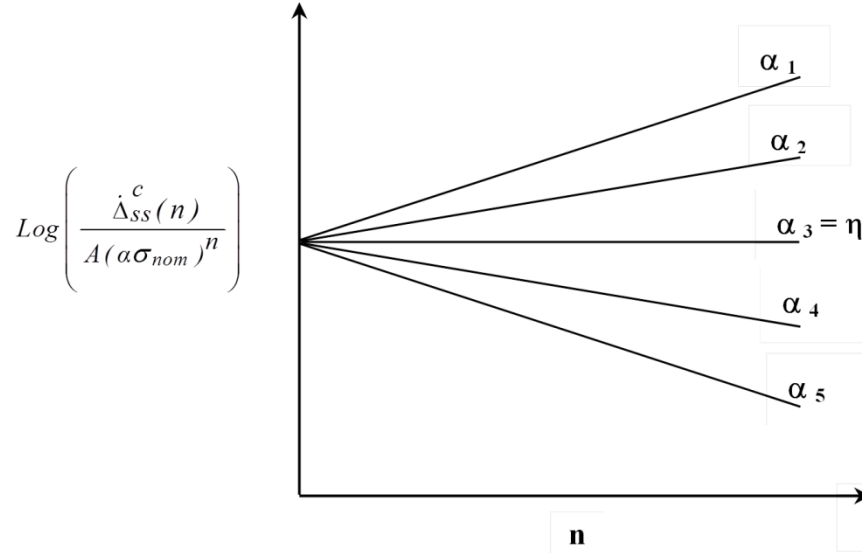
Fig. 4-1 Variation of $\log\left(\dot{\Delta}_{ss}^{c}(n) \Big/ A(\alpha\sigma_{nom})^{n}\right)$ with n.

4.2.3 Equivalent Gauge Length (EGL).

For a conventional uniaxial creep test, the creep strain at a given time is usually determined from the deformation of the gauge length (GL). If the gauge length elongation is Δ and the elastic portion is neglected, then

$$\varepsilon^{c} \approx \frac{\Delta}{GL} \tag{4.5}$$

For non-conventional small specimen creep tests, an equivalent gauge length (EGL) [47] can be defined, if the measured creep deformation can be related

to an equivalent uniaxial creep strain, in the same form as that of equation (4.5), i.e.

$$\varepsilon^c \approx \frac{\Delta}{\text{EGL}} \tag{4.6}$$

and

$$\dot{\varepsilon}^c \approx \frac{\dot{\Delta}}{\text{EGL}} \tag{4.7}$$

The EGL is related to the dimensions of the specimen. The creep strain and creep deformation given in equations (4.6) and (4.7) may be presented in a form related to the reference stress, σ_{ref}, i.e.

$$\varepsilon^c(\sigma_{ref}) \approx \frac{\Delta^c}{D} \tag{4.8}$$

and

$$\dot{\varepsilon}^c(\sigma_{ref}) \approx \frac{\dot{\Delta}^c}{D} \tag{4.9}$$

in which D (= $\beta\, d$) is the reference multiplier, which is, in fact, the EGL for the test. In some cases, the geometric changes, due to the specimen creep deformation with time, are small (e.g. for impression creep tests), and in such cases, the effects of geometric changes on D (EGL) can be neglected.

4.3 THE "TWO-BAR" SPECIMEN (TBS)

4.3.1 Specimen Geometry and Dimensions

The pin-loaded, Two Bar Specimen (TBS) type, shown in Fig. 4-2, has a simple geometry; specimen dimensions are defined by L_o, b, d, D_i, and k; where L_o is the uniform "bar" length, i.e. the distance between the centres of the loading pins, b is the bar width, d is the specimen thickness, D_i is approximately the diameter of the loading pins and k is the length of the loading pin supporting end.
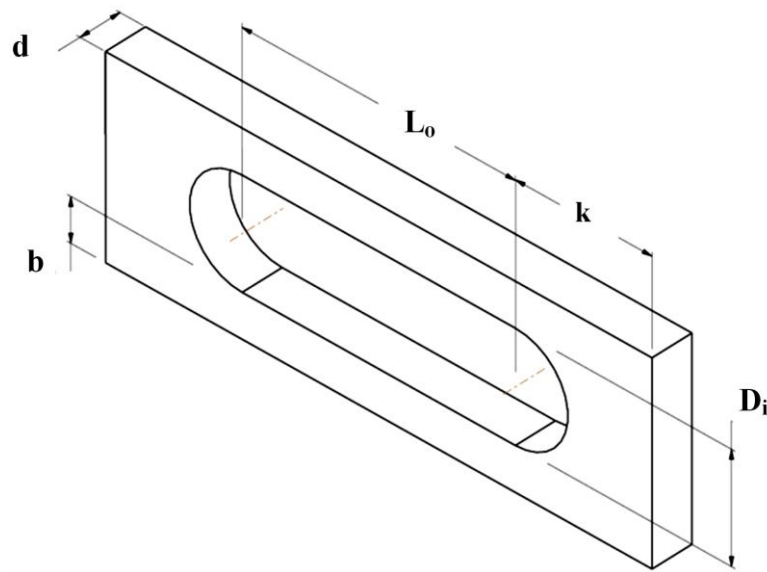
Fig. 4-2:   Two bar specimen geometry and dimensions.

4.3.2 Test Procedure.

The TBS testing technique is based on the principle of converting the specimen load-line deformation versus time curves, to the equivalent uniaxial strain versus time curves, using conversion relationships. The

conversion relationships, which are used to convert the specimen loading to the equivalent uniaxial stress, i.e., equation (4.4) and the specimen (pin) displacements to equivalent uniaxial strains and strain rates, i.e., equations (4.6) and (4.7), are functions of specimen dimensions and deformations. The (Two-Bar) specimen in Fig. 4-3 (b), is loaded by two loading pins and the displacement between the centres of the two loading pins is measured during the test. The loading fixtures generally have larger dimensions and higher stiffness, compared to the specimen, see Fig. 4-3, and are generally manufactured from a material which has a much higher creep resistance than the tested material. The conversion factors η and β are obtained using several finite element (FE) analyses as will be explained in Section 4.4.4.
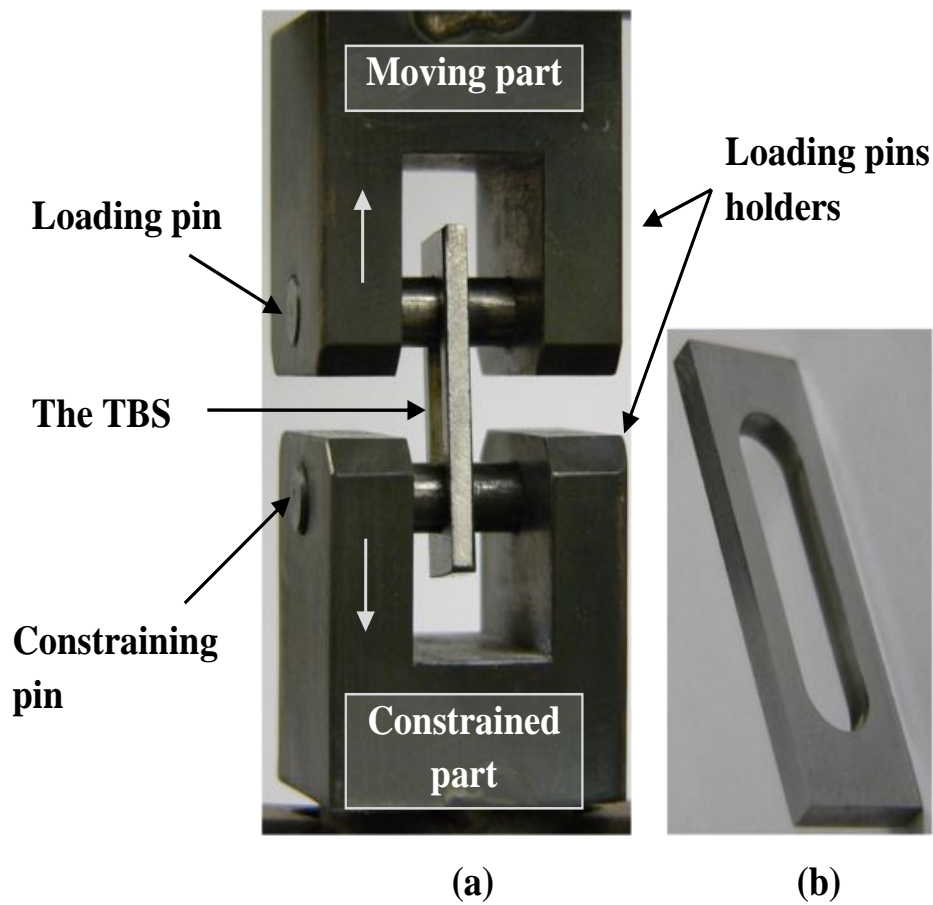
Fig. 4-3: (a) TBS experiment setup and loading application and (b) the TBS specimen.

4.4 FINITE ELEMENT ANALYSES FOR THE TBS

4.4.1 Scope of Investigation

The continuum damage material behaviour model, proposed by Liu-Murakami[11], has been used in the FE investigations, to obtain full creep curves and rupture data [101]. A limited study was also carried out, to assess the effects of the specimen depth, *d*, on the specimen failure time. Using

Norton's creep law, a series of elastic-creep analyses were also performed for a range of n values to determine the reference stress parameters η and β. Further FE analyses were used to study the effects of TBS dimensions on conversion factors, and also to determine the TBS recommended dimension ratio ranges. Finally FE analyses were used to obtain preliminary validation of the testing technique using 3D analyses and Norton's law. This was also used to assess the accuracy of the conversion relationship and of the conversion factors in Section 4.7. The ABAQUS finite element software package [70] was used for the FE analyses.

4.4.2 Material Behaviour Models

The Norton material model, i.e. $\dot{\varepsilon}^c = A\sigma^n$, was used in FE analyses to obtain the TBS steady state deformation rates, where A and n are material constants [13]. The Liu-Murakami model [11] is used to obtain full deformation-time creep curves for the TBS. The model consists of a pair of coupled creep/damage equations, i.e.

$$\frac{d\varepsilon_{ij}^C}{dt} = \frac{3}{2} A\sigma_{eq}^{n-1} S_{ij} Exp\left[\frac{2(n+1)}{\pi\sqrt{1+3/n}}\left(\frac{\sigma_1}{\sigma_{eq}}\right)^2 \omega^{3/2}\right] \tag{4.10}$$

$$\frac{d\omega}{dt} = \frac{M[1-Exp(-q_2)]}{q_2}(\sigma_r)^{\chi} Exp(q_2\omega) \tag{4.11}$$

where ω is the damage parameter ($0 < \omega < 1$), where $\omega = 0$ (no damage) and $\omega = 1$ (failure). A and n are the material constants in Norton's law, *M, χ and q_2* are also material constants, which can be obtained by curve fitting to uniaxial creep curves [3, 11] The rupture stress, σ_r, in equation (4.11) is given by:

$$\sigma_r = \alpha\sigma_1 + (1-\alpha)\,\sigma_{eq} \qquad (4.12)$$

where σ_1 is the maximum principal stress, σ_{eq} is the von-Mises equivalent stress and α is a material constant representing the multi-axial stress state ($0 < \alpha < 1$). The parameter α can be determined using experimental and FE creep rupture analyses results for notched bar specimens at different stresses [3]. A FORTRAN subroutine, CREEP, was used to implement the Liu-Murakami damage model for the FE analyses. The material constants for P91 at 600°C, which were used in the FE analyses for the Liu-Murakami model, were reported in [102].

4.4.3 Specimen Modeling

The 3D FE analyses were carried out using meshes which consist of 20-noded brick elements. Because of the symmetry, it was only necessary to model one quarter of the specimen and one half of the specimen thickness, d, as shown in Fig. 4-4. The boundary conditions, i.e. $u_x = 0$ on plane A, $u_y = 0$ on plane B and $u_z = 0$ on plane C, are also indicated in Fig. 4-4.
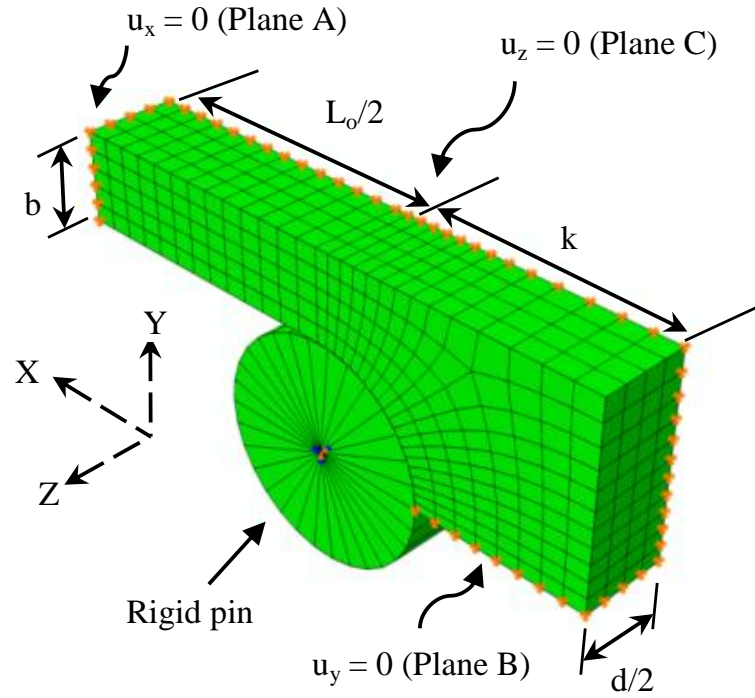
Fig. 4-4:   Finite element mesh and the boundary conditions.

The specimen is loaded and constrained through two loading pins which are assumed to be "rigid" in the FE model. The applied load was calculated for the required stress using equation (4.4). The Liu-Murakami damage model [11] was used in the FE analyses to predict the TBS rupture time, as illustrated in Fig. 4-5. The material creep constants for P91 steel at 600°C have been used to predict the failure life for the specimen.

The failure time form the FE analyses for the TBS was determined as the time at which the damage parameter, ω, approached unity, i.e., reaches the maximum value of 0.99 in the integration points in all of the elements on a path through the cross section area of the bar, as illustrated in Fig. 4-6. [101]. As the damage parameter, ω, reaches unity when using the Kachanov model, see equation (2.45), the creep strain rate reaches infinity. This cause numerical problem for the FE analyses therefore, a value less than one, 0.99, was chosen as the maximum allowed (or a critical) value of damage. Because the the Liu and Murakami model was originally based on the Kachanov model, the critical value of damage for this model was also taken as 0.99, as well. It is worth noting that the FE results are sensitive to that value of damage. Therefore, it must be kept the same throughout all of relevant analyses.
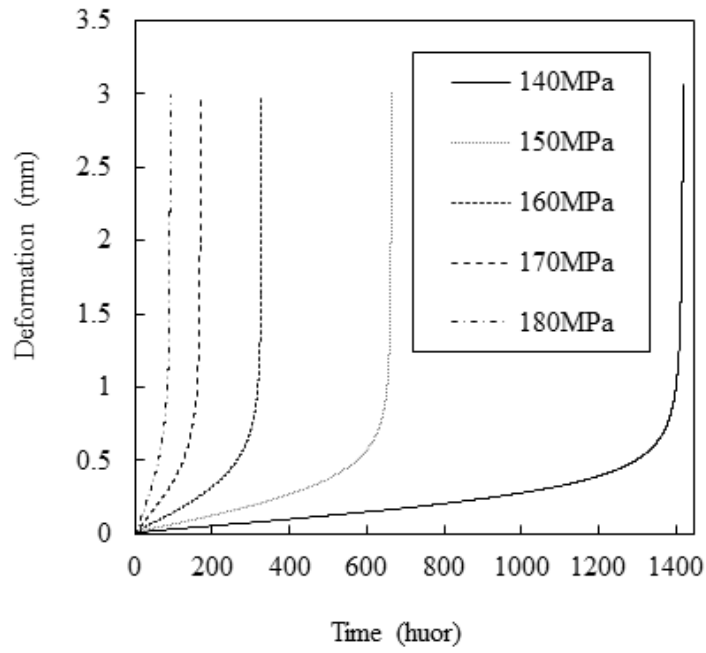
Fig. 4-5: Creep deformation versus time for P91 at 600°C, obtained from TBS-FE analyses for different stress levels.
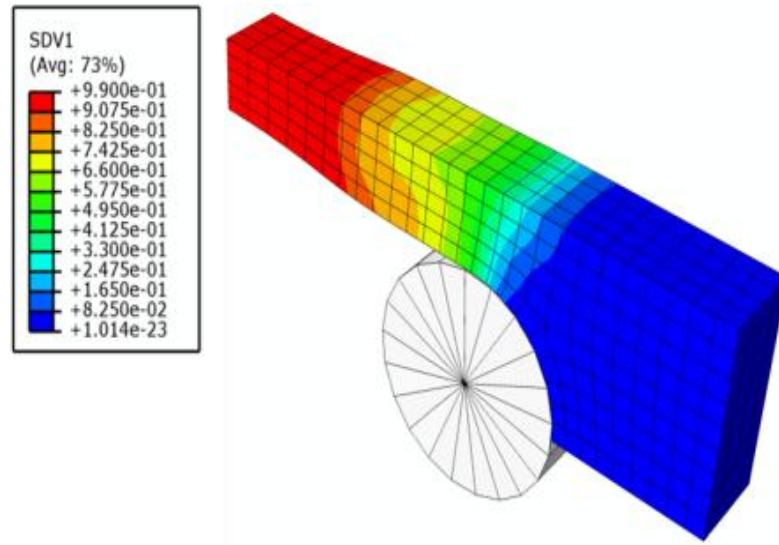
Fig. 4-6: Contour plot of damage parameter, ω, in the TBS for P91 at 600°C, (σ = 180 MPa, t_f = 90.81 hour).

The Liu-Murakami model [11] was also used to assess the effects of the friction between the loading pins and the specimen surfaces during loading

application. Various coefficients of friction (µ) were used in the FE analyses, to investigate the effects of the contact properties between the loading pins and the specimen surfaces, as described in Table 4-1. It has been found that for a large range of the coefficient of friction, the specimen failure times remained practically unchanged indicating that the contact friction does not have any measurable effect on the creep deformation.

Table 4-1:   Illustrate the effect friction coefficient factor on the specimen failure time for (P91 steel, T= 600°C, σ = 170MPa).

Friction coefficient factor (µ)	t_f (hour)
0.001	169.025
0.01	169.011
0.1	169.067
0.15	169.103
0.2	169.099

4.4.4   The determination of the reference stress parameters for the TBS

FE analyses was used to determine the reference stress parameters, i.e. the conversion factors η and β, for the TBS. Accurate determination of the reference stress parameters allows the equivalent gauge length (EGL) and the corresponding uniaxial stress for the specimen to be accurately obtained. Using a Norton material model, FE analyses were performed to obtain the steady-state deformation rates between the two loading pins for a range of n values. Similar to Fig. 4-1. the steady state deformation rates, $\dot{\Delta}_{ss}^{c}$ are

normalised, by $L_O A(\alpha \dfrac{P}{2bd})^n$, where P is the applied load [5]. However,

because only a quarter of the specimen is used in the FE analyses and half of

the specimen thickness, (see Fig. 4-4), the obtained minimum deformation

rates have to be doubled and the nominal stress will be $\dfrac{P}{0.5\,bd}$. Several α'

values were considered for all of the deformation rate values, with different

n-values. The value of α' which makes $log\left(\dfrac{2\dot{\Delta}_{ss}^c}{L_O A(\alpha' \dfrac{P}{0.5\,bd})^n}\right)$ practically

independent of n is the required α' value. This value (corresponding to the

solid line in Fig. 4-7), is the reference stress parameter, η, for the particular

TBS geometry and dimensions. The value of β can then be obtained from the

intercept of the solid line in Fig. 4-7. The procedure is described in more

detail in reference [5].

$$Log\left(\frac{2\,\dot{\Delta}_{ss}^{c}}{L_o\,A(\alpha\frac{P}{0.5\,bd})^n}\right)$$
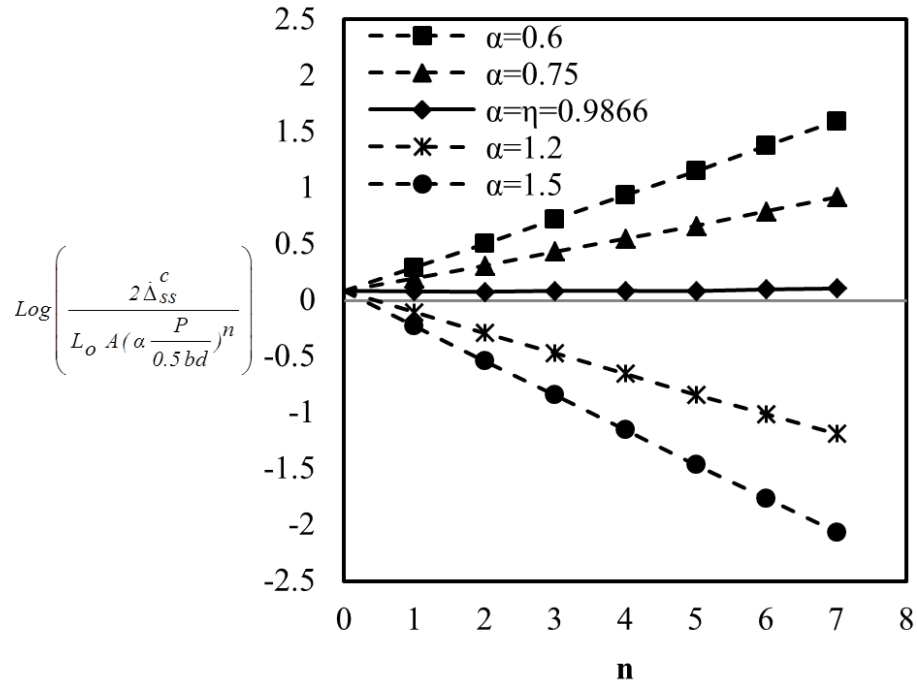
Fig. 4-7   Determination of β and η for the TBS.

4.5   EFFECTS OF TBS DIMENSIONS ON CONVERSION FACTORS AND FAILURE TIME

4.5.1   Effects of Specimen Dimension Ratios on the η and β Values

The specimen dimensions that can be used for testing are not rigidly fixed in order to allow specimens to be constructed from different shapes and volumes of material samples that may be available. The specimen geometry is defined by dimension ratios, i.e., $\frac{L_o}{D_i}$, $\frac{k}{D_i}$ and $\frac{b}{D_i}$ (see Fig. 4-2). Since the conversion factors η and β are geometry dependent, the three dimension ratios will have an effect on the conversion factors. Consequently, making the most appropriate choice of specimen, dimension ratios may affect the

127

conversion factors, and lead to the most accurate interpretation of the MSR and rupture data. A series of 3D steady state creep analyses using Norton's law have been carried out to assess the effects of the dimension ratios on the η and β values using meshes which consist of 20-noded brick elements as in Fig. 4-4. The nominal stress in the specimen bars were kept constant. Rigid pins were used throughout and the contact conditions, material properties and pin diameter were kept the same for all cases. The total TBS deformation rate measured at the centres of the loading pins, $\dot{\Delta}_{total}$, can be approximated by:-

$$\dot{\Delta}_{total} = \dot{\Delta}_{L_o} + \dot{\Delta}_k \tag{4.13}$$

where $\dot{\Delta}_{L_o}$ is the deformation rate of the uniform bars of length L_o and $\dot{\Delta}_k$ is the deformation rate (in the loading direction) of the supporting material around the loading and constraining pins. In fact, $\dot{\Delta}_k$ is a combination of two deflections, i.e. ($\dot{\Delta}_k^c$ and $\dot{\Delta}_{k(bending)}$), where $\dot{\Delta}_k^c$ is the creep deformation rate in the contact region and $\dot{\Delta}_{k(bending)}$ is the deformation rate as result of the bending in the supporting material (if k is small enough for significant bending to occur, see Fig. 4-4).

4.5.1.1 The effect of $\frac{L_o}{D_i}$ ratio

Several $\frac{L_o}{D_i}$ ratios were considered for this study. During this study the other two dimension ratios $\frac{k}{D_i}$ and $\frac{b}{D_i}$ were fixed at constants values. However, the

ratio $\frac{k}{D_i}$ was large enough to avoid any significant bending in the supporting material. The study was repeated for three different $\frac{b}{D_i}$ ratios as indicated in Fig. 4-8 .As the $\frac{L_o}{D_i}$ ratio increases with a constant $\frac{k}{D_i}$ and $\frac{b}{D_i}$ ratios, the contribution of the $\dot{\Delta}_{L_o}$ to the total specimen deformation rate increases, therefore the conversion factors approach a value of unity for very high $\frac{L_o}{D_i}$ ratios. As the ratio $\frac{L_o}{D}$ increases significantly the specimen deformation is predominantly uniaxial, where η and β are both close to unity, as illustrated in Fig. 4-8. However, as the $\frac{L_o}{D_i}$ ratio reduced, the contribution of the $\dot{\Delta}_{L_o}$ to the total specimen deformation rate decreases, resulting in an increase in the β value and a decrease in the η value for small $\frac{L_o}{D_i}$ ratios.
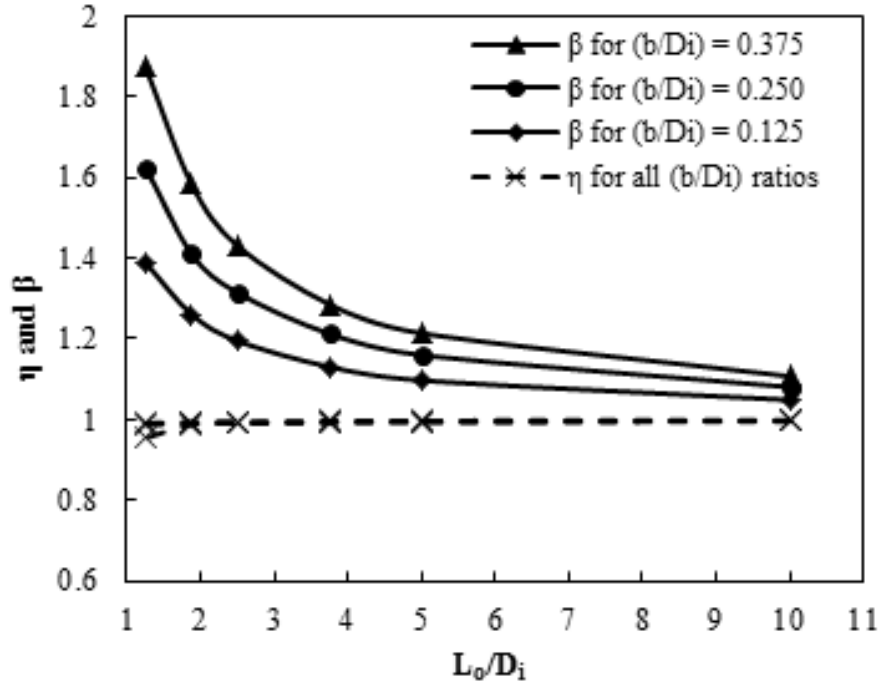
Fig. 4-8: Variations of β and η parameters with various $\frac{L_o}{D_i}$ ratios; the ratio $\frac{k}{D_i}$ for the specimens was 2 for all cases.

4.5.1.2 The effect of $\frac{k}{D_i}$ ratio

For this investigation seven $\frac{k}{D_i}$ ratios were used, while the other two dimension ratios $\frac{L_o}{D_i}$ and $\frac{b}{D_i}$ were fixed at constant values. The study was repeated for three different $\frac{L_o}{D_i}$ ratios. In this case, the changes in the total specimen deformation rate, i.e., equation (4.13), will be governed only by the changes in the loading pins supporting material deflections. When the supporting material is large enough to prevent significant bending, the contribution of $\dot{\Delta}_k$ to the total specimen deformation rate becomes constant; and therefore the conversion factors become constant for any $\frac{k}{D_i}$ ratios above about 1.25, as illustrated in Fig. 4-9. However, for very small $\frac{k}{D_i}$ ratios, where

130

significant bending in the k region may occur, the contribution of $\dot{\Delta}_k$ to the total specimen deformation rate will be significant. Therefore, the conversion factors, in particular the β value, changes significantly with $\frac{k}{D_i}$ when k is relatively small, as illustrated in Fig. 4-9.
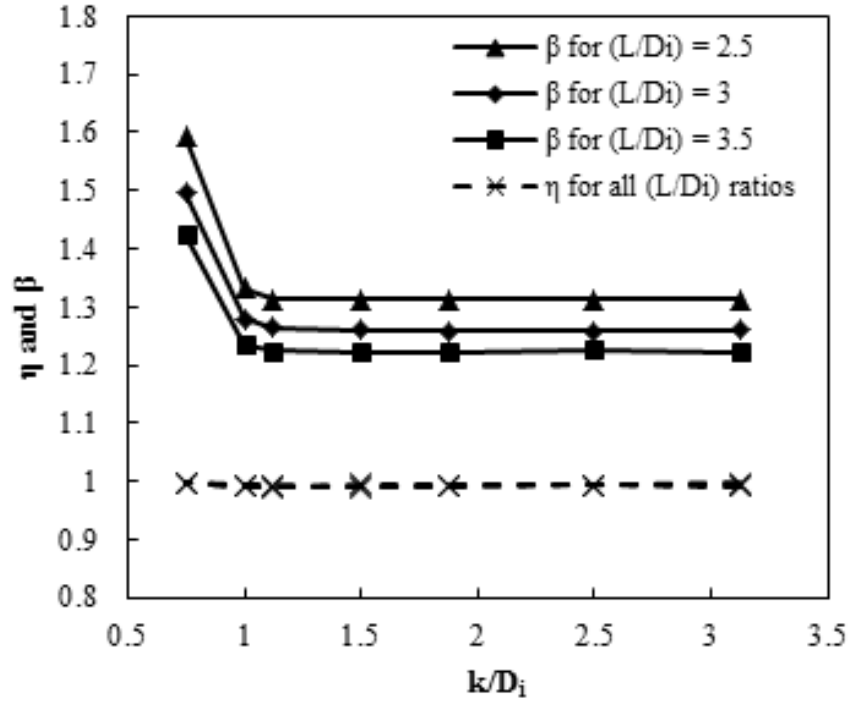
Fig. 4-9:   Variations of β and η parameters with various $\frac{k}{D_i}$ ratios; the ratio $\frac{b}{D_i}$ for the specimens was 0.25 for all cases.

4.5.1.3 The effect of $\frac{b}{D_i}$ ratio.

Six $\frac{b}{D_i}$ ratios were used in this study, while the other two dimension ratios $\frac{L_o}{D_i}$ and $\frac{k}{D_i}$ were fixed at constant values. The study was repeated for three different $\frac{L_o}{D_i}$ ratios as in Fig. 4-10. Changing the $\frac{b}{D_i}$ ratio requires modification

131

to the applied load in order to maintain a constant nominal stress level for all specimens used in the study. However, increasing the load magnitude, P, with constant contact area between the loading pins and the loading pins supporting material, i.e. k region, (see Fig. 4-4), results in an increase in the localised deformation rate in the contact region. In this case, $\dot{\Delta}_k$ in equation (4.13) is proportional to the ratio $\frac{b}{D_i}$ for a constant loading pin diameter.

For small $\frac{b}{D_i}$ ratios, i.e. $\sim \leq 0.2$, the deformation rate in the loading pin supporting material (contact region) is not large and the contribution of $\dot{\Delta}_k$ to the total specimen deformation rate in equation (4.13) is very small compared to $\dot{\Delta}_{L_o}$. Therefore, as expected, the conversion factors are close to unity. The applied load increases with the ratio $\frac{b}{D_i}$, consequently causing large deformation in the loading pins supporting material. Therefore, the contribution of the deformation rate caused by the loading pin supporting material deflections to the overall specimen deformation rate increases with the increases of the $\frac{b}{D_i}$ ratio as shown in Fig. 4-10. However, the values of η remain practically constant and close to unity for all $\frac{b}{D_i}$ ratios used in the study.
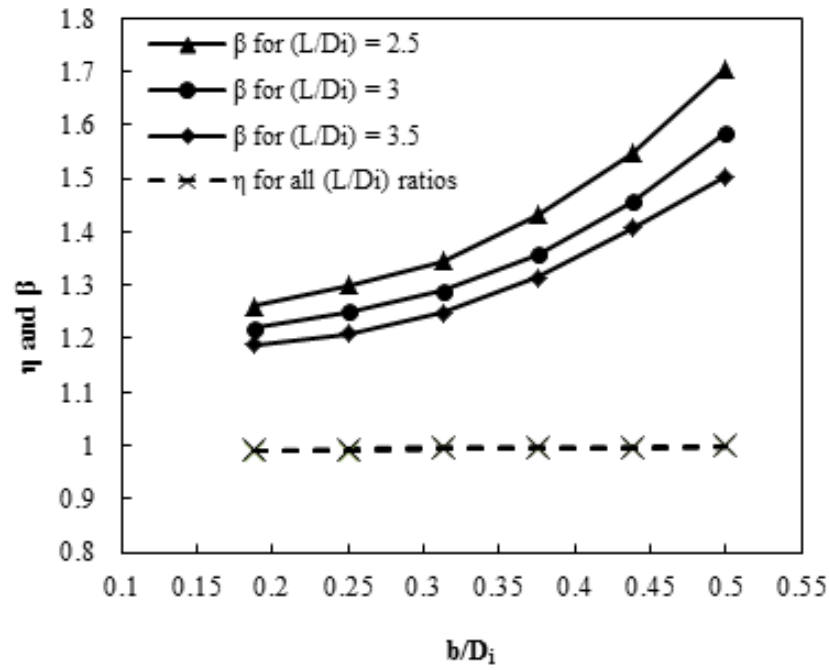
Fig. 4-10: Variations of β and η parameters with various $\dfrac{b}{D_i}$ ratios; the ratio $\dfrac{k}{D_i}$ for the specimens was 2 for all cases..

4.5.1.4 The effect of $\dfrac{d}{D_i}$ ratio

The effect of TBS depth, d, on the η and β values was investigated using FE analyses. The two extremes of behaviour, i.e. plane stress condition ($d \approx 0$) and plane strain condition ($d \approx \infty$), were investigated using meshes consisting of 8-noded for the plane stress, PS, and 8-noded, plane strain, PE, elements, respectively. The intermediate behaviour was also investigated using meshes which consist of 20-noded, 3D brick element (see Fig. 4-4). Various values of d were used, while all other specimen dimensions were kept constant for the analyses. The 3D specimen model dimensions L_o, K, β and D_i were 20, 6, 2 and 5mm, respectively, where the specimen depth, d, in

the 3D analyses, were taken to be 0.25, 1.00, 1.50, 2.00, 2.50, 3, 10 and 20 mm. The applied loads for the 3D cases were increasing with the specimen depth increase in order to maintain the same nominal stress in the uniform part of the specimen, L_o.

The results presented in Fig. 4-11 and Fig. 4-12 show that under plane stress conditions, where d is very small, i.e., close to zero, β and η have the highest values, which are 1.306 and 0.999, respectively. Under plane strain conditions, where d considered to be very large i.e. the d/D_i ratio is effectively infinite, β and η have the lowest values, which are 1.031 and 0.912, respectively. The β values obtained from the 3D analyses were as expected, varying between those obtained from the plane stress and the plane strain conditions, i.e. as the $\frac{d}{D_i}$ ratio increases, the values of β decreases and for very small $\frac{d}{D_i}$ ratio, β become almost equal to those obtained from plane stress condition as seen in Fig. 4-11 . On the other hand, the η values obtained from the 3D analyses remain practically constant, being nearly equal to the values obtained for plane stress conditions as can be seen from Fig. 4-12.
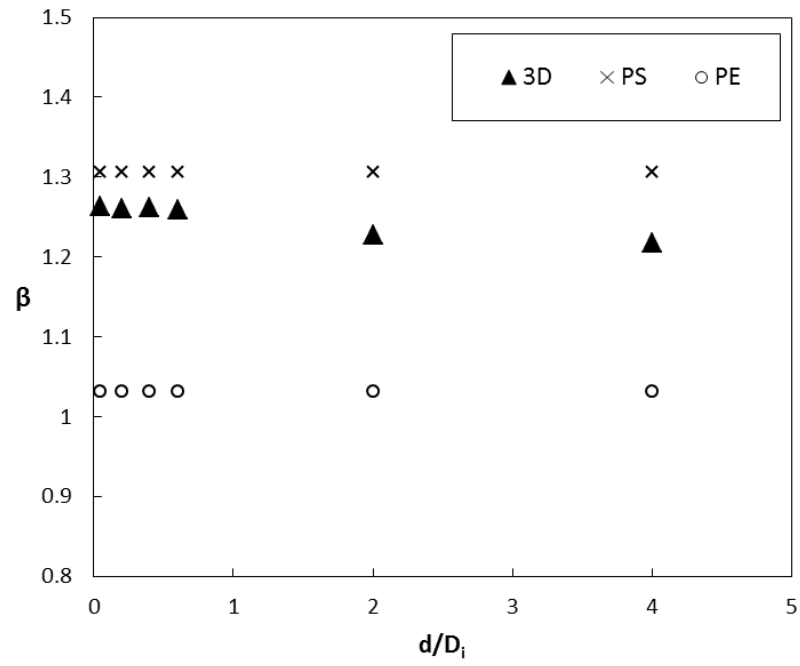
Fig. 4-11: The effects of d/D_i ratio on β values for specimen with L_o =20, K= 6mm, b=2mm and D_i =5 mm.
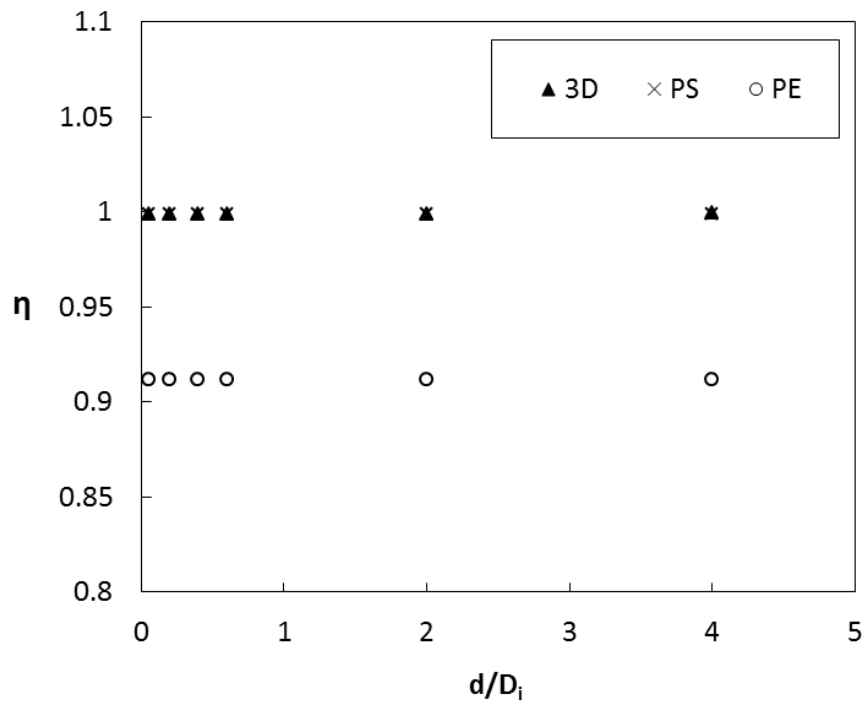
Fig. 4-12: The effects of d/D_i ratio on η values for specimen with L_o =20, K= 6mm, b=2mm and D_i =5 mm.

4.5.2 The effect of the loading pin diameter, D_i, on the Conversion Factors

The variations of β and η parameters with D_i have been also investigated using five D_i values, (i.e. D_i = 5, 6, 7, 8, and 9 mm). The bar width, b, changes with D_i, and the supporting material behind the loading pin were kept large enough to prevent significant bending for all cases, whereas L_o remains constant for all cases at 18 mm; the b value was increased with each reduction in D_i. The applied load, P, has to be increased as b increases in order to maintain the same stress levels for all cases. However, increasing the applied load and reducing the loading pin diameter at the same time results in significant deflections in the supporting material behind the loading pin. Therefore, the contribution of the $\dot{\Delta}_k$, in equation (4.13), to the total specimen deformation increases significantly for small D_i. From Fig. 4-13 one can deduce that β is inversely proportional to D_i. i.e.,

$$\beta \propto \frac{1}{D_i}$$

In contrast, η remains practically constant and close to unity for this range of D_i. It was practical to keep the loading pin diameter, D_i, constant during each dimension ratio study, i.e. $\frac{b}{D_i}$, $\frac{L_o}{D_i}$ and $\frac{k}{D_i}$, because changing , D_i will affect both the supporting material behind the loading pin and the $\frac{b}{D_i}$ ratio, if the rest of the specimen dimensions are assumed to be constant.

In actual creep testing situations the loading pin diameter, D_i, should not be very small in relation to other specimen dimensions in order to (i) avoid high stress concentration and significant deformation in the pin region, (ii) maintain sufficient stiffness in order to avoid significant bending in the loading pins during the test.
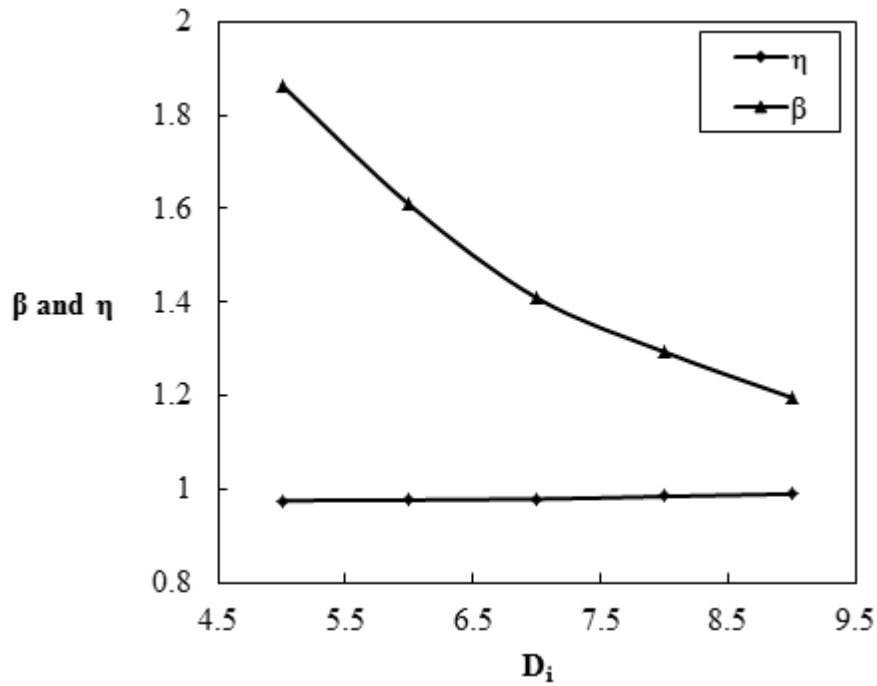
Fig. 4-13:   Variations of β and η parameters with D_i, for specimens with L_o = 18 mm and b = (0.5, 1, 1.5, 2 and 2.5mm).

4.5.3   The effect of TBS depth, *d,* on the failure time

The volume and shape of the small sample of material available for testing dictates the specimen dimensions including the specimen thickness. Therefore, the effect of TBS depth, *d,* on the failure time and on the minimum strain rate was investigated using FE analyses. Liu-Murakami damage model [3, 11] was used to obtain the TBS time to failure while Norton's model was

used to obtain the minimum strain rates. The investigation was carried out using a 3D specimen model with meshes consisting of 20-noded, 3D brick elements (see Fig. 4-4). The 3D specimen model dimensions for the damage analysis, L_o, K, b and D_i were 20, 8, 1 and 5 mm, respectively, whereas for the Norton's model they were 16, 8.5, 2 and 5 mm, respectively. Six values of d were chosen for both cases while the rest of the specimen dimensions were kept constant including the loading pin diameter. The applied load was increased with the d value in order to maintain the same nominal stress in the uniform part of the specimen for all cases. Equation (4.7) has been used to convert the FE, TBS minimum displacement rates to minimum strain rates. As seen from Fig. 4-14 and Fig. 4-15 the effect of specimen thickness on both the failure time and the minimum strain rate for constant stress is practically negligible.
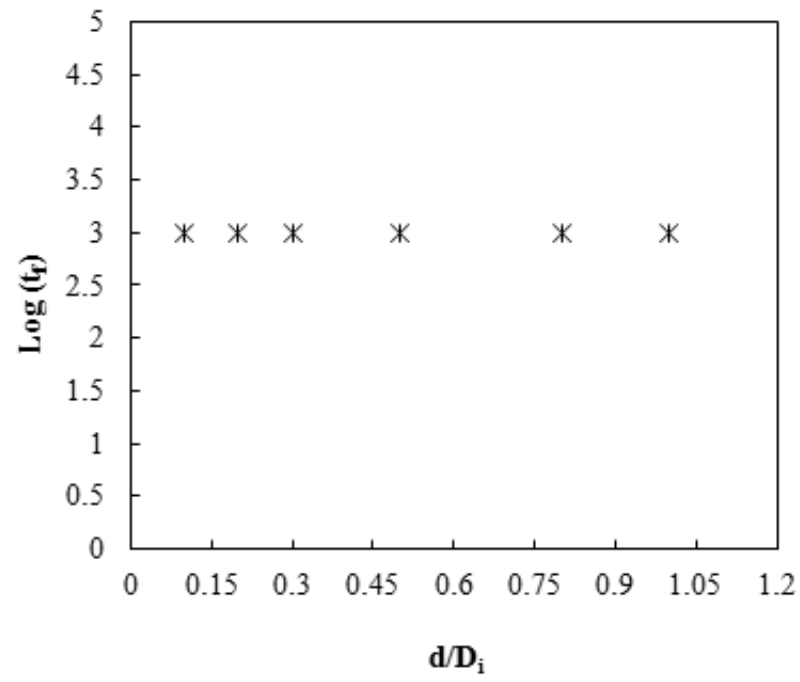
Fig. 4-14:   The effect of the TBS depth, *d*, on the failure time.
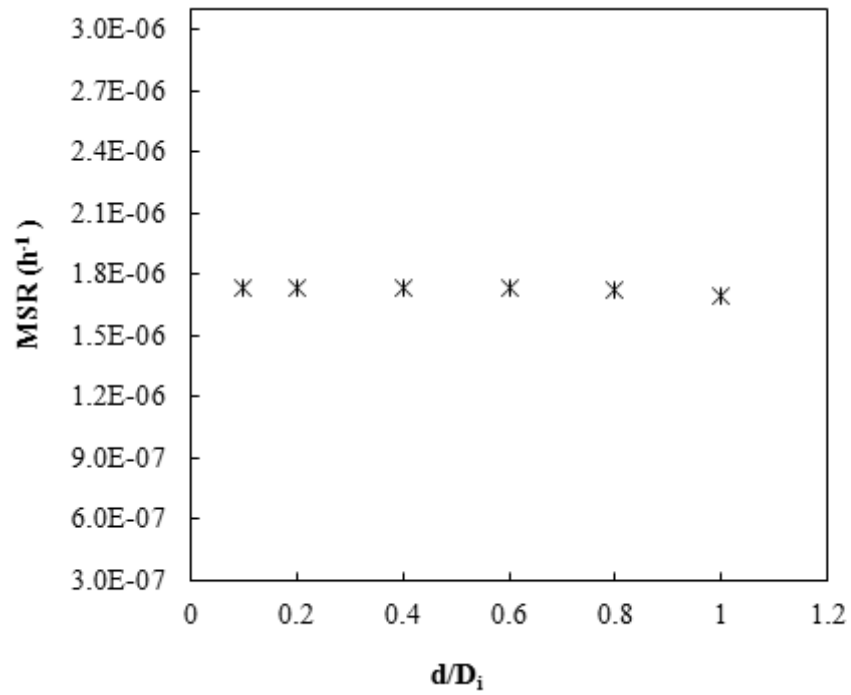
Fig. 4-15:   The effect of the TBS depth, *d*, on the minimum strain rate.

4.6 RECOMMENDED SPECIMEN DIMENSION RATIO RANGES

The actual specimen dimensions chosen for a particular application may be dictated by the shape and size of the small sample of material available. However, the specimen is designed to obtain creep properties from the overall specimen creep deformation; not from the localised deformation (which occurs in the contact area between the loading pins and the loading pins supporting material). In order to make a suitable choice of the specimen dimension ratios, with minimum localized deformation in the contact areas, the FE analyses results presented in Fig. 4-8 to Fig. 4-13 can be used as a guide.

It is recommended that specimen dimension ratios, which minimise the contribution of the deformation in the loading pins supporting material, should be used when it is possible, as indicated in Fig. 4-8 to Fig. 4-13. The η values, for the range of specimen dimension ratios, should be close to unity and practically independent of the specimen dimensions. However, the β values are always dependent on the magnitude of to the contribution of the deformation rate in the loading pins supporting material to the total specimen deformation rate, i.e. β is dependent on $\frac{\dot{\Delta}_k}{\dot{\Delta}_{total}}$. Hence the recommended ranges of specimen dimension ratio are given in Table 4-2. The specimens which were experimentally tested had dimension ratios, (see

Fig. 4-3 (b) , which fall in the range of the dimension ratios given in Table 4-2.

Table 4-2:   The recommended TBS dimension ratio ranges for a constant D_i.

Dimension ratios	Range
L_o/D_i	~ $\geq$ 2.0 - 5.0
k/D_i	~ $\geq$ 1.0
b/D_i	~ 0.2 - 0.47
b/d	~ 1.0

4.7   PRELIMINARY FE VALIDATION

Preliminary validation of the testing technique was carried out using 3D- FE analyses and Norton's law, to assess the accuracy of the conversion relationships, i.e., equation (4.7) and conversion factors, i.e., η and β. The specimen steady state deformation rates were obtained for several n values, theoretically, using equation (4.14),

$$\dot{\Delta} = L_O \times \beta \times A\left(\eta\sigma\right)^n \tag{4.14}$$

and numerically using FE analyses. The specimen dimensions, L_o, k, b, d and D_i were (13.0, 6.5, 2.0, 2.0 and 5.0 mm), respectively. These specimen dimensions result in conversion factors β and η values of 1.4557 and 0.9966 respectively. For this study the magnitude of the material constant A in Norton's law was 1E-16 for all cases, and the applied load corresponded to a constant stress of 50MPa. The load was calculated using equation (4.4).

141

The correlation between the steady state displacement rates obtained theoretically and numerically is remarkably good as shown in Fig. 4-16. Another FE analysis was carried out using different specimen dimensions and therefore different conversion factors. The dimensions L_o, k, b, d and D_i for the second specimen were 20.0, 6.0, 1.0, 1.0 and 6.0 mm, respectively, for which β and η were 1.179 and 0.991, respectively. For this study the material constant A in Norton's law was 1E-17 and the applied load corresponded to a stress of 80MPa. The specimen steady state deformation rates were obtained theoretically using equation (4.7) and (4.14), and numerically using FE for a number of n values. Again, very good agreement was obtained between the two sets of results, as seen in Fig. 4-17.
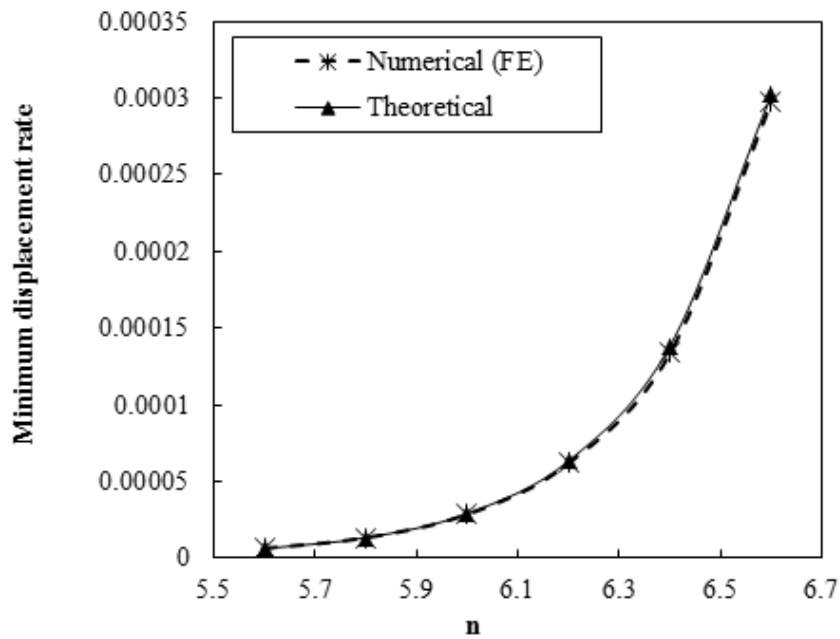
Fig. 4-16:   The steady state deformation rates obtained from the TBS theoretically and numerically (FE) using $\beta =1.4557$.
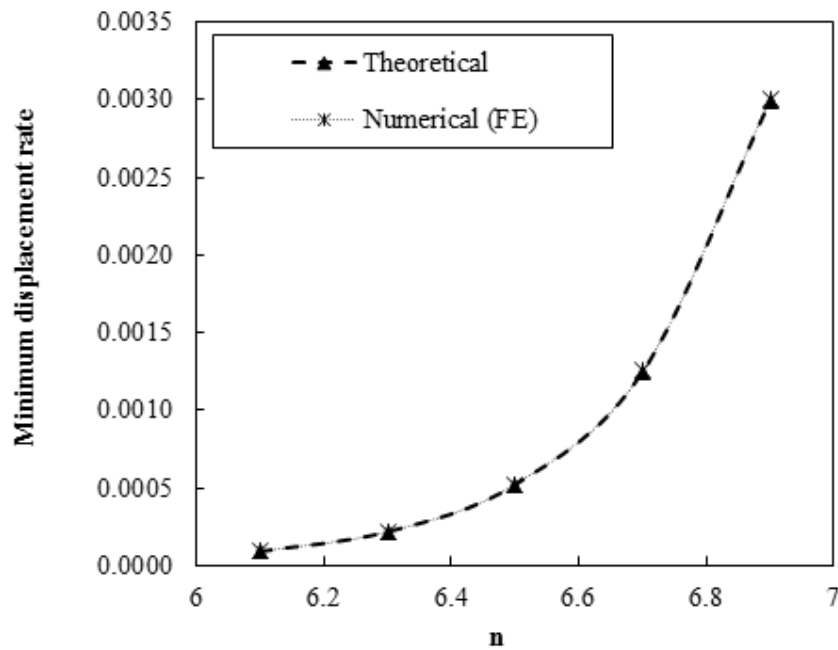
Fig. 4-17:   The steady state deformation rates obtained from the TBS theoretically and numerically (FE) using $\beta = 1.179$.

4.8   DISCUSSION AND CONCLUSIONS

The novel, small TBS is close in its behaviour to that of a miniature uniaxial specimen. The main advantage of the small TBS type, over other miniature creep test specimen types, is that a full creep strain versus time curve, till rupture, can be obtained by using such a specimen type. Another advantage is that the specimen has a simple geometry and can be easily machined and tested. Similar to the small ring creep test specimen [103], the measured deformation of the TBS is related to the overall creep deformation of the specimen, not to the local area of contact between the specimen and the loading device.

143

The conversion factors η and β depend on specimen dimension ratios and are independent of the tested material. Loading the specimen through loading pins makes it possible to achieve accurate aligning and hence to avoid possible bending effects, as would be experienced if a small cylindrical uniaxial specimen was used, where the loading is applied through "stiff" connection of the specimen ends. The design of the TBS requires a compromise between minimising the overall specimen dimensions and producing, as close as possible, a uniaxial state of stress. In addition, excessive deformation/stress concentration near the pin connections and bending of the supporting material behind the pins should be avoided. Also, the specimen design should be such that the creep deformation of the two uniform "bars" will dominate the overall specimen deformation.

The minimum dimensions of the TBS should take into consideration metallurgical effects, i.e. the grain size of the tested material should be much smaller than the smallest dimension of the specimen. In order to ensure that "bulk" properties are obtained a sufficient number of grains should be maintained in the uniform part cross section area of the specimen [7, 104, 105]. The changes in the conversion factors may be significant, and are dependent on the specimen dimensions especially for β as can be seen from Fig. 4-12 and Fig. 4-13. However, as long as the accurate conversion factors

144

are used in the conversion relationship, for the particular specimen dimensions, accurate creep data can be obtained.

From the preliminary validations, it can be seen that despite a significant differences in β values between case one, β =1.4557, and case two, β =1.179, a remarkably good agreement has been achieved between theoretical and numerical results, as shown in Fig. 4-16 and Fig. 4-17. However, any design which involves large deformation in the loading pin region should be avoided; because the aim of the new TBS testing technique is to obtain creep properties from the overall specimen, not from the small local area of contact between the loading pins and the specimen.

CHAPTER 5.

EXPERIMENTAL TESTING FOR THE TBS AND VALIDATION

_____

5.1   INTRODUCTION

The preliminary validations which were presented in Chapter 4, using FE analyses to assess the accuracy of this novel testing method, produced remarkably good agreement between the numerical and the theoretical results. However, experimental validations are also necessary for the new testing method in order to strengthen the case for the use of the finite element analyses and theoretical predictions presented in Chapter 4. This chapter is mainly concerned with the experimental programme of the TBS creep testing, the specimen manufacturing possesses and the experimental setup.

Two versions of P91 steels are considered for the validation program (i) the first is a typical, as-received, P91 pipe material, designated using the ASTM code as A-369 FP91, and (ii) a P91 pipe cast (indicated here as Bar 257), which has much lower creep rupture strength than the mean code data for P91 steel. The minimum strain rate and failure life are obtained using the new specimen type and these compared with those obtained from the

corresponding uniaxial creep data. These results demonstrate that the specimen type is capable of producing full uniaxial creep strain curves, minimum creep strain rate and failure time, with a high level of accuracy. The advantages of this new testing technique are discussed; conclusions and recommendations are also given in the last section of this chapter.

5.2 SPECIMEN DIMENSIONS, LOADING AND EXPERIMENT SET-UP

5.2.1 Specimens preparation

The tested specimens were manufactured and tested within the faculty of engineering at the University of Nottingham. Electrical discharge cutting system (EDM) was used to manufacture the specimens [106]. It was convenient to use this cutting method to manufacture the specimens, because of the small size of the TBS dimensions and the strong need to obtain identical bars with a good finish. The Two bar specimen cutting operation is described in Fig. 5-1 and the EDM cutting operation properties and specifications have been described in Section 3.6.1.

The cutting operations were performed with a circulating cooling liquid [94, 95]. Various cooling liquid types can be used in the EDM cutting operations. Some sensitive, micro scale, EDM machines uses oil based cooling liquids [107], whereas other EDM machines uses de-ionised water as the cooling

liquid, e.g., the AQ750L machine which was used to cut the TBSs for the present work. The cooling liquid plays a significant role in the TBS cutting operation and on the surface finishing [108]. The major benefits of this cooling liquid can be summarised as:-

➢ Extending the lifespan of the cutting wire

➢ Reducing the spark during the cutting operation

➢ Cooling the specimen during the cutting operation

In practical situations, the TBS can be easily manufactured from small material samples removed for example from component surfaces, using one of the Surface Sampling System (SSam) techniques. The technique can be easily used to remove small scoop samples from the component surfaces without affecting the component safe operation.

Specimens can also be constructed from small material zones such HAZ or WM of a weldment. Small thin pieces of material can be removed from these zones with dimensions of $\sim 1 \times \sim 4.5 \times \sim 40$ mm, a piece with these dimensions can be conveniently cut out of the HAZ or WM of arc welded steam pipes or pipe bends along the welding direction. Three TBSs can be easily constructed from such samples using the EDM cutting system, as illustrated in Fig. 5-1. In order to ensure that identical uniform bars are obtained, the cutting start and end points are located in the region behind the loading pins (see Fig. 5-1), In order to ensure a high quality surface

finish, especially in the uniform part of the specimen (L_o), the specimens were carefully polished to their final dimensions.
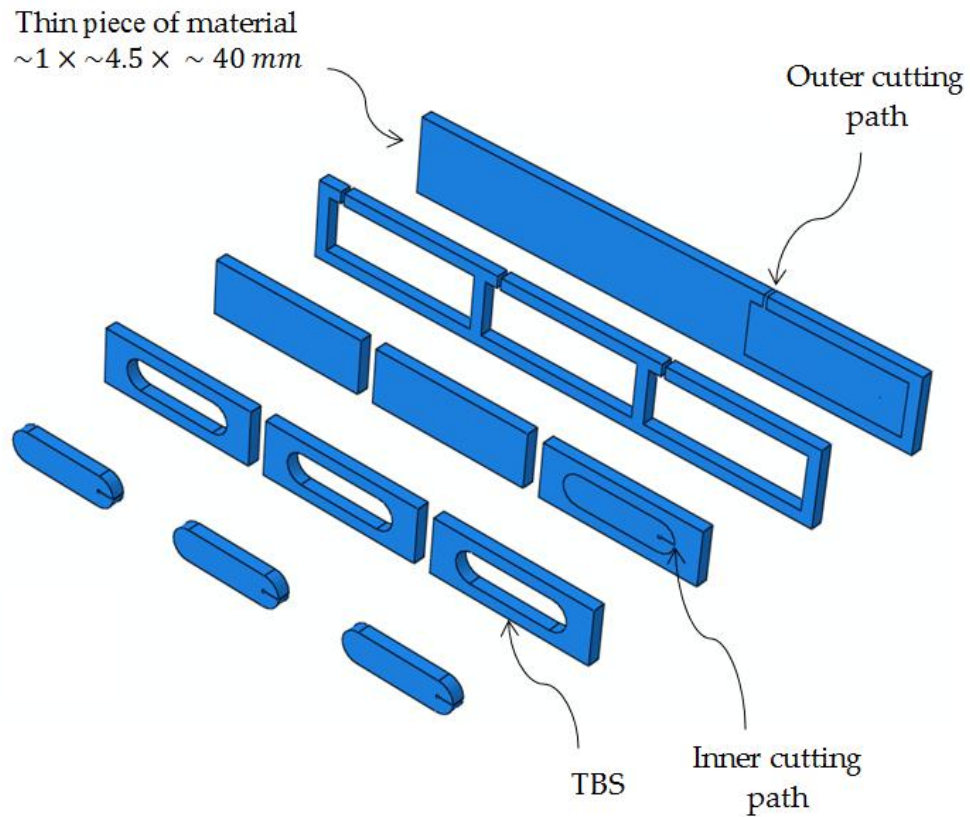
Fig. 5-1:   The TBS cutting operation using thin piece of material removed from the HAZ/WM regions and the EDM cutting system

5.2.2   Specimens Loading and Experimental Setup

A tensile load is applied to the TBS through pin connections; using two loading pins (see Fig. 5-2), a creep testing machine "Tinius Olsen H25KS" has been used to test the specimen (see Fig. 3-18). The specific specimen dimensions used for L_o, k, b, d and D_i were 13.0, 6.5, 2.0, 2.0 and 4.974 mm, respectively. These dimensions were used because small material samples, with dimensions of approximately 30 × 20 × 3 mm, can be conveniently

removed from a component surface using the nun destructive Surface Sampling System (SSam), [46]. However, these specimen dimensions can be easily scaled down by 25% or 50% if necessary. Furthermore, because the recommended specimen dimensions (see Section 4.6) have been given as ratios, i.e. variable rather than fixed values, the specimen can be made with even smaller dimensions, if needed. The loading pins diameter is 4.974 mm, which result in a clearance between the loading pins and the specimen surface of about 0.026 mm, this clearance is just enough to allow the specimen to achieve accurate aligning during the loading application. The loading pins and the loading pin holders (see Fig. 5-2) were manufactured from a Nickel-base Superalloy (Nimonic 80A), which has much higher creep resistance than the tested material; this ensures that the deformation of the loading fixture is negligible. The reference stress parameters for the tested Two-bar specimen are reported in Table 5-1. These parameters have been obtained using the same procedure described in Section 4.4.4,

Table 5-1   The reference stress parameters for the tested Two-bar specimen

η	0.9966
β	1.4557

Also the specific set of dimension ratios for the tested Two-bar, i.e. $\frac{L_o}{D_i}$ = 2.6, $\frac{b}{D_i}$ = 0.4 and $\frac{k}{D_i}$ = 1.3, with a loading pin diameter D_i of 4.974 mm. These

150

dimensions fall within the recommended TBS dimension ratios ranges
presented in Table 4-2.

(a)
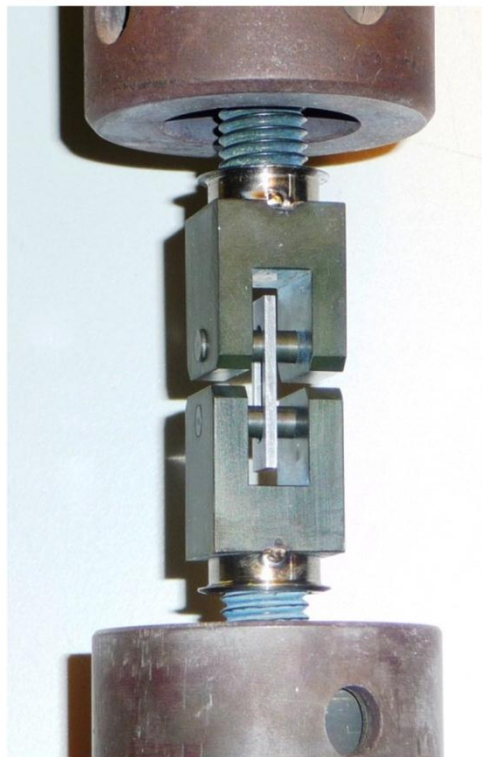
(a)

Fig. 5-2 Photos of the TBSs (a) and the TBS loading arrangement (b)

5.3 MINIMUM CREEP STRAIN RATES AND CREEP RUPTURE DATA FOR THE P91 STEEL AT 600°C.

The TBSs were constructed using P91 steel parent material [2]This material is used extensively in the pipework of power plants. P91 is a high strength, steel capable of operating at elevated temperatures. Table 5-2 shows the chemical composition of the tested P91 steel parent material (PM). Conventional uniaxial creep test specimens (see Fig. 2-5) were manufactured using P91 steel and creep tested at 600°C. The tests were carried out at stress levels of 140, 150, 160, 170 and 180 MPa; the uniaxial creep-time curves are shown in Fig. 5-3. It can be seen that the strain time curves exhibit relatively small primary creep behaviour and comparatively long secondary and tertiary regions.

Table 5-2   Chemical compositions for the P91 steels (wt%)

Material	C	Mn	Si	N	Cr	Mo	Nb	Cu	V
A-369 FP91	0.109	0.443	0.307	0.042	8.350	0.948	0.165	0.152	0.210
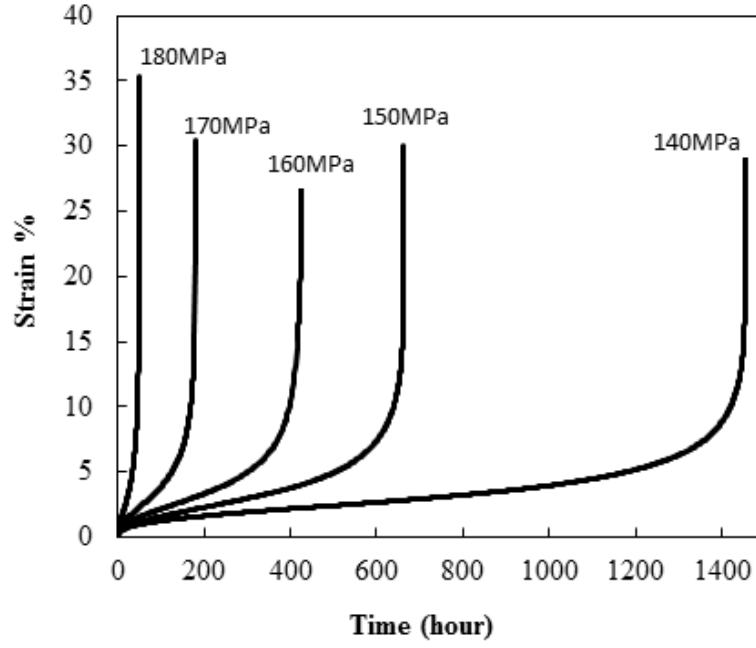
Fig. 5-3:   Creep strain versus time curves obtained from uniaxial tests for P91 steel at 600°C

Five TBSs were creep tested (see Fig. 5-4 and Fig. 5-6) with loads corresponding to uniaxial stresses of 140, 150, 160, 170 and 180 MPa, respectively, where equation (5.1) was used to calculate the applied load for each stress.

$$\sigma_{ref} = \eta\, \sigma_{(nom)} \tag{5.1}$$

where σ_{ref} is the reference stress, which, in this case, uses the corresponding uniaxial stresses, η, the reference stress parameter for the specimen and $\sigma_{(nom)}$ is the nominal stress in the uniform part of the specimen. The conversion relationship, i.e. equation (5.2), has been used to convert the TBS

153

minimum creep deformation rates, measured between the centres of the loading pins, to the equivalent uniaxial minimum creep strain rates, i.e.

$$\dot{\varepsilon}^c = \frac{\dot{\Delta}_{ss}^c}{\beta \, L_o} \qquad (5.2)$$

where $\dot{\varepsilon}^c$ is the equivalent uniaxial minimum creep strain rate, $\dot{\Delta}_{ss}^c$ is the TBS minimum creep deformation rate, L_o is the distance between the centres of the loading pins and β is the conversion factor, which is dependent on the relative specimen dimensions. The recorded deformation versus time curves obtained from the TBSs tests are shown in Fig. 5-5. The converted TBS minimum creep strain rates and the equivalent uniaxial minimum creep strain rates are plotted together using Log-Log scales in Fig. 5-7. The correlation between the uniaxial and the TBS data is good.

| (a) | (b) | (c) |
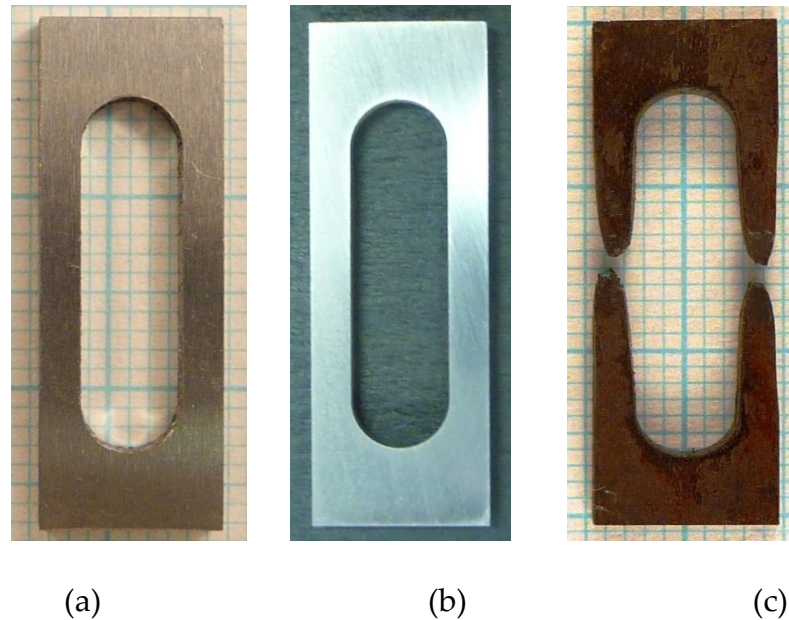
Fig. 5-4:   Untested specimen (a), polished specimen ready for testing (b), and tested specimen (c)
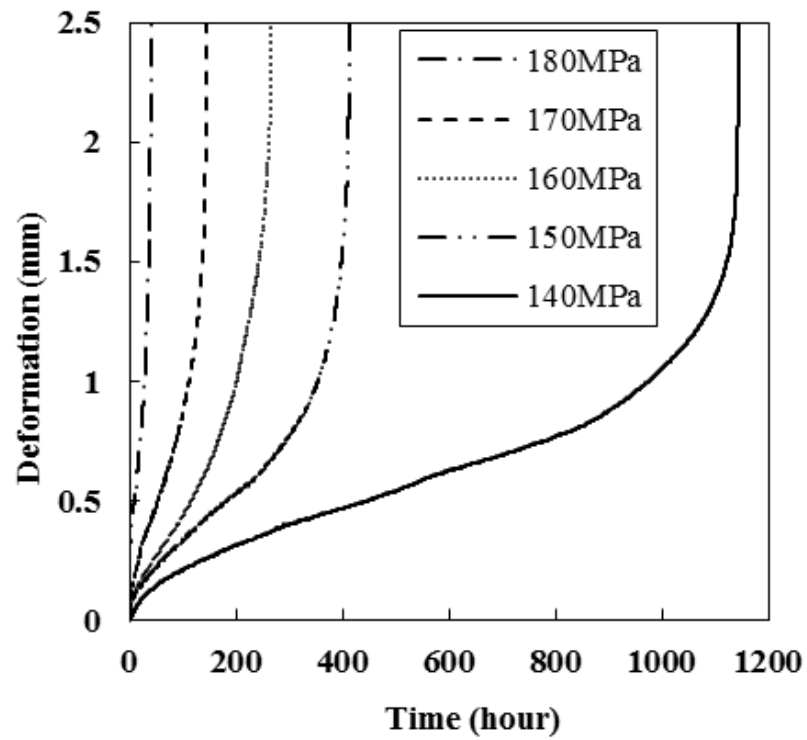
Fig. 5-5:   Deformation versus time curves obtained from the two bar specimens made
from a P91 steel tested at 600°C

Fig. 5-6:   The appearance of the tested TBSs made of P91 steel, and creep tested using
various stresses at 600°C, together with an untested specimen
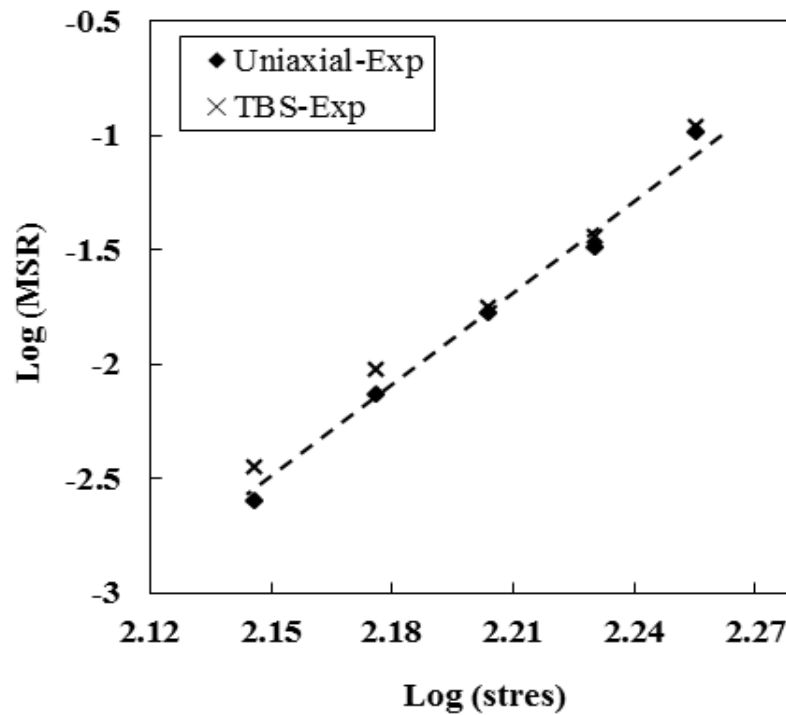
Fig. 5-7:   Minimum creep strain rate data for P91steel at 600°C

The TBS is unlike the small punch creep test (SPCT), where the specimen shape and dimensions change significantly during the test, from flat surface disk to a hemispherically ended shape. The changes in the overall TBS specimen shape and dimensions during the test are relatively insignificant (see Fig. 5-4 and Fig. 5-6). The changes in dimensions of some of the tested TBS are reported in Table 5-3.

Table 5-3: The dimensions of the tested TBSs made of P91 steel and tested at 600°C. The original specimens dimensions L_o, d, b and k were 13.0, 2.0, 2.0 and 6.5 respectively all dimensions are in (mm)

stress	L_o*	d*	b*	k*
140	16.26	1.95	1.99	6.49
150	15.63	1.98	1.95	6.43
160	17.25	1.92	1.87	6.53
170	16.54	1.94	1.94	6.51
180	-	-	-	-
Average	16.42	1.94	1.93	6.49
Changes%	26.30	2.62	3.12	0.153

(*) approximate dimension for the tested specimen

Table 5-3 demonstrates that, the average changes in the TBSs dimensions, i.e., L_o, d, b and k are about 26%, 2.6%, 3% and 0.15%, respectively. Table 5-3 also shows that the uniform part of the specimen dominates the TBS deformation; L_o experiences a relatively large elongation of approximately 26% of the original length. The changes of L_o, is about 3.5 mm, which make the ratio L_o/D_i at failure $\approx$ 3.3, whereas the L_o/D_i at the beginning of the test was 2.6. The total change of the L_o/D_i ratio during the test is about 0.9. The data presented in Fig. 4-8, shows that between these two L_o/D_i ratios, i.e. 2.6 and 3.3, both η and β factors remain practically constant. Since the changes in the specimen geometry and dimensions are insignificant, as indicated in Table 5-3, it is reasonable to assume that the conversion factors remain practically constant throughout the test duration. Hence, the TBS deformation time curves presented in Fig. 5-5 can be conveniently converted to strain versus time curves using equation (5.3), i.e.

$$\varepsilon^c = \frac{\Delta^c}{\beta \, L_o} \qquad (5.3)$$

where ε^c is the equivalent uniaxial creep strain, Δ^c is the TBS creep deformation , β is the reference stress parameter and L_o is the distance between the centres of the loading pins. The converted TBS strain-time curves are compared with the corresponding uniaxial curves in Fig. 5-8. The failure time versus applied stress for the TBS tests and the corresponding uniaxial tests are plotted together in Fig. 5-9, using (log-log scales). Again good correlation between the uniaxial and the TBS data is found.
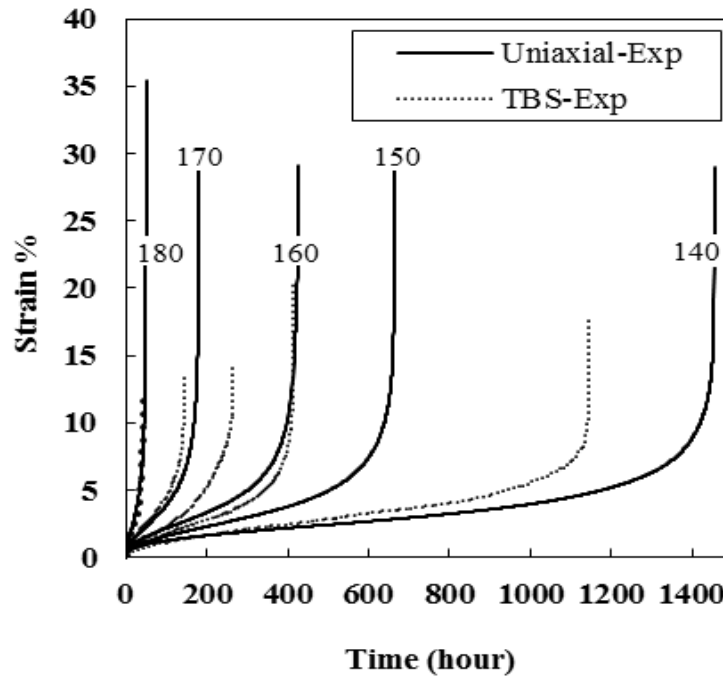
Fig. 5-8: Converted TBS creep strain versus time curves together with the corresponding uniaxial creep strain versus time curves, for P91steel at 600°C, the stresses in [MPa].
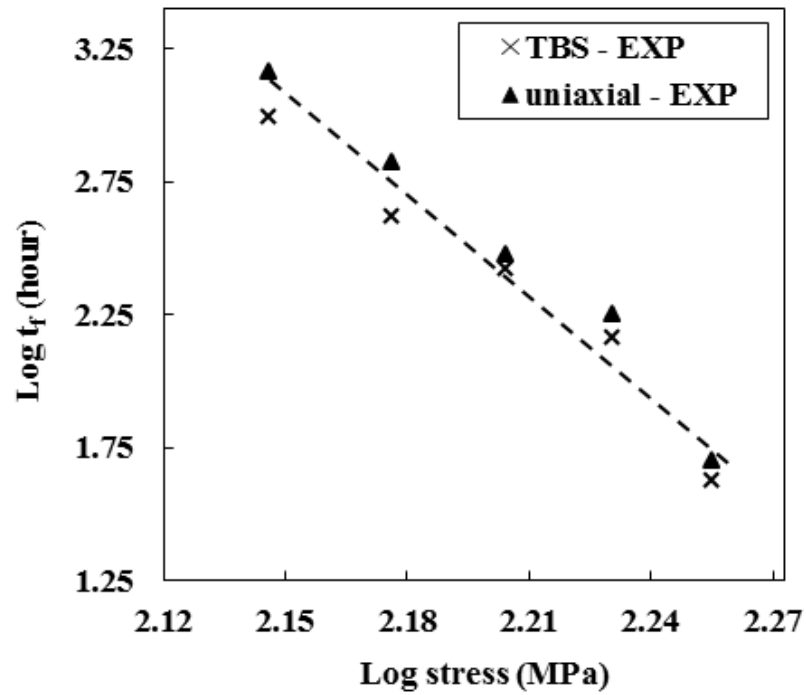
Fig. 5-9:   Creep rupture data obtained from the TBSs and the corresponding uniaxial
specimens for P91steel at 600°C

Table 5-4   Comparison between experimental MSRs (%) obtained from TBSs and the
corresponding uniaxial MSRs (%) for P91 steel at 600°C

Stress [MPa]	Uniaxial MSR [h⁻¹]	TBS MSR [h⁻¹]	Difference %
140	0.0025	0.00351	28.7
150	0.0074	0.0095	22.1
160	0.0166	0.01769	6.1
170	0.0321	0.03605	10.9
180	0.1037	0.10902	4.8

Table 5-5   Comparison between the failure time obtained from the TBSs and from the
corresponding uniaxial tests for P91 steel at 600°C

Stress [MPa]	Uniaxial (t_f)[h]	TBS (t_f)[h]
140	1454	1143
150	663	413
160	426	265
170	179	143
180	50	41

An investigation has been carried out to assess the differences between some of the TBS tests data and the corresponding uniaxial creep test data, as shown in Table 5-4 and Table 5-5. It is concluded that the differences are due to the scattering in the material, manufacturing and polishing procedures. However, for this material, an exact straight line fit between the log MSRs versus log stress (see Fig. 5-7) or log time to failure versus log stress (see Fig. 5-9), was not obtained even from full size conventional creep test specimens. Therefore, more TBS testing for this and other materials, at different stresses and temperature, should be carried out for the purpose of further validation.

5.4   MINIMUM CREEP STRAIN RATES AND CREEP RUPTURE DATA FOR THE (BAR-257) P91 STEEL AT 650°C

For further validation, Bar-257 P91 steel has been used to manufacture the TBSs. The material is also a modified 9Cr steel, a high strength, high ductility steel capable of operating at high temperatures. However, this material is weaker than typical P91 pipe material steel. Table 5-6 shows the chemical composition of the Bar-257 steel parent material (PM)[40]. Five conventional uniaxial creep test specimens were made from the same material and creep tested at 650°C; the tests were carried out at stresses of 70, 82, 87, 93 and 100 MPa, respectively. Strain time curves obtained from the uniaxial tests are shown in Fig. 5-10. The curves exhibit a relatively small primary creep region

and comparatively long secondary and tertiary regions. Pronounced tertiary

creep begins at a strain level of about 5.5%.

Table 5-6 Chemical compositions for (Bar-257) P91 steels (wt%)

Material	C	Mn	Si	N	Cr	Mo	Nb	Cu	V
Bar 257	0.11	0.36	0.022	0.048	8.74	0.98	0.12	0.08	0.21
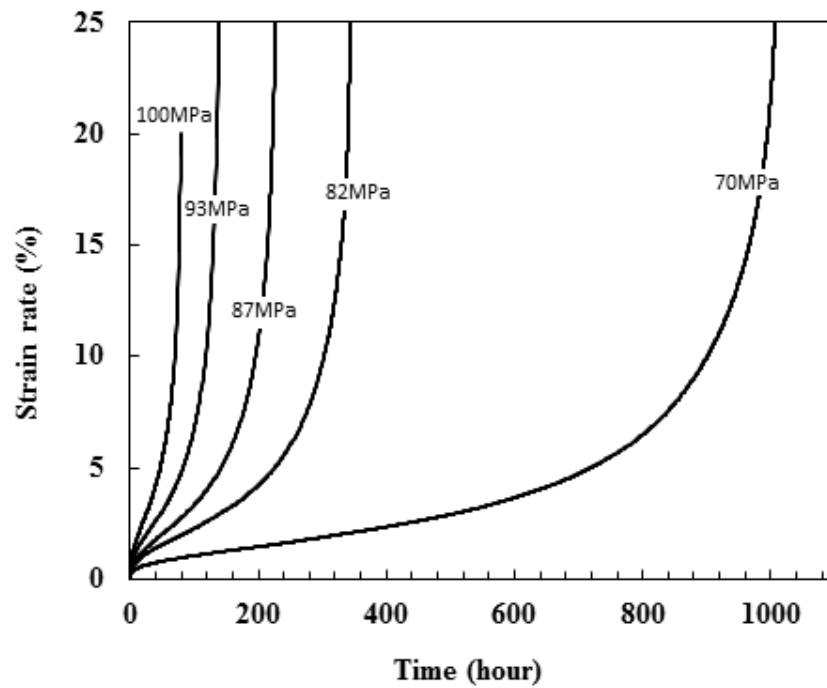
Fig. 5-10:   Creep strain versus time curves obtained from uniaxial tests for (Bar-257) P91 steel, tested at 650°C

Using the same material, five TBSs were manufactured, using the same

manufacturing process as that described in Section 5.2. The specimens were

creep tested at 650°C with loads corresponding to uniaxial stresses of 70, 82,

87, 93 and 100 MPa, respectively, equation (5.1) was used to calculate the

applied load for each stress. The deformation time curves obtained from the TBSs are shown in Fig. 5-11. The curves exhibit relatively small primary creep regions and relatively long secondary and tertiary regions. The measured dimensions of the tested TBSs which are made of P91 (Bar-257) steel, for all of the stress levels are reported in Table 5-7.

Table 5-7 The dimensions of the tested TBS, made of P91 (Bar-257) steel, tested at 650°C. The original specimen dimensions L_o, d, b and k were 13.0, 2.0, 2.0 and 6.5 respectively all dimensions are in (mm).

Stress	L_o*	d*	b*	k*
70	18.29	1.88	1.98	6.5
82	17.05	1.94	1.95	6.5
87	17.9	1.9	1.84	6.5
93	18.22	1.88	1.92	6.5
100	17.49	1.82	1.93	6.52
Average	17.79	1.88	1.92	6.50
changes %	26.92	6.15	3.95	0.06

(*) approximate dimension for the tested specimen

Table 5-7 shows that, the changes in the TBSs dimensions, i.e., L_o, d, b and k are about 27%, 6%, 4% and 0.06%, respectively. Table 5-7, shows that the changes in most of the TBS dimensions are relatively insignificant, apart from L_o, which increased by approximately 27%. The average change of the L_o value is about 4.7 mm, which makes the ratio L_o/D_i at failure to be about 3.54, whereas L_o/D_i ratio at the beginning of the tests was 2.6. Hence, the total change of the L_o/D_i ratio during the test is about 0.94. The data presented in Fig. 4-8, shows that between these two values of L_o/D_i, both η and β factors, remain practically constant. Since the conversion factors (η and β) remain

practically constant as the test progresses, it was considered to be reasonable

to use the relationship presented by equation(5.3), to convert the TBSs

deformation versus time curves presented in Fig. 5-11, to strain versus time

curves. The converted TBSs creep strains together with the corresponding

uniaxial creep strains are plotted in Fig. 5-12, which indicates excellent

agreement between the two sets of results.
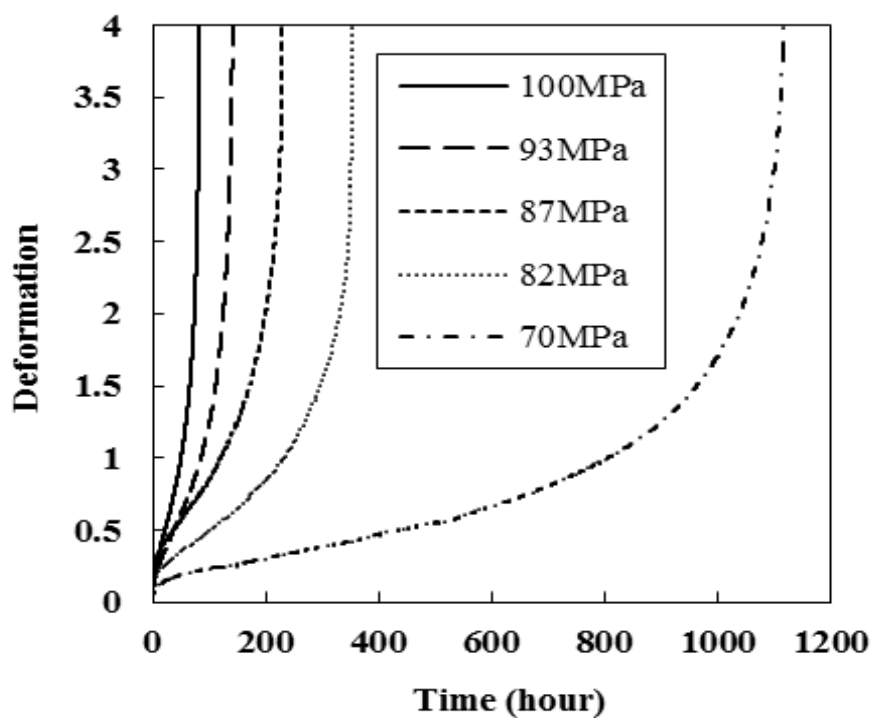
Fig. 5-11:   The TBS Deformation versus times curves for (Bar-257) P91 steel at 650$^\text{o}$C
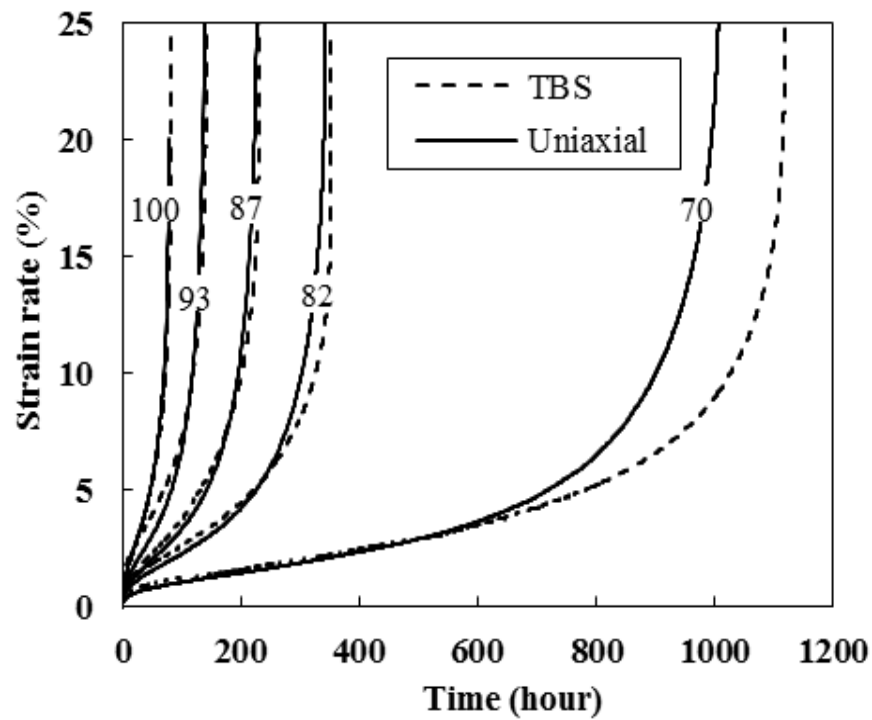
Fig. 5-12:   Converted TBS creep strain curves for various stress together with the
corresponding uniaxial creep strain versus time curves for (Bar-257) P91 steel
at 650°C, the stresses in [MPa]

The TBSs minimum creep strain rates were obtained from the deformation

versus time curves and equation (5.2). The results are compared with the

corresponding uniaxial minimum creep strain rates in Fig. 5-13, from which

it can again be seen that remarkably good agreement exists between the two

sets of results. The TBSs time to failure are also compared with the

corresponding uniaxial times to failure in Fig. 5-14. The level of agreement

between the TBSs and the corresponding uniaxial data is found to be

excellent. The slight difference between the uniaxial and the TBS data is

presented in Table 5-8 and Table 5-9; this is most likely to be related to the

unavoidable scattering in the material or due to the specimens manufacture

or polishing procedures.
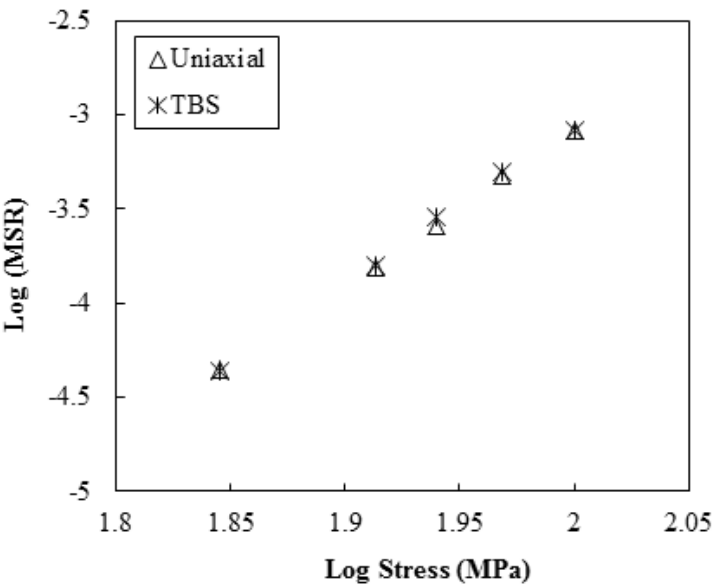
Fig. 5-13:   TBSs and the corresponding uniaxial Minimum creep strain rate data for (Bar-257) P91 steel at 650°C.
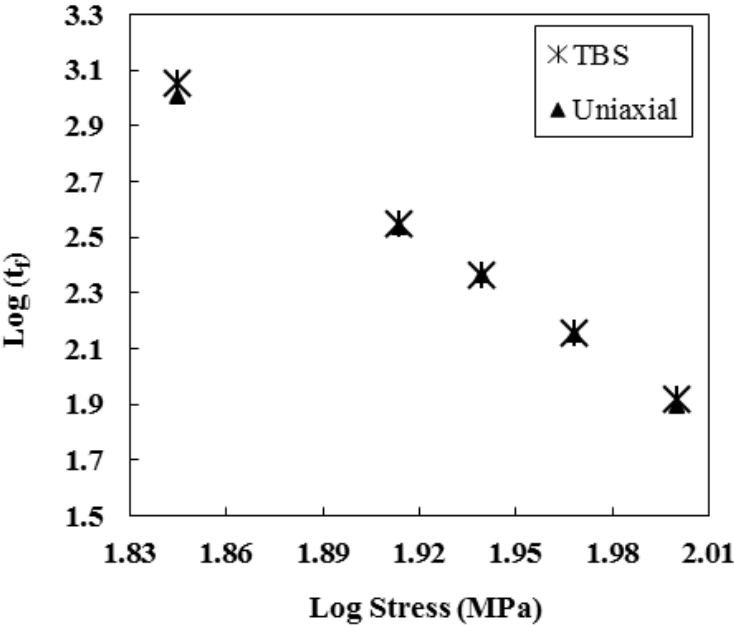
Fig. 5-14:   Creep rupture data obtained from TBSs testes and the corresponding uniaxial testes for (Bar-257) P91steel at 650°C.

Table 5-8:   Comparison between experimental MSRs (%) obtained from TBSs and the
corresponding uniaxial MSRs (%) for (Bar-257) P91 steel at 650°C

Stress [MPa]	Uniaxial MSR [h^{-1}]	TBS MSR [h^{-1}]	Difference %
70	0.00442	0.004463	0.9
82	0.015501	0.015737	1.4
87	0.02592	0.028392	8.7
93	0.04721	0.049429	4.4
100	0.08325	0.083993	0.8

Table 5-9:   Comparison between the failure time obtained from the TBSs and from the
corresponding uniaxial tests for (Bar-257) P91 steel at 650°C

Stress [MPa]	Uniaxial (t_f)[h]	TBS (t_f)[h]
70	1010	1117
82	343	351
87	230	229
93	140	142
100	78.6	83
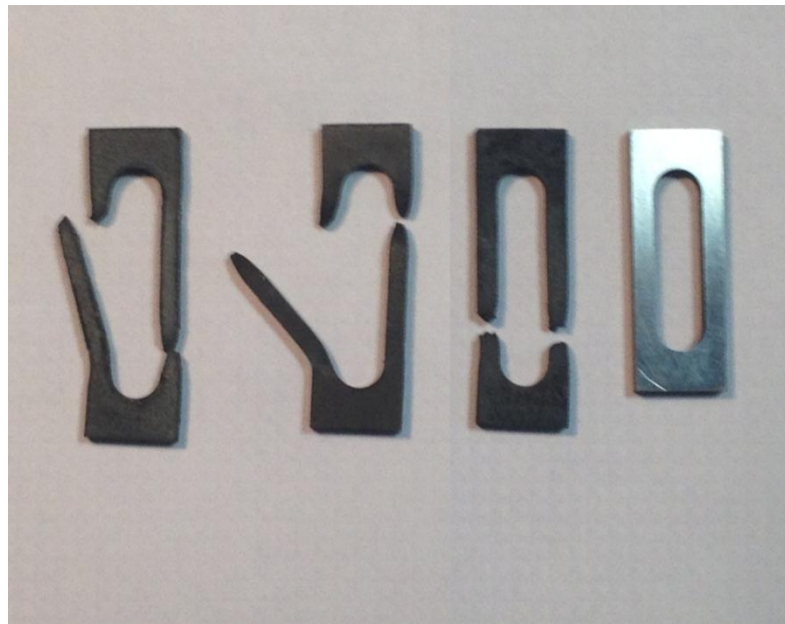
Fig. 5-15 Tested TBSs mad of (Bar-257) P91 steel, and creep tested using various stresses at
650°C, together with untested specimen

The appearance of some of the tested TBSs (see Fig. 5-6 and Fig. 5-15), show

signs of bending in one of the specimen bars. This type of bending indicates

that failure may occur in one bar before the other, and that this leads to

bending in the other bar before the testing machine finally stops; the

machine was set to stop when excessive deformations occurs, i.e., at failure.

However, the results presented in Fig. 5-5, Fig. 5-8, Fig. 5-11 and Fig. 5-12

indicate that throughout most of the test duration, i.e., during the primary ,

secondary stages and most of tertiary stage, the strain rates in the two bars

are equal, i.e., that the two bars hold the load together till the specimen

approaches the failure time.

5.5 DISCUSSION AND CONCLUSIONS

In order to assess the creep strength of service-aged materials, small

specimen creep testing methods have been found to be an extremely useful.

The method can be used to produce data to help in the process of predicting

the remaining lifetime of components [8, 47]. Most miniature creep test

specimen types, available to date, do not have the capability of obtaining

reliable creep rupture data [8]. The small punch creep test method is claimed

to be capable of producing creep rupture data, using small disks of material.

However, to date, there is no universally accepted procedure which can

correlate small punch creep test data with corresponding uniaxial creep test

results. The TBS test technique proposed in this thesis has shown that, the

technique is capable of obtaining both steady state creep and creep rupture data with reasonable accuracy. Useable specimen dimensions can be readily obtained for a wide range of material sizes. Hence, specimens can be easily extracted from small samples of material, for example, from the small scoop sample removed from the surface of the components, as shown in Fig. 2-14; or from thin piece of material removed from HAZ or WM of a weldment (see Fig. 5-1).

The limited amount of test data obtained so far, for a P91steel, at 600°C, and for (Bar-257) P91 steel at 650°C, have shown good agreement between the MSRs obtained from the TBS tests and the corresponding conventional uniaxial creep tests (see Fig. 5-7and Fig. 5-13). Good agreement is also found to be existing between the TBSs failure times and the corresponding conventional specimens failure times (see Fig. 5-9 and Fig. 5-14). However, care must be taken when manufacturing and polishing the specimens to ensure that uniform bar thicknesses and depths are achieved.

CHAPTER 6.

DETERMINATION OF MATERIAL CREEP CONSTANTS USING MINIATURE CREEP TEST SPECIMENS

_____

6.1   INTRODUCTION

Many power plants in the UK/US are now operating beyond their original designed life. Hence, there is a need to assess the creep strength of the many high temperature components within these plants. Standard size uniaxial creep test specimens (see Fig. 2-5), and Bridgman notch specimens (see Fig. 2-7) are used to assess the creep strength and to determine the full set of material constants for many creep modals, such as the Norton, the Kachanov and the Liu-Murakami damage models. However, both specimen types require relatively large material samples to be used in order to manufacture them [3, 109].

In many real life situations, involving in-service components, a standard specimen cannot be removed from components without (i) compromising their structural integrity, (ii) major subsequent repairing operations to the tested component [110]. Normally only small samples of material can be removed from these in-service engineering components for creep assessment, using one of the surface sampling techniques (see Fig. 2-13)

e.g.[6, 27, 111]. Therefore, this chapter is mainly concerned with the determination of creep constants, for the Norton model, the Kachanov and the Liu-Murakami damage models, using various small creep test specimen techniques. The small ring creep testing method [10] and the impression creep testing method [9, 52, 98], are often used to determine secondary creep data for materials.

In this chapter, the results of both testing techniques have been used to obtain the secondary creep constants, i.e., Norton's constants (A and n). The results are compared with the corresponding uniaxial data, using (Bar-257) P91 steel at 650°C, a 316 stainless steel at 600°C and a 2-1/4Cr1Mo weld metal at 640°C. However, neither of these testing methods is able to be used to obtain tertiary creep and creep rupture data. Hence it has been recognised that there is a need to develop miniature creep test specimen types and the associated testing techniques, from which reliable creep deformation and creep rupture data can be derived.

This issue has been addressed in this chapter by using two small-sized creep test specimens, (i) the recently developed two-bar specimen type (TBS), which can be used to obtain both minimum uniaxial creep strain rate data and creep rupture data [101, 112], and (ii) the novel small notched specimen, which is suitable for use in predicting the multiaxial creep behaviour for a

given material. The small notched specimen loading, testing procedure and specimen manufacturing process are also described. The FE analysis method has been used to assess the small notched specimen failure time and location, and also to assess the effects of the notch radius on the specimen failure time. These specimens can be easily constructed from the HAZ or WM zones of a weld. They can be made from small scoop samples removed from component surfaces [46]. The Two-bar and notched specimens both have simple geometries and can be conveniently machined and loaded (through pin-connections) and then tested using tensile load.

The (Bar-257) P91 steel at 650°C, and the P91 steel at 600°C have been used to assess the accuracy of both testing techniques. The material creep constants for the Kachanov and Liu-Murakami models, i.e., *A, n, M, B, Ø, χ, α* and q_2 have been obtained using the TBS and the small notched specimens and the constants are compared with those obtained from the corresponding conventional uniaxial and Bridgeman notch tests. The results show remarkably good agreement between the two sets of results. This chapter also includes the major advantages of these new, small specimen testing techniques over the other small specimen creep testing techniques.

6.2 COMMONLY USED SMALL CREEP TEST SPECIMENS FOR OBTAINING THE SECONDARY CREEP DATA

The most common small specimen creep test methods used to determine the secondary creep constants are (i) the small ring specimen testing technique [47], which is described in detail in Chapter three and (ii) the impression creep testing technique which has been described in Chapter two. For both methods, the steady state load line deformation rates are converted to the equivalent uniaxial minimum strain rate (MSR), using conversion relationships. The two specimen types and the loading arrangements are shown in Fig. 6-1
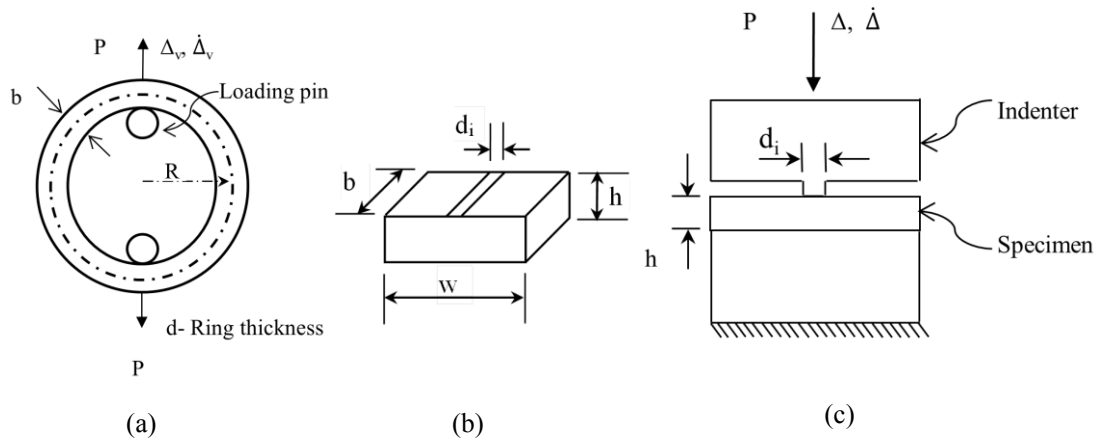
Fig. 6-1 Specimens and loading arrangement for a small ring creep test (a) and an impression creep test (b, c)

The minimum creep strain rates (MSRs), for various stresses have been obtained using small ring specimens with R=10 mm, b/d=1 and R/d = 5, for (bar-257) P91 steel at 650°C. The conversion relationships given by equations (2.31) and (2.32), are used to convert the applied load to the equivalent

uniaxial stress and the minimum load line deformation rate to the equivalent

uniaxial strain rate. The MSRs are shown together with the corresponding

uniaxial MSRs in Fig. 2-35 [27]. The impression creep test has been used to

obtain the MSRs for two materials (i) a 2-1/4Cr1Mo weld metal at 640$^{\text{o}}$C and

(ii) a 316 stainless steel at 600$^{\text{o}}$C [54]. The conversion relationships, given by

equations (2.12) and (2.13), are used to convert the pressure under the

indenter to the equivalent uniaxial stress, and the load line for the indenter

displacement rate to the equivalent uniaxial strain rate. The results are

plotted together with the corresponding uniaxial tests in Fig. 2-21.

6.3 COMMONLY USED SMALL CREEP TEST SPECIMENS FOR OBTAINING CREEP RUPTURE DATA

6.3.1 Small punch creep testing technique (SPCT).

The small punch creep test method involves applying a constant load, through a

spherical punch or a ball, to a thin disc, at an elevated temperature (see

Fig. 6-2). Typical small disc dimensions are ~ 0.5mm thickness and ~ 4mm

radius and the ball radius is typically ~1.25mm. The load line deformation is

recorded throughout the test duration[113]. The resulting plot of punch load

line displacement against time curve looks similar to that of a creep curve which

would be obtained from a conventional creep test specimen. Many attempts

have been made to introduce conversion parameters to relate the applied load to

the corresponding equivalent uniaxial stress and to convert the punch load line

deformation to the equivalent uniaxial strain. These attempts are discussed in detail in [8, 62, 67, 114], and therefore only a brief description is given here. The SPCT exhibits large elastic and plastic deformations and an increasing contact area between the disk and the loading ball during the test. There are no universally agreed conversion factors to relate SPCT data to the corresponding uniaxial data, and therefore it was decided not to use the SPCT method in this work.
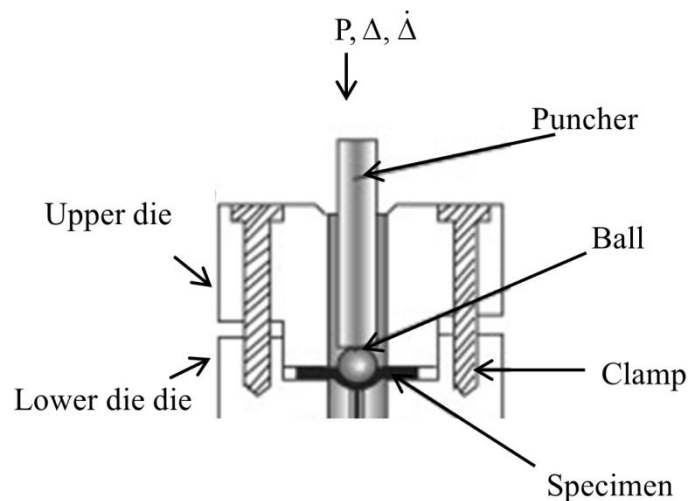
Fig. 6-2 Specimen and loading arrangement for a small Punch creep test

6.3.2 Small two-bar specimen creep testing technique (TBS)

The TBS testing technique is capable of obtaining both the secondary and the creep rupture data, using small material samples. The method was described in Chapter 4, and therefore only a brief description will be given in this chapter. The specimen is loaded through pin connections (see Fig. 6-3), and the specimen deformation is recorded throughout the test duration.

Conversion relationships are used, i.e. equations (5.1), (5.2) and (5.3), to convert the applied load to the corresponding uniaxial stress and to convert the TBS deformation and deformation rate to the corresponding uniaxial strain and strain rate [101, 112]. The TBS validation results will be used in this chapter to determine the material constants for the secondary and the tertiary creep regions.
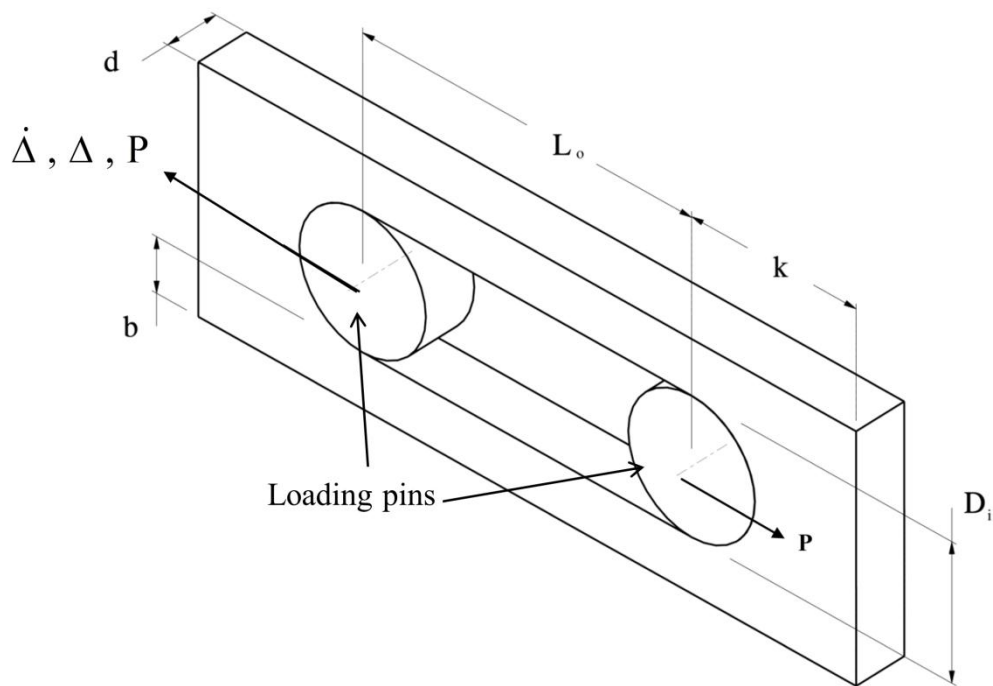
Fig. 6-3 Specimens and loading arrangement for the small Two-bar creep test

The TBSs were creep tested using two materials (i) the (Bar-257) P91steel at 650°C [115] and (ii) the typical P91 steel at 600°C [112]. These materials are used extensively in power plants pipework. For (Bar-257) P91 steel, the specimens were creep tested at 650°C with loads corresponding to uniaxial stresses of 70, 82, 87, 93 and 100 MPa [40]. For the typical P91 steel, the

specimens were creep tested at 600ºC with loads corresponding to uniaxial stresses of 140, 150, 160, 170 and 180 MPa [109]. The TBS converted strain versus time curves for both materials are shown together with the corresponding uniaxial strains in Fig. 5-8 and Fig. 5-12. The MSRs and the failure times obtained from the TBSs and from the corresponding uniaxial tests for the two materials are also compared in Fig. 5-7, Fig. 5-9, Fig. 5-13 and Fig. 5-14

6.4 DETERMINATION OF MATERIAL CONSTANTS FOR CREEP MODELS

6.4.1 Determination of Norton model material constants (*A* and *n*)

Norton's law is the most commonly used model to describe the secondary creep region (steady state region), because of its simplicity/accuracy [13], i.e., $\dot{\varepsilon}^c = A\sigma^n$, where *A* and *n* are temperature dependent material constants, σ is the stress and $\dot{\varepsilon}^c$ is the minimum strain rate (MSR) which depend only on the strass and the temperature. The material constants *A* and *n* for (Bar-257) P91 steel at 650ºC, the P91steel at 600ºC, the 316 stainless steel at 600ºC and a 2-1/4Cr1Mo weld metal at 640ºC, were obtained using the impression, the ring and the TBS creep test results which are presented in Fig. 2-35, Fig. 5-7 and Fig. 5-13. All creep data for a 316 stainless steel at 600ºC and a 2-1/4Cr1Mo weld metal at 640ºC, which have been used to obtain *A* and *n* for these materials are from the literature See Table 6-2 [57]. The uniaxial and the

176

ring creep tests data for the (Bar-257) P91 steel at 650°C, which have been used to obtain A and n for this material were also taken from the literature [27]. However, all TBS creep tests which have been used to obtain the material creep properties for the (Bar-257) P91 steel at 650°C and the P91 steel at 600°C, were part of this work. The A and n constants were obtained by plotting the MSRs against the applied stresses on a log–log scale and then determining a line of best fit. The slope of the line of best fit is n and the intercept is log (A). The material constants obtained using the impression, the small ring and small TBS creep tests and from the corresponding uniaxial tests are compared in Table 6-1, Table 6-2 and Table 6-3 respectively.

Table 6-1 Norton's law material constants obtained from the ring and the corresponding uniaxial creep test specimens for (Bar-257) P91 steel at 650°C

Test type	(Bar-257) P91 steel at 650°C
Ring specimen Creep test	n=7.24
	A=1.70216E-18
Uniaxial creep test	n=8.462
	A=1.092×E-20

Table 6-2 Norton's law material constants obtained from the impression and the corresponding uniaxial creep test specimens, for a 316 stainless steel at 600°C and a 2-1/4Cr1Mo weld metal at 640°C

Test type	316 stainless steel at 600°C	2-1/4Cr1Mo weld metal at 640°C
impression creep test	n= 9.438	n= 6.6799
	A=5.87489E-28	A=1.13E-17
Uniaxial creep test	n= 10.782	n= 6.4295
	A=3.92645E-31	A= 3.17E-17

Table 6-3 Norton's law material constants obtained from the TBS and the corresponding uniaxial creep test specimens for (Bar-257) P91 steel at 650°C and P91 steel at 600°C

Test type	(Bar-257) P91 steel at 650°C	P91 steel at 600°C
Two-bar specimen creep test	$n=8.455$ $A=1.0914E-20$	$n=13.77$ $A=9.506E-35$
Uniaxial creep test	$n=8.462$ $A=1.092 \times E-20$	$n=13.69$ $A=1.00E-34$

The Norton's Law material constants A and n which have been obtained using the Ring, the Impression and the TBS creep testing techniques, (see Table 6-1, Table 6-2 and Table 6-3), are used to predict the MSRs for different stress levels. The results are compared with the MSRs obtained based on the material constants obtained using the uniaxial specimens. Remarkably good correlation is found between the two sets of results, as seen from Table 6-4 to Table 6-7

Table 6-4 Comparison between the calculated MSRs using Norton's law and the material constants A and n obtained from (i) the Ring specimen, (ii) the TBS and (iii) the uniaxial creep test specimens for (Bar-257) P91steel at 650°C

Stress [MPa]	Uniaxial MSR [h^{-1}]	Ring MSR [h^{-1}]	TBS MSR [h^{-1}]
50	3.4E-06	2.5E-06	2.5E-06
55	6.7E-06	5.4E-06	5.8E-06
60	1.2E-05	1.1E-05	1.2E-05
65	2.2E-05	2.3E-05	2.3E-05
70	3.8E-05	4.3E-05	4.4E-05

Table 6-5 Comparison between the calculated MSRs using Norton's law and the material constants *A* and *n* obtained from (i) the TBS and (ii) the uniaxial creep test specimens for P91 steel at 600°C

Stress [MPa]	Uniaxial MSR [h^{-1}]	TBS MSR [h^{-1}]
50	2.3E-11	1.8E-11
55	8.7E-11	6.6E-11
60	2.9E-10	2.2E-10
65	8.7E-10	6.5E-10
70	2.4E-09	1.8E-09

Table 6-6 Comparison between the calculated MSRs using Norton's law and the material constants *A* and *n* obtained from (i) the Impression and (ii) the uniaxial creep test specimens for 316 stainless steel at 600°C

Stress [MPa]	Uniaxial MSR [h^{-1}]	Impression MSR [h^{-1}]
50	6.3E-12	8.1E-13
55	1.5E-11	2.2E-12
60	3.5E-11	5.8E-12
65	7.5E-11	1.3E-11
70	1.5E-10	3.0E-11

Table 6-7 Comparison between the calculated MSRs using Norton's law and the material constants *A* and *n* obtained from the (i) Impression and the (ii) uniaxial creep test specimens for 2-1/4Cr1Mo weld metal at 640°C

Stress [MPa]	Uniaxial MSR [h^{-1}]	Impression MSR [h^{-1}]
50	2.5E-06	2.6E-06
55	4.7E-06	4.9E-06
60	8.5E-06	8.5E-06
65	1.4E-05	1.4E-05
70	2.3E-05	2.3E-05

6.4.2 Determination of material constants for damage models (*A, n, M, χ, B, Ø, and q$_2$*)

The most commonly used damage models are the Kachanov material behaviour model [18] and the Liu-Murakami model[11]. Both are capable of modeling the entire creep strain curves. The models consist of pairs of

coupled creep/damage equations which are capable of representing the damage in the material during creep; both models have been described in Section 2.6. The material constants for Kachanov and Liu-Murakami models, i.e., (A, n M, χ, B, $\varnothing$, and q_2) for (Bar-257) P91 steel at 650°C and for P91 steel at 600°C have been obtained using TBS results for both materials which are presented in Fig. 5-7, Fig. 5-8, Fig. 5-9, Fig. 5-12, Fig. 5-13 and Fig. 5-14.

The constants (A and n) for both Liu-Murakami and Kachanov models are the same as those for Norton's model which have been obtained in Section 6.4.1. The material constants M and χ for the P91 steel at 600°C and for the (Bar-257) P91 steel at 650°C were obtained by plotting the TBS failure times against the applied stresses on (log–log) scales and then determining a line of best fit (see Fig. 5-9 and Fig. 5-14). The slope of the line of the best fit is ($-\chi$) and the intercept is (-log M). The values of B and $\varnothing$ were determined by calculating the creep strain curves using Kachanov damage model, i.e., equation (2.49) for different values of $\varnothing$. Then by fitting these calculated creep curves to the experimental TBS creep strain curves, i.e., (Fig. 5-8 and Fig. 5-12), the $\varnothing$ value and the corresponding B value (satisfying $M= B(1 + \varnothing)$) that give the best fit to the experimental data were considered to be the most accurate $\varnothing$ value for the material. Both B and $\varnothing$ mainly govern the creep strain rate in the tertiary region on the strain versus time curves for the Kachanov damage model.

The material constant q_2 in the Liu-Murakami model was obtained in a similar way to the constant $\emptyset$ in the Kachanov model. Creep strain-time curves were calculated using a time marching technique for different values of q_2 keeping all the other material constants the same and then fitting to the TBS experimental results. The value of q_2 which gives the best fit was then taken as the material constant. The constant q_2 *is* similar to (B and $\emptyset$) in Kachanov model; it mainly governs the creep strain rate in the tertiary region on the strain-time curves. The TBS experimental, converted creep strain versus time curves and the fitted curves for the Kachanov and Liu-Murakami models, for both materials, are shown in Fig. 6-4 and Fig. 6-5. The calculated creep strain curves for the Liu-Murakami model have been obtained using the uniaxial form of Liu-Murakami model as in the following relationship:-

$$\Delta\varepsilon = A\sigma^n Exp\left[\frac{2(n+1)}{\pi\sqrt{1+3/n}}\omega^{3/2}\right]\Delta t \qquad (6.1)$$

where Δt is a time increment, taken to be the TBS experimental time increments, where $\Delta t = t_{i+1} - t_i$. The values of ω are increased with t_i, from zero (no damage) to unity (at failure).
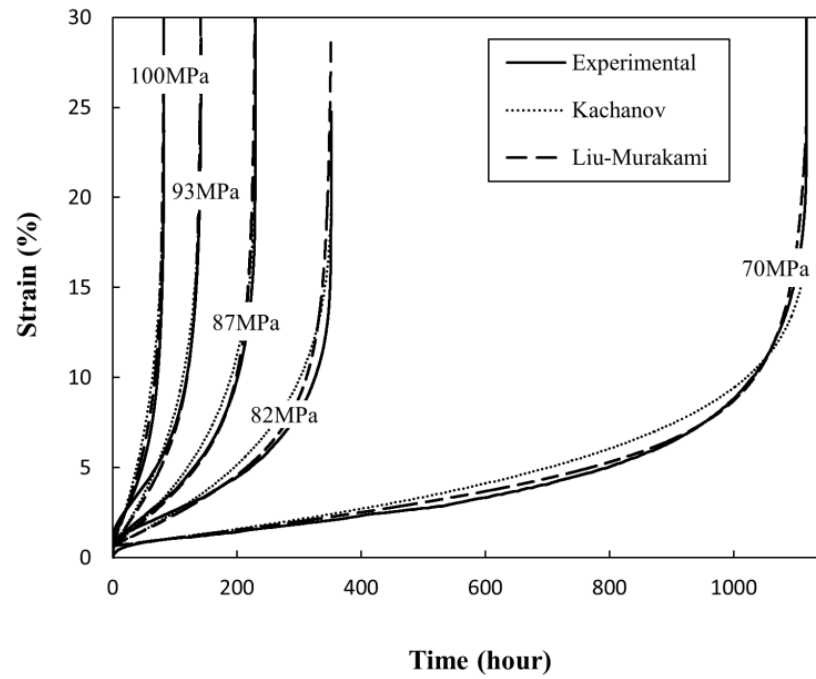
Fig. 6-4 The experimental converted TBS creep strain curves, for (Bar-257) P91 steel at 650°C and the fitted creep strain curves using the Kachanov model with Ø=9.5 and the Liu-Murakami model with q_2= 4.00
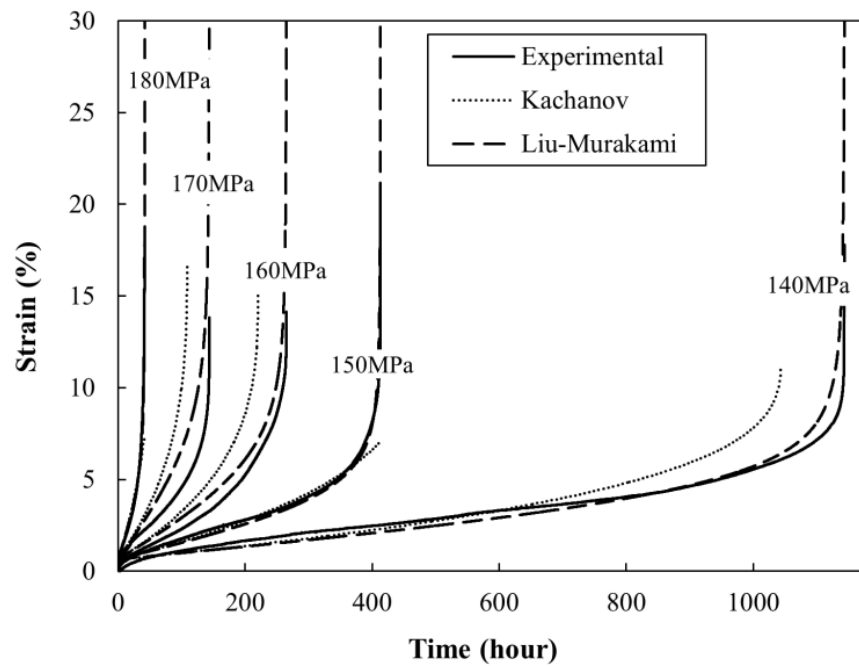
Fig. 6-5 The experimental converted TBS creep strain curves, for P91 steel at 600°C and the fitted creep strain curves using the Kachanov model with Ø=19.00 and the Liu-Murakami model with q_2=7.00

6.5 DETERMINING THE MULTIAXIAL STRESS STATE PARAMETER (α) USING SMALL NOTCHED SPECIMEN

After fitting Kachanov and Liu-Murakami models to the converted experimental TBS creep strain curves to find the majority of damage models material constants, i.e., (A, n M, χ, B, $\varnothing$, and q_2), the multiaxial stress state parameter, α, can be obtained. This can be done by comparing FE failure times for notched bars (using a range of α values) with the experimental notched bar failure times. Traditionally Bridgman notches specimens (see Fig. 2-7) are used to determine the constant α. However, in this thesis the new small specimen test type has been used to determine the parameter α. Similar to the small TBS, the small notched specimen can be manufactured using small material samples, removed from for example, the HAZ or WM regions of welds or from small scoop samples removed from a component surface using one of the small sampling techniques [46].

6.5.1 Analysis and design of a small notched specimen

The small notched specimen has a simple geometry and it can be easily loaded through loading pins which allow good aligning to be achieved during the loading application. The specimen dimensions are defined by R the notch radius, h the notch region height, w the notch depth, H the specimen height, d the specimen depth, L the specimen length and D_i the loading pin diameter; these dimensions are shown in Fig. 6-6.
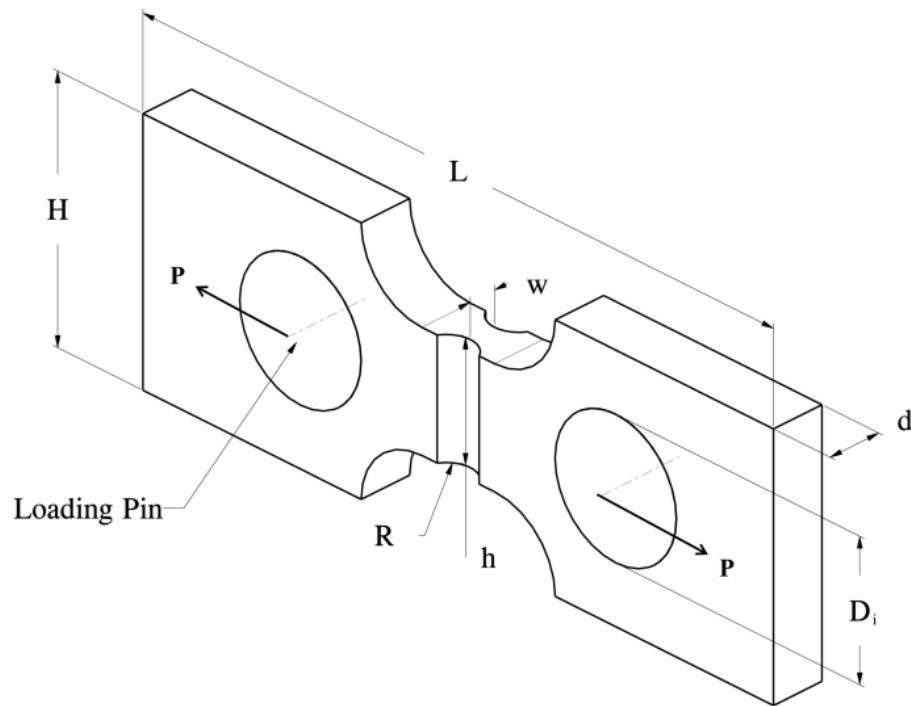
Fig. 6-6 Small notched specimen dimensions and loading application

6.5.2 Finite element analyses (FE)

6.5.2.1 Specimen Modeling

In order to assess the specimen design and the failure location of the specimen, 3D-FE analyses have been carried out using meshes which consist of 20-noded brick elements. Because of the symmetry, it was only necessary to model one quarter of the specimen and one half of the specimen thickness, d, as shown in Fig. 6-7. The boundary conditions, i.e. $u_x = 0$ on plane A, $u_y = 0$ on plane B and $u_z = 0$ on plane C, are also indicated in Fig. 6-7. The specimen is loaded and constrained through two loading pins which are assumed to be "rigid" in the FE model. The applied loads were calculated to ensure that the stresses at the notch tip (the smallest cross section area), i.e., ($w \times h$), are

184

representative of the stresses used in laboratory tests. For accurate determination of the specimen failure time, the mesh density has been refined at the critical notched region. The Liu-Murakami damage model was used in the FE analyses to predict the small notched specimen rupture time. The FE analyses failure time for the small notched specimen was determined as the time at which the damage parameter, ω, approaches unity, i.e., reaches the maximum value of 0.99 in the integration points in all of the elements on a path through the cross section area of the bar, as illustrated in Fig. 6-8. The ABAQUS finite element software package was used for the FE analyses [70].
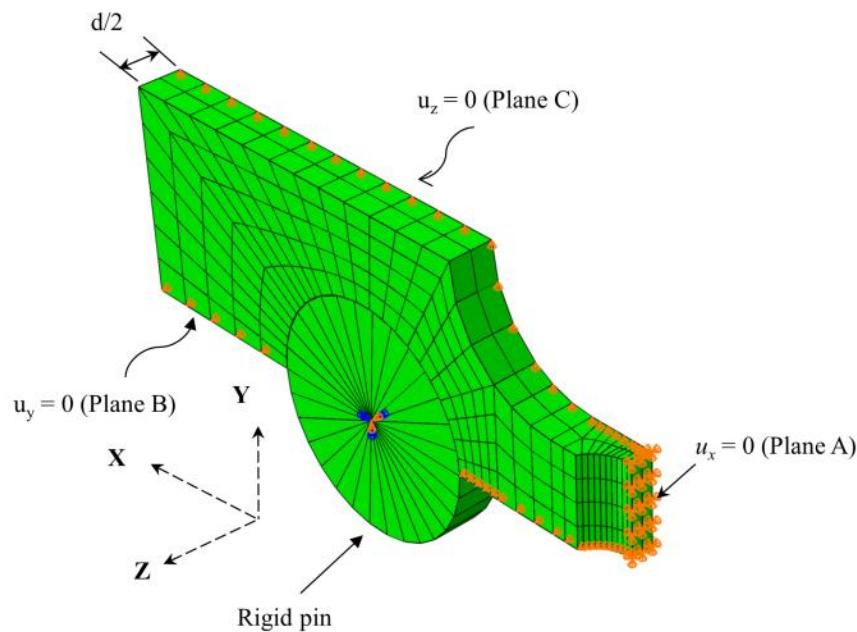
Fig. 6-7 Finite element mesh and the boundary conditions
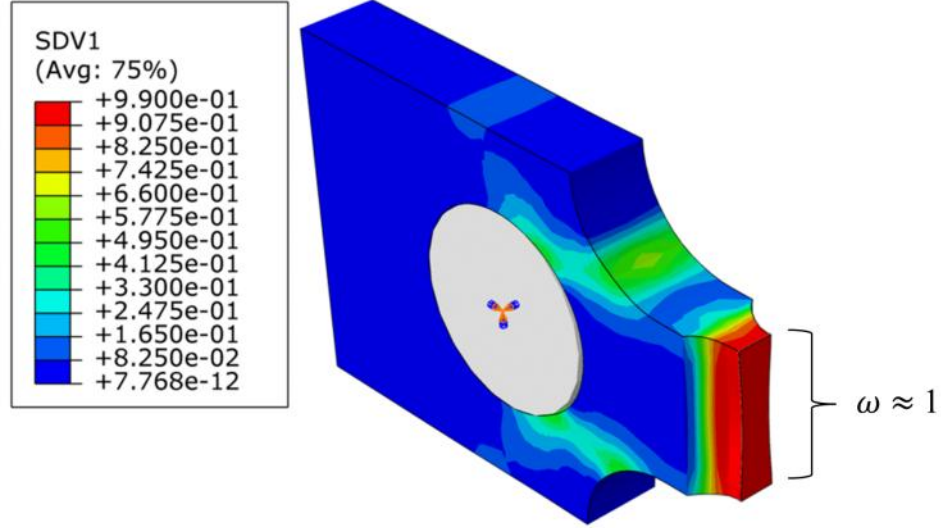
Fig. 6-8 Contour plot of damage parameter, ω, in the small notched specimen for (Bar-257) P91 at 650°C

6.5.2.2 Effects of the notch radius (R/w) on the specimen failure time

FE investigations have been carried out to assess and compare the effect of α on (i) the uniaxial specimen failure time, (ii) the Bridgman notch specimen failure time and (iii) the small notched specimen, with various R/w ratios, on failure time. For the small notched specimen, several R values have been chosen, whereas the rest of the specimen dimensions were kept constant including the notch depth, w, for all cases. The material creep constants for (Bar-257) P91 at 650°C with stress of 70MPa were used in the Liu-Murakami damage model to determine the specimen failure times for a range of α values.

In this study, the Bridgman notch specimen was taken as the reference and the aim was to determine which R/w ratio gives the closest failure times to

186

those of the Bridgman notched specimens with the same α values. The failure times for the uniaxial specimen, the Bridgman notch specimen and the small notched specimen, with different R/w ratios, are plotted against α values in Fig. 6-9. The results indicate, as expected, that the α has no effect on the uniaxial specimen failure times and it has a significant effect on the Bridgman notch specimen failure times. The effect of α on the small notch specimen failure times varies between that of the uniaxial specimen and that of the Bridgman notch specimen and it is inversely proportional to the R/w ratio. Failure times for small R/w ratios are closer to the failure times of the Bridgman notch specimen for the same α values, whereas for large R/w ratios the failure times are closer to those of the uniaxial specimen with the same α values. On this basis, the small notch specimens should be manufactured with the smallest R/w ratio that is practically possible. However, manufacturing small notched specimens with relatively small R values e.g., R=0.5 mm, with good surface finish can be challenging and expensive, and therefore the test specimens were designed with R=1 mm and R/w=1.
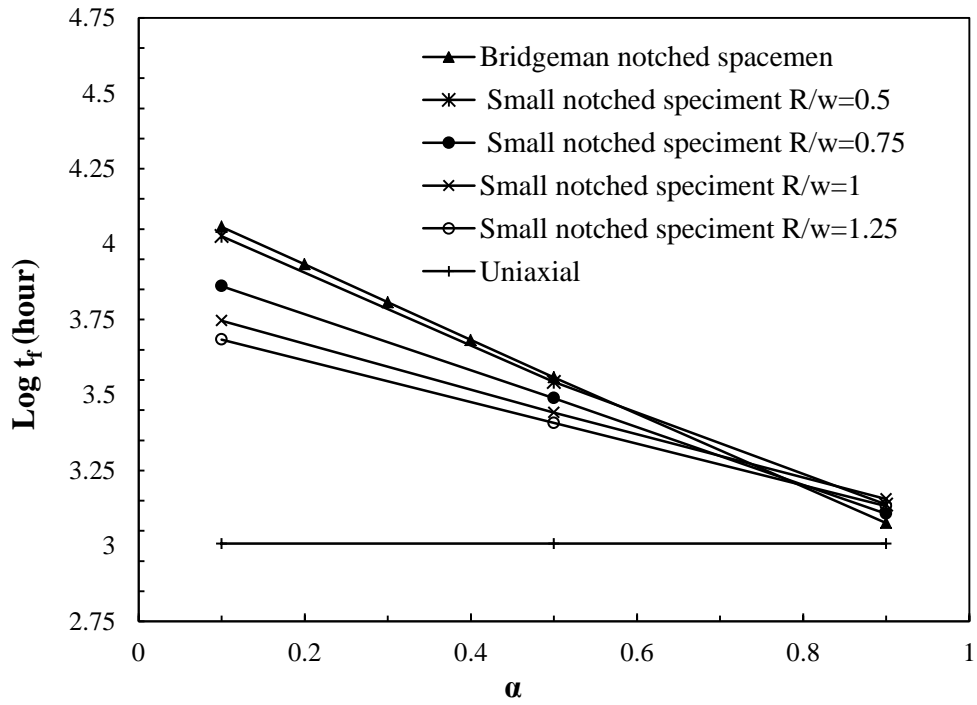
Fig. 6-9 The effect of α value on the uniaxial specimen, Bridgman notch specimen and small notched specimens, with varies R/w ratios, w=1 mm for all small notched cases

6.5.3 Specimen Manufacturing and Test Procedure

Due to the small size of the notched specimen (see Fig. 6-6 and Fig. 6-10), the electrical discharge method (EDM) was found to be the most suitable for specimen manufacture. The specific specimen dimensions for $L, H, d, R, h,$ w and D_i were 26, 9, 2, 1, 4, 1 and 4.98 mm, respectively. These dimensions were chosen because small material samples, with the dimensions of approximately (30 × 20 × 3 mm), can be easily removed from the power plant high temperature components surfaces using one of the surface sampling techniques (SSam) without affecting their safe operation [46]. The constant

loading is applied to the specimen through loading pins, and the specimen

deformation is recorded throughout the test until rupture occurs see Fig. 6-11.
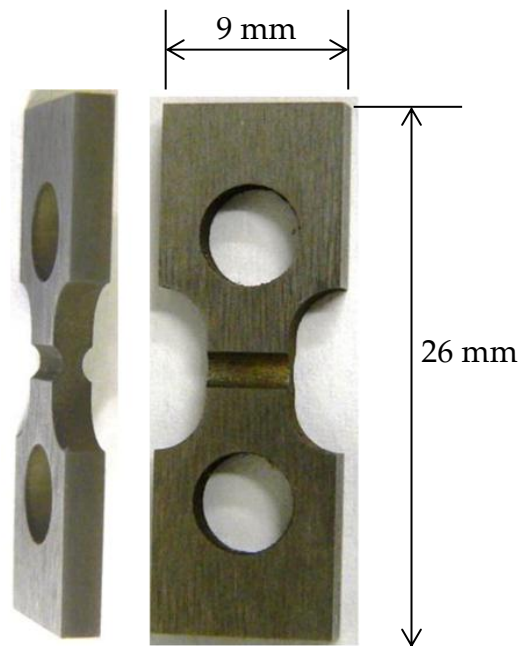
Fig. 6-10 A photo of the small notched specimens manufactured using an EDM machine

Fig. 6-11 A photo of the tested small notched specimen made of (Bar-257) P91 steel, and creep tested using 82MPa, at 650°C.

6.5.4 Determining the α value for (Bar-257) P91 steel at 650°C

The parameter α governs the rupture stress in the Kachanov and Liu-Murakami models. The rupture stress is given by $\sigma_r = \alpha\sigma_1 + (1-\alpha)\sigma_{eq}$. The α parameter ranges from 0 to 1, when $\alpha = 0$ the rupture stress is governed by the equivalent stress (σ_{eq}), and when $\alpha = 1.0$ the rupture stress is governed by the maximum principal stress (σ_1). The parameter α can be determined by fitting the experimental failure times of the small notched specimens to the numerical failure times using finite element (FE) analyses for various α values.

Two experimental small notched specimen creep tests have been carried out at 82 and 100MPa, using (Bar-257) steel at 650°C. Corresponding FE analyses of the small notched specimens were carried out using various α values which result in different failure times for each α value in the FE analyses. The α value that gives a failure time corresponding to the experimental failure time is taken to be the correct α value for the material (see Fig. 6-12). Scatter in the material properties or variations in the surface finish quality of the specimen, especially in the critical, notch region, can affect the experiment failure times. In this case, the average α value is taken to be the required value.
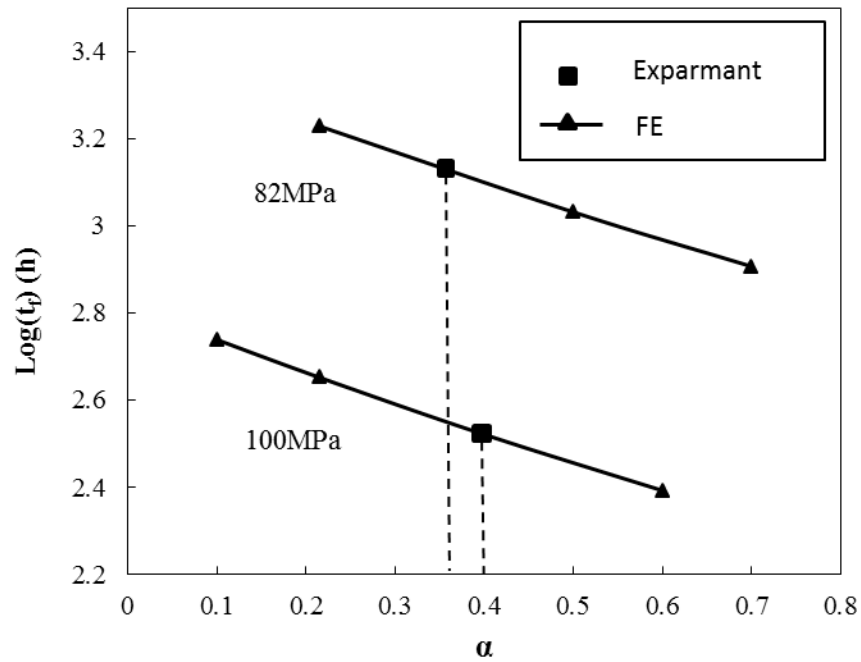
Fig. 6-12 Determining the α value for (Bar-257) P91 steel at 650°C using small notched specimens

6.6 SUMMARY OF P91 STEEL MATERIAL CONSTANTS

The full set of the material constants which are to be used in the Norton, Kachanov and Liu-Murakami models have been obtained, using only the small TBS, and the small notched specimen, for (Bar-257) P91 steel at 650°C and the P91steel at 600°C. The results are compared, in Table 6-8 and Table 6-9, with those obtained from the full size uniaxial and the Bridgman notch specimens [43, 116].Remarkably good agreement was found to exist between the two sets of results.

Table 6-8 Creep material constants for the (Bar-257) P91 steel at 650°C, obtained using (i) uniaxial specimen, (ii) the small TBS and (iii) the small notched specimen.

Material	A	n	m	B	ϕ	χ	α	q_2
uniaxial	1.092×10^{-20}	8.462	-4.754×10^{-4}	3.537×10^{-17}	7.346	6.789	0.312	3.2
TBS	1.0884×10^{-20}	8.455	-3.5×10^{-4}	3.052×10^{-18}	9.5	7.276	0.37	4.00

α was obtained using the small notched specimen (the average of two tests)

Table 6-9 Creep material constants for the P91 steel at 600° C , obtained using (i) uniaxial specimen and (ii) the small TBS.

Material	A	n	B	ϕ	m	χ	α	q_2
uniaxial	1.00×10^{-34}	13.69	2.12×10^{-27}	18.00	0.00	10.96	0.3	6.00
TBS	9.5×10^{-35}	13.77	4.931×10^{-30}	19.00	0.00	11.64	-	7.00

The material constants obtained from the TBS tests for (Bar-257) P91steel at 650°C, (see Table 6-8), have been used to perform FE analyses, using the Liu-Murakami damage model, in order to predict the strain versus time curves for the TBS. The FE prediction of the strain versus time curves are compared with the corresponding experimental uniaxial strain versus time curves in Fig. 6-13. Remarkably good agreement is found between the TBS, FE prediction strain curves and the experimental uniaxial strain curves.
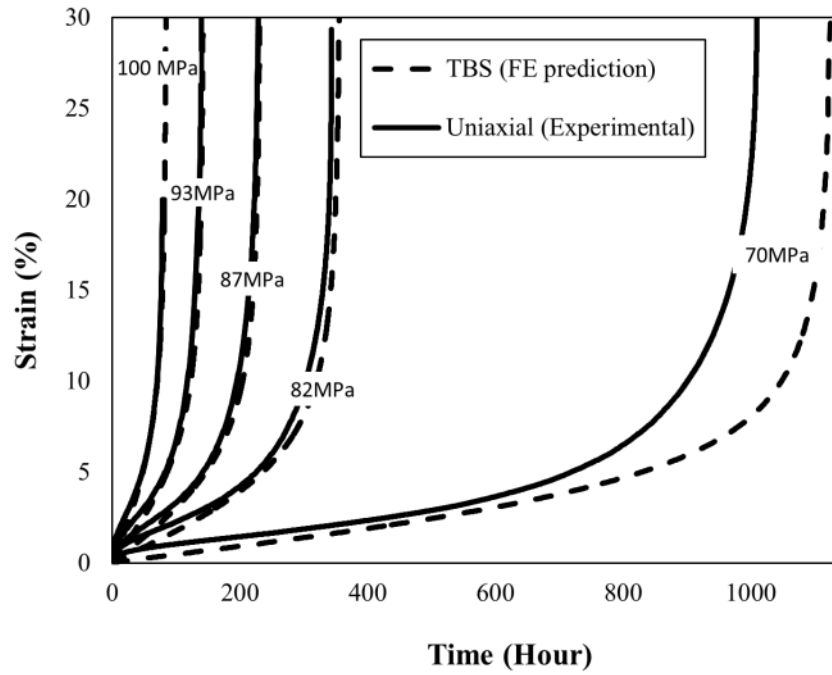
Fig. 6-13 Comparison between (i) the converted TBS creep strain versus time curves obtained from the FE analyses, using the material constants obtained from the TBS creep tests, and (ii) the corresponding experimental uniaxial creep strain versus time curves, for (Bar-257) P91 steel at 650°C

6.7 DISCUSSION AND CONCLUSIONS

The small creep test specimen methods described in this chapter have been shown to be capable of obtaining a full set of material properties for a variety of creep models, including the Norton's law, the Liu-Murakami model and the Kachanov model. Some of the testing techniques can only be used to obtain secondary creep data, for example, the small ring testing [27] and the impression creep testing [53] methods, can be used for this purpose. Other small specimen types, such as the TBS testing technique [112] are capable of obtaining both secondary creep and rupture creep data. The small ring and the impression creep testing techniques have been used to obtain the steady

193

state constants, i.e., *A* and *n* in Norton's law for a 2-1/4Cr1Mo weld metal, at 640°C, 316 stainless steel, at 600°C and (Bar-257) P91 steel, at 650°C. Both testing techniques have shown good correlations with the corresponding uniaxial test data, as presented in Table 6-1 to Table 6-7. The small TBS has been used to obtain Norton's law constants as well as most of the Liu-Murakami and Kachanov material constants, i.e., *A, n, M, B, ϕ, χ* and *q_2*, for P91 steel at 600°C and (Bar-257) P91 steel at 650°C. Very good agreement was found to exist between the materials constants obtained using the small TBS tests and with those of the corresponding conventional uniaxial tests, as presented in Table 6-8 and Table 6-9. The multiaxial stress state parameter *α* has been also obtained for the (Bar-257) P91 steel at 650°C using a novel small notched specimen (see Fig. 6-6). The result is compared with the corresponding Bridgman notch specimen results in Table 6-8.

The specimen has a relatively simple geometry and therefore it can be easily machined and loaded, since the loading of the specimen, through pin connections, makes it possible to achieve accurate aligning. Useable specimen dimensions can be readily obtained for a wide range of available material sizes. Hence, the TBS and the small notched specimen can be easily extracted from small samples of material, such as, for example, small scoop samples removed from the surfaces of components and from the HAZ or WM regions of welds [46]. Both testing techniques can be considered to be

non-destructive techniques (NDT), as the specimens can be made from small material samples taken from the operating components surfaces without affecting their safe operation.

The FE results presented in Fig. 6-9 can be used as a guide to the design of the small notched specimen. The slope of the *Log (t_f)* versus α plot indicates the accuracy of the chosen design; steeply sloping line tends to give more accurate and easy to determine values of α for the material. The process of choosing specimen dimensions involves a compromise related to the volume of the material available from which a specimen can be made, the available/affordable manufacturing technique and the *R*/w ratio. However, the failure times for the notched specimen are sensitive to the notched region finish and to the small changes in the *R*/w ratio, as indicated in Fig. 6-9. The work presented in this thesis has shown that results of tests on small TBS and small notched specimens can be used to obtain a full set of material constants for damage models. When compared with those obtained using full size specimens, the agreement is very good.

CHAPTER 7.

DISCUSSION, CONCLUSIONS AND FUTURE WORK

_____

7.1   DISCUSSION

This thesis is mainly concerned with the development of small specimen creep testing techniques and the associated specimen types. Small specimens creep testing methods have been found to be extremely useful for assessing the creep strength of service-aged materials. The methods can be used to produce data to help in the process of predicting the remaining lifetime of components [8, 47]. Also it can be used to determine the relative creep properties of materials produced as part of an alloy development programme e.g.[4, 98]. The small ring specimen test method can be used to determine the secondary creep strain properties. Also, the minimum creep strain rates, obtained using the ring specimen, for a service-aged material, can be used, with the Monkman-Grant relationship, to predict the approximate component life.

The usefulness of the small ring specimen test method depends on the ease with which specimens can be manufactured and tested and the ease with which the measured deformations can be converted to the corresponding

uniaxial creep data. It should be noted that the expressions for the σ_{ref} and the $\dot{\varepsilon}^c(\sigma_{ref})$ do not contain any material properties, i.e., the conversion process (from small ring specimen data to corresponding uniaxial data) is material independent. Also, the measured deformation is not related to localised creep strains which occur at the region of contact between the test specimen and the loading device (e.g. the impression creep test method); it depends on the bending which occurs at every circumferential position of the ring.

Hence, it is not necessary to have a loading device with significantly higher creep strength than the material being tested. In addition, creep testing of circular, small ring specimens, is made easy by the self-centering property of the specimen. Having a relatively high EGL is a significant advantage of the ring specimen. Typical ring test dimensions, i.e. R = 5 mm and d = 1 mm, result in a β-value of about 0.5, leading to an EGL of about the same magnitude as a conventional uniaxial creep test specimen with a 50 mm gauge length.

In some situations, the dimensions and shape of the small samples of material available may make it more beneficial to test elliptical, rather than circular, specimens. In this case, two types of geometry have been investigated, i.e. "concentric-ellipses" and "offset-ellipses". The offset-ellipse

approach is recommended, because the concentric-ellipse geometry has a variable thickness, which causes an increase in the ring deformation rate, and as a consequence, the β value increases. The results of the ring specimen FE analyses results show that the ring dimensions may have a significant effect on both the η and β values. The experimental results for a Nickel base Superalloy 738 Material, tested at 800°C, and a (Bar-257) P91 steel, tested at 650°C, indicate that the small ring test data can be converted into corresponding uniaxial data, with remarkably good accuracy.

The small TBS which is presented in Chapter 4 is very close in its behaviour to that of a miniature uniaxial specimen. The main advantage of the small TBS type, over other miniature creep test specimen types, is that a full creep strain versus time curve, up to rupture, can be obtained by using this specimen type. Similar to the ring specimen, the measured deformation of the TBS is related to the overall creep deformation of the specimen, not to the local area of contact between the specimen and the loading device. The conversion factors η and β depend on specimen dimension ratios and are independent of the tested material. The TBS has a simple geometry and can be easily machined and tested. In addition loading the specimen through loading pins makes it possible to achieve accurate aligning and hence avoiding possible bending effects, as would be experienced if a small

cylindrical uniaxial specimen was used, where the loading is applied through "stiff" connection of the specimen ends.

The design of the TBS requires a compromise between minimising the overall specimen dimensions and producing, as close as possible, a uniaxial state of stress in the uniform part of the specimen (failure location). In addition, excessive deformation/stress concentration near the pin connections and bending of the supporting material behind the pins should be avoided. Also, the specimen design should be such that the creep deformation of the two uniform "bars" will dominate the overall specimen deformation. The minimum dimensions of the TBS should take into consideration metallurgical effects, i.e. the grain size of the tested material should be significantly smaller than the smallest dimension of the specimen, in order to ensure that "bulk" properties are obtained. A sufficient number of grains should be maintained in the uniform cross section area region of the specimen [7, 104, 105]. The changes in the conversion factors may be significant, and are dependent on the specimen dimensions especially for β. However, preliminary validation using FE analyses shows that as long as the accurate conversion factors are used in the conversion relationships, for the particular specimen dimensions, accurate creep data can be obtained.

The experimental validation of the TBS has been carried out in Chapter 5, where it has been shown that, the TBS testing technique is capable of obtaining both steady state creep and creep rupture data with remarkably good accuracy. Useable specimen dimensions can be readily obtained for a wide range of material sizes. Hence, specimens can be easily extracted from a small sample of material, for example, from the small scoop sample removed from the surfaces of the components, or from thin pieces of material removed from the HAZ or WM regions of a weldment. Furthermore, the specimen dimensions which have been used in this thesis can be easily scaled down by 100% i.e., 6.50, 3.25, 1.00, 1.00 and 2.50 for L_o, k, d, b and D_i.

Although at present there is only a limited amount of test data available, for a P91 steel, at 600°C, and for a (Bar 257) P91 steel at 650°C, the results to date indicate remarkably good agreement between the MSR and rupture data obtained from the TBS tests and the corresponding conventional uniaxial creep tests. The experimental results obtained for the small creep test specimens, which are presented in Chapter 6 have been shown to be able to be used to obtain a full set of material constants, for a variety of creep models, including the Norton's law, the Liu-Murakami damage model and the Kachanov damage model. The small ring and the impression creep testing techniques have been used to obtain the steady state constants, i.e., A

and n in Norton's law for, 316 stainless steel at 600°C, 2-1/4Cr1Mo weld metal at 640°C, and (Bar-257) P91 steel at 650°C.

Both testing techniques have shown good correlation with the corresponding uniaxial test data. The small TBS has been used to obtain Norton's law constants as well as most of the Liu-Murakami and Kachanov material constants, i.e., *A, n, M, B, ϕ, χ* and *q_2*, for (Bar-257) P91 steel at 650°C and for P91 steel at 600°C. Very good correlation was found to exist between the material constants obtained using the small TBS tests and the corresponding conventional uniaxial tests. The multiaxial stress state parameter α has been also obtained for the (Bar-257) P91 steel at 650°C, using a novel small notched specimen. The result is compared with the corresponding Bridgman notch specimen results.

The notched specimen has a relatively simple geometry and therefore it can be easily machined and loaded. In addition, loading the specimen through pin connections makes it possible to achieve accurate aligning. Useable specimen dimensions can be readily obtained for a wide range of material sample sizes. Hence, the small notched specimen can be easily manufactured from small samples of material, such as, for example, the small scoop samples removed from the surfaces of components and from the HAZ or WM regions of welds [46]. This testing technique can be considered as non-destructive

testing (NDT) technique, as the specimens can be easily made from small material samples taken from the operating components, surfaces.

The small notch specimen FE investigation which was carried out to establish the effects of the R/w ratio on the specimen failure times can be used as a guide to the design of the small notched specimen. The slope of the *Log (t_f)* versus α plot indicates the accuracy of the chosen design; a steeply sloping line tends to give more accurate and easy to determent values of the α value for a material. The process of choosing specimen dimensions is a compromise between the volume and shape of the material available from which to make the specimen, and of the available or affordable manufacturing technique required as well as the R/w ratio. However, it should be noted that the failure times for the notched specimen are sensitive to the notched region finish and to the small changes in the R/w ratio.

7.2   CONCLUSIONS

1- The small ring creep test specimen and impression creep test specimen are capable of obtaining accurate secondary creep data when compared with the corresponding uniaxial creep data.

2- It is recommended that a circular ring specimen with $d=2$, $R/d \approx 5$, and $b_0/d \approx 1$ should be used where practical; this ring geometry will allow easy interpretation of the test data.

3- Care must be taken when manufacturing and polishing the small two-bar and the notched specimens, to ensure good finishing is achieved according to the ASTM E2714 – 13 (standards test for creep-fatigue testing).

4- The results of small TBS and notched specimen tests can be used to obtain the full set of material constants for the Norton's law, the Liu-Murakami and the Kachanov damage models.

5- Very good correlation is found between the material constants obtained from the TBS and the small notched specimens and those obtained from the full size specimens.

6- The small ring, the impression, the TBS and the notched specimens, can be easily manufactured from small samples of material, such as for example, the small scoop samples removed from the surfaces of components and from the HAZ or WM regions of welds.

7- TBS designs which result in large deformation in the loading pin region should be avoided, because the aim of the novel TBS testing technique is to obtain creep properties from the overall specimen and not from a small volume of material near a region in the vicinity of the contact between the loading pins and the specimen. The TBS design

should be such that the creep deformation of the two uniform "bars" will dominate the overall specimen deformation.

7.3   FUTURE WORK

1- More creep tests, using the small notched specimen, should be carried out in order to demonstrate the repeatability of the testing method.

2- The small notched specimen tests in the future should be carried out using a smaller R/w ratio (see Fig. 6-6) and a more accurate EDM cutting machine to obtain a better notch finishing.

3- More TBS creep tests should be carried out using different specimen dimensions, materials and testing conditions.

4- Statistical analysis of the TBS results should be carried out to demonstrate repeatability of the TBS testing method.

5- The small TBS and the notched specimens should be manufactured entirely from the HAZ and WM regions of welds and creep tested in order to obtain full set of material creep constants for these regions.

REFERENCES

1.   Hyde, T.H., A.A. Becker, W. Sun, and J.A.Williams, *Finite-element creep damage analyses of P91 pipes.* International Journal of Pressure Vessels and Piping, 2006. **83**: p. 10.

2.   Shibli, I.A. and N. Le Mat Hamata, *Creep crack growth in P22 and P91 welds — overview from SOTA and HIDA projects.* International Journal of Pressure Vessels and Piping, 2001. **78**(11–12): p. 785-793.

3.   Saber, M., D.W.J. Tanner, S. Wei, and T.H. Hyde, *Determination of creep and damage properties for P92 at 675 ℃.* The Journal of Strain Analysis for Engineering Design, 2011. **46**(8): p. 842-851.

4.   Peravali, S., T.H. Hyde, K.A. Cliffe, and S.B. Leen, *Development and use of an anisotropic damage model for the high-temperature life assessment of a P91 weldment.* The Journal of Strain Analysis for Engineering Design, 2008. **43**(5): p. 361-382.

5.   Hyde, T.H. and W. Sun, *Evaluation of conversion relationships for impression creep test at elevated temperatures.* International Journal of Pressure Vessels and Piping, 2009. **86**(11): p. 757-763.

6.   Parker, J.D. and J.D. James, *Creep behaviour of miniature disc specimens of low alloy steel.* ASME, PVP 279, Developments in a Progressing 1994: p. 167-172.

7.   Garzillo, A., C. Guardamagna, L. Moscotti, and L. Ranzani, *A technique for the residual life assessment of high temperature components based on creep-rupture testing on welded miniature specimens.* International Journal of Pressure Vessels and Piping, 1996. **66**(1–3): p. 223-232.

8.   Yingzhi L. and Roman S. *Determination of Creep Properties From Small Punch Test*. in *Pressure Vessels and Piping Division Conference*. 2008. Chicago, Illinois, USA.

9.   Li, J.C.M., *Impression creep and other localized tests.* Materials Science and Engineering: A, 2002. **322**(1–2): p. 23-42.

10.   Hyde, T.H., B.S.M. Ali, and W. Sun, *Interpretation of Small Ring Creep Tests Data.* The Journal of Strain Analysis for Engineering Design, 2013. **48**(4): p. 269-278.

11.   Liu, Y. and S. Murakami, *Damage localization of conventional creep damage models and proposition of a new model for creep damage analysis.* JSME International Journal 1998. **41**(1): p. 57-65.

12.   Fournier, B., F. Dalle, M. Sauzay, J. Longour, M. Salvi, C. Caës, I. Tournié, P.F. Giroux, and S.H. Kim, *Comparison of various 9–12%Cr steels under fatigue and creep-fatigue loadings at high temperature.* Materials Science and Engineering: A, 2011. **528**(22–23): p. 6934-6945.

13.   Penny, R.K. and D.L. Marriott, *Design for creep*1995, London: Chapman & Hall.

14.   Evans, R.W. and B. Wilshire, *Creep of metals and alloys*1985, London: the Institute of Metals.

15.   Callister, W.D., *Materials Science And Engineering An Introduction* 7th Edition ed2007: John Wiley and Sons, Inc.

16.   George, E.D. and D. Bacon, *Mechanical Metallurgy*1988, UK McGraw-Hill Book Company (UK) Limited.

17.   Brooks, C.R. and A. Choudhury, *Failure Analysis of Engineering Materials*2001: McGraw-Hill.

18.   Kachanov, L.M., *Time of the fracture process under creep conditions* SSSR, 1958. **8**(26).

19.   Ennis, P. and A. Czyrska, *Recent advances in creep-resistant steels for power plant applications.* Sadhana, 2003. **28**(3): p. 709-730.

20.   Berbenni, S., V. Favier, and M. Berveiller, *Impact of the grain size distribution on the yield stress of heterogeneous materials.* International Journal of Plasticity, 2007. **23**(1): p. 114-142.

21.   Ning, Y., Z. Yao, Z. Yang, H. Guo, and M.W. Fu, *Flow behavior and hot workability of FGH4096 superalloys with different initial microstructures by using advanced processing maps.* Materials Science and Engineering: A, 2012. **531**(0): p. 91-97.

22.   Hansen, N., *Hall–Petch relation and boundary strengthening.* Scripta Materialia, 2004. **51**(8): p. 801-806.

23.   Callister, W.D., *Material Science and Engineering: An Introduction*1999: John Wiley & Sons Incorporated.

24.   Indrawan, I.G.B., H. Rahardjo, and E.C. Leong, *Effects of coarse-grained materials on properties of residual soil.* Engineering Geology, 2006. **82**(3): p. 154-164.

25.   Mackenzie, A.C., *On the use of a single uniaxial test to estimate deformation rates in some structures undergoing creep.* International Journal of Mechanical Sciences, 1968. **10**(5): p. 441-453.

26.   Johnsson, A., *Reference stress for structures obeying the prandtl and dorn creep laws.* Int. J. Mech. Sci., 1974. **Vol 16(5)**: p. 298-305.

27.   Hyde, T.H. and W. Sun, *A novel, high-sensitivity, small specimen creep test.* The Journal of Strain Analysis for Engineering Design, 2009. **44**(3): p. 171-185.

28.   Hyde, T.H., C.J. Hyde, and W. Sun, *Theoretical basis and practical aspects of small specimen creep testing.* The Journal of Strain Analysis for Engineering Design, 2012.

29.   Sim, R.G., *Evaluation of reference parameters for structures subject to creep.* ARCHIVE: Journal of Mechanical Engineering Science 1959-1982 (vols 1-23), 1971. **13**(1): p. 47-50.

30.   Wilshire, B. and D.R.J. Owen, *Engineering approaches to high temperature design : Recent advances in creep and fracture of engineering materials and structures* 21983, Swansea,Pineridge press,1983.

31.   Hyde, T.H., K.A. Yehia, and A.A. Becker, *Interpretation of impression creep data using a reference stress approach.* International Journal of Mechanical Sciences, 1993. **35**(6): p. 451-462.

32.   Hyde, T.H., W. Sun, and J.A. Williams, *Requirements for and use of miniature test specimens to provide mechanical and creep properties of materials: a review.* International materials reviews, 2007. **52**(4): p. 213-255.

33.   Hyde, T.H., A.A. Becker, W. Sun, A. Yaghi, J.A. Williams, and S. Concari, *Determination Of Creep Properties For P91 Weldment Materials At 625ºC*, in *5th International Conference on Mechanics and Materials in Design*, J.F.S.G.a.S.A. Meguid, Editor 2006: Porto-Portugal.

34.   Kurumlu, D., E.J. Payton, M.L. Young, M. Schöbel, G. Requena, and G. Eggeler, *High-temperature strength and damage evolution in short fiber reinforced aluminum alloys studied by miniature creep testing and synchrotron microtomography.* Acta Materialia, 2012. **60**(1): p. 67-78.

35.   Webster, G.A., S.R. Holdsworth, M.S. Loveday, K. Nikbin, I.J. Perrin, H. Purper, R.P. Skelton, and M.W. Spindler, *A Code of Practice for conducting notched bar creep tests and for interpreting the data.* Fatigue & Fracture of Engineering Materials & Structures, 2004. **27**(4): p. 319-342.

36.   McMeeking, R.M., *Crack tip energy release rate for a piezoelectric compact tension specimen.* Engineering Fracture Mechanics, 1999. **64**(2): p. 217-244.

37.   Lei, Y., *Finite element crack closure analysis of a compact tension specimen.* International Journal of Fatigue, 2008. **30**(1): p. 21-31.

38.   Xuan, F., S. Tu, and Z. Wang, *A modification of ASTM E 1457 C* estimation equation for compact tension specimen with a mismatched cross-weld.* Engineering Fracture Mechanics, 2005. **72**(17): p. 2602-2614.

39.   Davies, C.M., D.W. Dean, K.M. Nikbin, and N.P. O'Dowd, *Interpretation of creep crack initiation and growth data for weldments.* Engineering Fracture Mechanics, 2007. **74**(6): p. 882-897.

40.   Hyde, T.H., M. Saber, and W. Sun, *Testing and modelling of creep crack growth in compact tension specimens from a P91 weld at 650°C.* Engineering Fracture Mechanics, 2010. **77**(15): p. 2946-2957.

41.   Hyde, C.J., T.H. Hyde, W. Sun, and A.A. Becker, *Damage mechanics based predictions of creep crack growth in 316 stainless steel.* Engineering Fracture Mechanics, 2010. **77**: p. 2385-2402.

42.   Biglari, F., K.M. Nikbin, I.W. Goodall, and G.A. Webster, *Determination of fracture mechanics parameters J and C∗ by finite element and reference stress methods for a semi-elliptical flaw in a plate.* International Journal of Pressure Vessels and Piping, 2003. **80**(7–8): p. 565-571.

43.   Hyde, T.H., M. Saber, and W. Sun, *Creep crack growth data and prediction for a P91 weld at 650°C.* International Journal of Pressure Vessels and Piping, 2010. **87**(12): p. 721-729.

44.   Paulraj, M.P., S. Yaacob, M.S.A. Majid, M.N.F.M. Kazim, and P. Krishnan, *Structural Steel Plate Damage Detection using Non Destructive Testing, Frame Energy based Statistical Features and Artificial Neural Networks.* Procedia Engineering, 2013. **53**(0): p. 376-386.

45.   Exponent. *Surface Sampling Systems*. 2011 [cited 2013 25/3/2013]; Available from: http://www.exponent.com/SSam/.

46.   Hyde, C.J., T.H. Hyde, and W. Sun. *Small ring specimen creep testing of a Nickel-based superalloy.* in *Determination of mechanical properties of materials by small punch and other miniature testing techniques* 2012. Ostrava, Czech Republic.

47.   Hyde, T.H. and W. Sun, *Some considerations on specimen types for small sample creep tests.* Materials at High Temperatures, 2010. **27**: p. 157-165.

48.   Tabuchi, M., T. Watanabe, K. Kubo, M. Matsui, J. Kinugawa, and F. Abe, *Creep crack growth behavior in the HAZ of weldments of W containing high Cr steel.* International Journal of Pressure Vessels and Piping, 2001. **78**(11-12): p. 779-784.

49.   Takamoto, I., I. Yuichi, S. Masao, K. Yusuke, T. Takafumi, and F. Masaharu. *Development Of Miniature Creep Testing For High Temperature Materials Verification Testing.* in *Determination of mechanical properties of materials by small punch and other miniature testing techniques* 2012. Ostrava, Czech Republic.

50.   Jianhua, S., Q. Zhenmei, and L. Xiang, *Influence of Oxidation to Small Punch Creep Test.* 2007. **353-358** p. 461-464.

51.   Mälzer, G., R.W. Hayes, T. Mack, and G. Eggeler, *Miniature Specimen Assessment of Creep of the Single-Crystal Superalloy LEK 94 in the 1000 °C Temperature Range.* Metallurgical and Materials Transactions A, 2007. **38**(2): p. 314-327.

52.   Mathew, M.D., Naveena, and D. Vijayanand, *Impression Creep Behavior of 316LN Stainless Steel.* Journal of Materials Engineering and Performance, 2012. **22**(2): p. 1-6.

53.   Sastry, D.H., *Impression creep technique—An overview.* Materials Science and Engineering: A, 2005. **409**(1–2): p. 67-75.

54.   Sun, W., T.H. Hyde, and S.J. Brett. *Use Of Impression Creep Test Method For Determining Minimum Creep Strain Rate Data.* in *Determination of mechanical properties of materials by small punch and other miniature testing techniques* 2012. Ostrava, Czech Republic.

55.   Cigada, A., *Struttura e proprietá dei materiali metallici*1993, Novara, ITALY.

56.   Hyde, T.H. and W. Sun, *Multi-step Load Impression Creep Tests for a 1/2Cr1/2Mo1/4V Steel at 565°C.* Strain, 2001. **37**(3): p. 99-103.

57. Sun, W., T.H. Hyde, and S.J. Brett, *Application of impression creep data in life assessment of power plant materials at high temperatures.* Materials Design and Applications, 2008: p. 222-175.

58. Phaniraj, C., B.K. Choudhary, S.R.K. Bhanu, and B. Raj, *Relationship between time to reach Monkman–Grant ductility and rupture life.* Scripta Materialia, 2003. **48**(9): p. 1313-1318.

59. Kim, B.J., Y.B. Sim, J.H. Lee, M.K. Kim, and B.S. Lim, *Application of small punch creep test for Inconel 617 alloy weldment.* Procedia Engineering, 2011. **10**(0): p. 2579-2584.

60. Fleury, E. and J.S. Ha, *Small punch tests to estimate the mechanical properties of steels for steam power plant: I. Mechanical strength.* International Journal of Pressure Vessels and Piping, 1998. **75**(9): p. 699-706.

61. Evans, M. and D. Wang, *The small punch creep test: some results from a numerical model.* Journal of Materials Science, 2008. **43**(6): p. 1825-1835.

62. Hou, F., H. Xu, Y.F. Wang, and L. Zhang, *Determination of creep property of 1.25Cr0.5Mo pearlitic steels by small punch test.* Engineering Failure Analysis, 2013. **28**(0): p. 215-221.

63. Zhou, Z., Y. Zheng, X. Ling, R. Hu, and J. Zhou, *A study on influence factors of small punch creep test by experimental investigation and finite element analysis.* Materials Science and Engineering: A, 2010. **527**(10–11): p. 2784-2789.

64. Yang, Z. and Z. Wang, *Relationship between strain and central deflection in small punch creep specimens.* International Journal of Pressure Vessels and Piping, 2003. **80**(6): p. 397-404.

65. Zhao, L., H. Jing, L. Xu, Y. Han, J. Xiu, and Y. Qiao, *Evaluating of creep property of distinct zones in P92 steel welded joint by small punch creep test.* Materials & Design, 2012(0).

66. Ling, X., Y. Zheng, Y. You, and Y. Chen, *Creep damage in small punch creep specimens of Type 304 stainless steel.* International Journal of Pressure Vessels and Piping, 2007. **84**(5): p. 304-309.

67. Hyde, T.H., M. Stoyanov, W. Sun, and C.J. Hyde, *On the interpretation of results from small punch creep tests.* The Journal of Strain Analysis for Engineering Design, 2010. **45**(3): p. 141-164.

68. CEN, *Small Punch Test Method for Metallic Materials*, 2006, CEN: Brussels.

69. Hyde, T.H., F. Cortellino, J.P. Rouse, and W. Sun. *Small Punch Creep Testing and Data Analysis of a P91 Steel at 650oC*. in *Determination of mechanical properties of materials by small punch and other miniature testing techniques* 2012. Ostrava, Czech Republic.

70. ABAQUS, *ABAQUS 6.11-3 Standard user manual*2010, USA: ABAQUS, Inc.

71. Findeisen, A., M. Klatt, and H. Joachim Krautz, *Examination of the corrosion behaviour of selected power plant materials under various operating conditions*. Chemie der Erde - Geochemistry, 2010. **70, Supplement 3**(0): p. 193-199.

72. Tanner, D.W.J., A.A. Becker, and T.H. Hyde, *High temperature life prediction of a welded IN718 component*. Journal of Physics: Conference Series, 2009. **181**(1): p. 012027.

73. Giroux, P.F., F. Dalle, M. Sauzay, J. Malaplate, B. Fournier, and A.F. Gourgues-Lorenzon, *Mechanical and microstructural stability of P92 steel under uniaxial tension at high temperature*. Materials Science and Engineering: A, 2010. **527**(16–17): p. 3984-3993.

74. David, W.J.T., *Life assessment of welded Inconal 718 at high temperature* 2009, Thesis submitted to the University of Nottingham. p. 267.

75. Hyde, T.H., A.A. Becker, Y. Song, and W. Sun, *Failure estimation of TIG butt-welded Inco718 sheets at 620 oCunder creep and plasticity conditions*. Computational Materials Science, 2006. **35**: p. 6.

76. Metals, H.T. *INCONEL 617 TECHNICAL DATA*. 2012 [cited 2013 07/02/2013]; INCONEL 617 TECHNICAL DATA]. Available from: http://www.hightempmetals.com/techdata/hitempInconel617data.php .

77. Jin, S., L. Guo, T. Li, J. Chen, Z. Yang, F. Luo, R. Tang, Y. Qiao, and F. Liu, *Microstructural evolution of P92 ferritic/martensitic steel under Ar+ ion irradiation at elevated temperature*. Materials Characterization, 2012. **68**(0): p. 63-70.

78. Gampe, U. and P. Seliger, *Creep crack growth testing of P91 and P22 pipe bends*. International Journal of Pressure Vessels and Piping, 2001. **78**(11–12): p. 859-864.

79. Jason, D.P.P. *Why new U.S. supercritical units should consider T/P92 piping*. 2006 16/03/2013 [cited 2013 19th January]; Available from: http://www.powermag.com/issues/features/Why-new-U-S-supercritical-units-should-consider-TP92-piping_438_p4.html.

80. Vaillant, J.C., B. Vandenberghe, B. Hahn, H. Heuser, and C. Jochum, *T/P23, 24, 911 and 92: New grades for advanced coal-fired power plants--Properties and experience.* International Journal of Pressure Vessels and Piping, 2008. **85**(1-2): p. 38-46.

81. Hayhurst, D.R., *Creep rupture under multi-axial states of stress.* Journal of the Mechanics and Physics of Solids, 1972. **20**(6): p. 381-382.

82. Hyde, T.H., R. Li, W. Sun, and M. Saber, *A simplified method for predicting the creep crack growth in P91 welds at 650°C.* Proceedings of the Institution of Mechanical Engineers, Part L: Journal of Materials: Design and Applications, 2010.

83. Hyde T. H., Saber M., and S. W., *Determination of creep and damage properties for P92 at 675 °C.* 2011.

84. Hyde, T.H., M. Saber, and W. Sun, *Creep Crack Growth in a P91 Weld at 650°C*, in *WELDS*2009: Sanibel Harbour Resort & Spa, Fort Myers, Florida, USA.

85. Kim, B., C. Jeong, and B. Lim, *Creep behavior and microstructural damage of martensitic P92 steel weldment.* Materials Science and Engineering: A, 2008. **483-484**: p. 544-546.

86. Hyde, T.H., L. Xia, and A.A. Becker, *Prediction of creep failure in aeroengine materials under multi-axial stress states.* International Journal of Mechanical Sciences, 1996. **38**(4): p. 385-403.

87. Perrin, I.J., D.R. Hayhurst, and R.A. Ainsworth, *Approximate creep rupture lifetimes for butt welded ferritic steel pressurised pipes.* European Journal of Mechanics - A/Solids, 2000. **19**(2): p. 223-258.

88. Storesund, J. and S.T. Tu, *Geometrical Effect on Creep in Cross Weld Specimens.* International Journal of Pressure Vessels and Piping, 1995. **62**: p. 179-193.

89. Tanaka, Y., K. Kubushiro, S. Takahashi, N. Saito, and H. Nakagawa, *Creep-Induced Microstructural Changes in Large Welded Joints of High Cr Heat Resistant Steel.* Procedia Engineering, 2013. **55**(0): p. 41-44.

90. Nikbin, K., *Creep/Fatigue Crack Growth Testing, Modelling and Component Life Assessment of Welds.* Procedia Engineering, 2013. **55**(0): p. 380-393.

91. Joseph, A., S.K. Rai, T. Jayakumar, and N. Murugan, *Evaluation of residual stresses in dissimilar weld joints.* International Journal of Pressure Vessels and Piping, 2005. **82**(9): p. 700-705.

92. Tabuchi, M., A.T. Yokobori Jr, R. Sugiura, M. Yatomi, A. Fuji, and K. Kobayashi, *Results of a Japanese round robin program for creep crack growth using Gr.92 steel welds.* Engineering Fracture Mechanics, 2010. **77**(15): p. 3066-3076.

93. Hyde, T.H., B.S.M. Ali, and W. Sun, *Interpretation of small ring creep test data.* The Journal of Strain Analysis for Engineering Design, 2013. **48**(4): p. 269-278.

94. Beltrami, I., A. Bertholds, and D. Dauw, *A simplified post process for wire cut EDM.* Journal of Materials Processing Technology, 1996. **58**(4): p. 385-389.

95. Liu, C. and D. Esterling, *Solid modeling of 4-axis wire EDM cut geometry.* Computer-Aided Design, 1997. **29**(12): p. 803-810.

96. Hyde, T.H., C.J. Hyde, and W. Sun, *basis for selecting the most appropriate small specimen creep test type*, in *Pressure Vessel & Piping Conference* 2012, ASME Toronto, Canada.

97. Tabuchi, M., A.T. Yokobori Jr, R. Sugiura, M. Yatomi, A. Fuji, and K. Kobayashi, *Results of a Japanese Round Robin Program for Creep Crack Growth Using Gr.92 Steel Welds.* Engineering Fracture Mechanics, 2010. **77**(15):p.3066-3076.

98. Dorner, D., K. Röller, B. Skrotzki, B. Stöckhert, and G. Eggeler, *Creep of a TiAl alloy: a comparison of indentation and tensile testing.* Materials Science and Engineering, 2003. **357**(1–2): p. 346-354.

99. Johnsson, A., *An alternative definition of reference stress for creep.* Int. J. Mech. Sci., 1973. **16**(5): p. 298-305.

100. Hyde, T.H., K. Yehia, and W. Sun, *Observation on the creep of two-material structures.* J. Strain Analysis, 1996. **31** (6): p. 441-461.

101. Hyde, T.H., B.S.M. Ali, and W. Sun. *A Small Creep Test Specimen for Use in Determining Uniaxial Creep Rupture Data.* in *On the determination of*

mechanical properties of materials by small punch and other miniature testing techniques 2012. Ostrava, Czech Republic.

102. Li, R., T.H. Hyde, W. Sun, and B. Dogan. *Modelling And Data Interpretation Of Small Punch Creep Testing*. in *Pressure Vessels & Piping Division*. 2011. Baltimore, Maryland, USA: ASME.

103. Sun, W. and T.H. Hyde, *Determination of secondary creep properties using a small ring creep test technique.* Metallurgical Journal, 2010(LXIII): p. 185-193.

104. Evans, M. and D. Wang, *Optimizing the sensitivity of the small-disc creep test to damage and test conditions.* J. Strain Anal., 2007. **42**: p. 389-409.

105. Stratford, G.C., F. Dipersio, and J. Klapyt, *miniaturised creep testing using the small punch test technique*, in *Third International Charles Parsons Turbine Conference*1995. p. 419-428.

106. Ho, K.H., S.T. Newman, S. Rahimifard, and R.D. Allen, *State of the art in wire electrical discharge machining (WEDM).* International Journal of Machine Tools and Manufacture, 2004. **44**(12–13): p. 1247-1259.

107. Peng, Z., Z. Wang, Y. Dong, and H. Chen, *Development of a reversible machining method for fabrication of microstructures by using micro-EDM.* Journal of Materials Processing Technology, 2010. **210**(1): p. 129-136.

108. Mohd, A.N., D.G. Solomon, and M. Fuad, *A review on current research trends in electrical discharge machining (EDM).* International Journal of Machine Tools and Manufacture, 2007. **47**(7–8): p. 1214-1228.

109. Hyde, T.H., W. Sun, A.A. Becker, and J.A. Williams, *Creep properties and failure assessment of new and fully repaired P91 pipe welds at 923 K.* Journal of Materials:Design and Applications, 2004. **218**(3): p. 211-222.

110. Wolk, R.H. and J. McDaniel, *High efficiency coal fueled power generation.* Energy Conversion and Management, 1992. **33**(5–8): p. 705-712.

111. Hyde, T.H., W. Sun, and A.A. Becker, *Analysis of the impression creep test method using a rectangular indenter for determining the creep properties in welds.* International Journal of Mechanical Sciences, 1996. **38**(10): p. 1089-1102.

112. Hyde, T.H., B.S.M. Ali, and W. Sun, *Analysis and Design of a Small, Two-Bar Creep Test Specimen.* ASME J. Engineering Materials and Technology, 2013. **135**: p. 410061-410069.

113.   Izaki, T., T. Kobayashi, J. Kusumoto, and A. Kanaya, *A creep life assessment method for boiler pipes using small punch creep test.* International Journal of Pressure Vessels and Piping, 2009. **86**(9): p. 637-642.

114.   Yang, S., J. Zhou, X. Ling, and Z. Yang, *Effect of geometric factors and processing parameters on plastic damage of SUS304 stainless steel by small punch test.* Materials & Design, 2012. **41**(0): p. 447-452.

115.   Hyde, T.H., B.S.M. Ali, and W. Sun, *Small Two-bar specimen creep testing of (Bar-257) P91 steel at 650ᵒC.* ASME J. Engineering Materials and Technology 2013. **Under revision**.

116.   Rouse, J.P., W. Sun, T.H. Hyde, and A. Morris, *Comparative assessment of several creep damage models for use in life prediction.* International Journal of Pressure Vessels and Piping, 2013. **108–109**(0): p. 81-87.